

**RESULTS OF AN EXPERIMENT IN A ZION-LIKE GEOMETRY  
TO INVESTIGATE THE EFFECT OF WATER ON THE CONTAINMENT  
BASEMENT FLOOR ON DIRECT CONTAINMENT HEATING (DCH)  
IN THE SURTSEY TEST FACILITY: THE IET-4 TEST**

Michael D. Allen  
Thomas K. Blanchat  
Martin Pilch  
Robert T. Nichols\*

SAND--92-1241

DE93 002514

Severe Accident Phenomenology  
Sandia National Laboratories  
Albuquerque, NM

**ABSTRACT**

The fourth experiment of the Integral Effects Test (IET-4) series was conducted to investigate the effects of high pressure melt ejection on direct containment heating. Scale models (1:10) of the Zion reactor pressure vessel (RPV), cavity, instrument tunnel, and subcompartment structures were constructed in the Surtsey Test Facility at Sandia National Laboratories. The RPV was modeled with a melt generator that consisted of a steel pressure barrier, a cast MgO crucible, and a thin steel inner liner. The melt generator/crucible had a hemispherical bottom head containing a graphite limiter plate with a 3.5-cm exit hole to simulate the ablated hole in the RPV bottom head that would be formed by tube ejection in a severe nuclear power plant accident. The reactor cavity model contained 3.48 kg of water with a depth of 0.9 cm that corresponded to condensate levels in the Zion plant. A 43-kg initial charge of iron oxide/aluminum/chromium thermite was used to simulate corium debris on the bottom head of the RPV. Molten thermite was ejected into the scaled reactor cavity by 6.7 MPa steam.

IET-4 replicated the third experiment in the IET series (IET-3), except the Surtsey vessel contained slightly more pre-existing oxygen (9.6 mol.% vs. 9.0 mol.%), and water was placed on the basement floor inside the crane wall. The cavity pressure measurements showed that a small steam explosion occurred in the cavity at about the same time as the steam explosion in IET-1. The oxygen in the Surtsey vessel in IET-4 resulted in a vigorous hydrogen burn, which caused a significant increase in the peak pressure, 262 kPa compared to 98 kPa in the IET-1 test. IET-3, with similar pre-existing oxygen concentrations, also had a large peak pressure of 246 kPa. The total debris mass ejected into the Surtsey vessel in IET-4 was 40.72 kg, and gas grab sample analysis indicated that 297 g-moles of hydrogen were produced by steam/metal reactions. About 236 g-moles of hydrogen burned and 61 g-moles remained unreacted.

---

\*Ktech Corp., 901 Pennsylvania NE, Albuquerque, NM 87110

**MASTER**

28

# CONTENTS

<u>Section</u>	<u>Page</u>
1. INTRODUCTION . . . . .	1
2. EXPERIMENT DESCRIPTION . . . . .	1
2.1 Initial Conditions . . . . .	3
2.2 Measurements and Instrumentation . . . . .	3
2.2.1 Pressure Measurements . . . . .	3
2.2.2 Temperature Measurements . . . . .	4
2.2.3 Gas Composition . . . . .	5
2.2.4 Posttest Debris Recovery . . . . .	6
2.2.5 Debris Velocity . . . . .	6
3. EXPERIMENTAL RESULTS . . . . .	6
3.1 Blowdown History . . . . .	7
3.2 Pressure Measurements . . . . .	7
3.2.1 Surtsey Vessel Pressure . . . . .	8
3.2.2 Cavity Pressure . . . . .	8
3.2.3 Pressure Measured Inside the Seal Table Room . . . . .	9
3.2.4 Pressure Measured Inside the Subcompartment Structures . . . . .	10
3.3 Gas Temperature Measurements . . . . .	10
3.4 Debris Temperature Measurements . . . . .	11
3.5 Gas Composition Measurements . . . . .	12
3.6 Debris Recovery Summary . . . . .	13
3.7 Energy Balance . . . . .	14
4. SUMMARY . . . . .	17
5. REFERENCES . . . . .	66

## LIST OF TABLES

<u>Table</u>	<u>Page</u>
1. Instruments used in the IET-4 Experiment . . . . .	19
2. Initial Conditions for the IET-1, IET-3, and IET-4 Experiments . . . . .	26
3. Gas Concentrations Measured in the IET-4 Experiment . . . . .	27
4. Debris Recovery Summary for the IET-1, IET-3, and IET-4 Experiments . . . . .	28
5. Energy Balance for the IET-1, IET-3, and IET-4 Experiments . . . . .	29
6. Summary of the Results of the IET-1, IET-3, and IET-4 Experiments . . . . .	29

## LIST OF FIGURES

<u>Figure</u>	<u>Page</u>
1. Surtsey vessel, high-pressure melt ejection system, and subcompartment structures used in the IET-4 experiment . . . . .	30
2. Melt generator and MgO crucible used in the IET-4 experiment . . . . .	31
3. Schematic of the 1:10 linear scale model of the Zion reactor cavity . . . . .	32
4. High-pressure steam boiler, steam accumulator, melt generator, cavity, and Surtsey vessel layout . . . . .	33
5. Two-dimensional view of the subcompartment structures inside the Surtsey vessel . . . . .	34
6. Isometric view of the subcompartment structures inside the Surtsey vessel . . . . .	35
7. Top view of structures inside the Surtsey vessel . . . . .	36
8. Top view of the Surtsey vessel showing instrumentation ports . . . . .	37
9. Location of Surtsey vessel bulk gas temperature thermocouple arrays . . . . .	38
10. Gas grab sample bottle fill times . . . . .	39
11. Blowdown pressure history for the IET-4 experiment . . . . .	40
12. Steam blowdown temperatures measured in the steam accumulator tank with type-K thermocouples in the IET-4 experiment . . . . .	41
13. Surtsey vessel pressure versus time measured at level 1 in the IET-4 experiment . . . . .	42
14. Surtsey vessel pressure versus time measured at level 3 in the IET-4 experiment . . . . .	43
15. Surtsey vessel pressure versus time measured at level 5 in the IET-4 experiment . . . . .	44
16. Surtsey vessel pressure comparisons versus time for the IET-1, IET-3, and IET-4 experiments . . . . .	45
17. Cavity pressure and Surtsey vessel pressure versus time in the IET-4 experiment . . . . .	46

## List of Figures (continued)

<u>Figure</u>	<u>Page</u>
18. Comparison of the cavity pressures versus time for the IET-1, IET-3, and IET-4 experiments . . . . .	47
19. Seal table room absolute pressure and differential pressure compared to Surtsey vessel pressure in the IET-4 experiment . . . . .	48
20. Seal table room and Surtsey vessel pressure versus time in the IET-4 experiment . . . . .	49
21. Debris ejection timing into the seal table room in the IET-4 experiment . . . . .	50
22. Subcompartment absolute pressure and differential pressure compared to Surtsey vessel pressure in the IET-4 experiment . . . . .	51
23. Cavity floor, chute exit, and seal table room temperatures measured with type-K thermocouples in the IET-4 experiment . . . . .	52
24. Gas temperatures measured at levels 1, 3, and 5 in the Surtsey vessel with aspirated thermocouples in the IET-4 experiment . . . . .	53
25. Gas temperatures inside the subcompartment structures measured with aspirated thermocouples in the IET-1, IET-3, and IET-4 experiments . . . . .	54
26. Gas temperatures inside the seal table room measured with type-K aspirated thermocouples in the IET-3 and IET-4 experiments . . . . .	55
27. Comparison of the temperatures in the triangular vent space above RCPs 1A and 1D in the IET-3 and IET-4 experiments . . . . .	56
28. Temperature history of the east thermocouple array in the IET-4 experiment . . . . .	57
29. Temperature history of the west thermocouple array in the IET-4 experiment . . . . .	58
30. Relative pressure and bulk gas temperature increase in the Surtsey vessel in the IET-4 experiment . . . . .	59
31. Raw pyrometer output at the chute exit measured with a type 11x20 optical pyrometer in the IET-4 experiment . . . . .	60
32. Raw pyrometer output at the chute exit measured with a type 11x30 optical pyrometer in the IET-4 experiment . . . . .	61

## LIST OF FIGURES (concluded)

<u>Figure</u>	<u>Page</u>
33. Debris temperature at the chute exit measured with a type 11x20 optical pyrometer in the IET-4 experiment . . . . .	62
34. Debris temperature at the chute exit measured with a type 11x30 optical pyrometer in the IET-4 experiment . . . . .	63
35. Debris temperature measured with the graphite disk calorimeters in the IET-4 experiment . . . . .	64
36. Posttest sieve analysis of debris recovered from outside the subcompartment structures in the Surtsey vessel in the IET-4 experiment . . . . .	65

## ACKNOWLEDGMENTS

The authors express their gratitude to Michael Oliver, who was the electronics and instrumentation engineer for these experiments, and to James Ross, Tim Covert, and Robert Carolan, who were the mechanical technicians. The authors appreciate the technical review of this report provided by T. Y. Chu and Lubomyra N. Kmetyk. Editorial review was provided by Patty G. Guyer.

This work was funded by the Accident Evaluation Branch of the United States Nuclear Regulatory Commission.

## 1.0 INTRODUCTION

The Surtsey Test Facility at Sandia National Laboratories (SNL) is used to perform scaled experiments for the Nuclear Regulatory Commission (NRC) that simulate hypothetical high-pressure melt ejection (HPME) accidents in a nuclear power plant (NPP). These experiments are designed to investigate the phenomena associated with direct containment heating (DCH). High-temperature, chemically reactive melt is ejected by high-pressure steam into a 1:10 linear scale model of a reactor cavity. Debris is entrained by the steam blowdown into the Surtsey vessel, where specific phenomena, such as the effect of subcompartment structures, water in the cavity, and hydrogen generation and combustion, can be studied.

The fourth Integral Effects Test (IET-4) using a small scale model of the Zion Nuclear Generating Station was successfully conducted on March 20, 1992. The purpose of this test was to replicate the IET-3 test [Allen et al. 1992c], which was conducted with 0.09 MPa of air and 0.1 MPa of nitrogen in the Surtsey vessel, along with 3.48 kg of water in the scaled reactor cavity model. In addition, the IET-4 test was conducted with 71 kg of water on the basement floor inside the crane wall. The water on the floor of the cavity and containment basement were scaled to condensate levels in a NPP accident. Molten debris deflected back to the containment basement floor should be quenched by this water, but the interaction could produce additional hydrogen. The comparison between the IET-3 and IET-4 tests should provide a measure of the change in peak Surtsey vessel pressure due to debris quenching and combustion of additional hydrogen.

The Surtsey IET test series in the Zion configuration is being conducted at 1:10 linear scale, and Argonne National Laboratory (ANL) counterpart tests are being performed at 1:40 scale. Results of these experiments will allow assessment of scaling methodologies proposed by the Severe Accident Scaling Methodology - Technical Program Group (SASM-TPG)<sup>1</sup> and by SNL.<sup>2</sup>

## 2.0 EXPERIMENT DESCRIPTION

All tables and figures are located at the end of the text. Table 1 is a listing of the instrumentation used in the IET-4 experiment, including the channel number, type, purpose, and location of each instrument. The circled numbers in Figures 1 through 9 correspond to the channel numbers in the data acquisition system listed in Table 1.

---

<sup>1</sup> SASM - TPG, Nov. 1991, An Integrated Structure and Scaling Methodology for Severe Accident Technical Issue Resolution, NUREG/CR-5809, EG&G-2659, draft for comment, Idaho National Engineering Laboratory, Idaho Falls, ID.

<sup>2</sup> M. Pilch and M. D. Allen, A Scaling Methodology for Direct Containment Heating with Application to the Design and Specification of an Experiment Program for Resolving DCH Issues, SAND91-2784, to be published, Sandia National Laboratories, Albuquerque, NM.

Figure 1 is a composite view of the Surtsey vessel, the HPME delivery system, and the outer boundary of the subcompartment structures used in the IET-4 experiment. This figure shows the instrument penetration ports at six levels in the Surtsey vessel.

In the Surtsey IET tests, 1:10 linear scale models of the Zion reactor pressure vessel (RPV), cavity, in-core instrument tunnel, and subcompartment structures were used. The RPV was modeled with a melt generator that consisted of a steel pressure barrier, a cast MgO crucible, and a thin steel inner liner (Figure 2). The melt generator/crucible had a hemispherical bottom head containing a graphite limiter plate with a 3.5 cm exit hole to simulate the ablated hole in the RPV bottom head that would be formed by tube ejection and hole ablation in a NPP severe accident.

The cavity used in the IET-4 test (Figure 3) was a 1:10 linear scale model of the Zion reactor cavity that was designed to withstand internal pressures of 6.9 MPa with a safety factor of 4. The inclined portion of the instrument tunnel entered the bottom head of Surtsey at a 26° angle from vertical, as it does in Zion. A false concrete floor was constructed in the Surtsey vessel, similar to the floor of the Zion basement, so that the inclined portion of the instrument tunnel was about 2.7 times the correct scaled length of the inclined part of the Zion instrument tunnel. This floor was constructed in Surtsey to match the configuration of the ANL facility. Figure 4 shows the experiment configuration, with the layout of the high pressure steam boiler, accumulator, burst diaphragm, melt generator, and cavity connection to the Surtsey vessel.

The subcompartment structures included 1:10 linear scale models of the crane wall, four steam generators (SG), four reactor coolant pumps (RCP), the opening in the floor of the seal table room for the instrument guide tubes, the seal table room, the biological shield wall, the refueling canal, the radial beams and the gratings at the RCP deck, and the operating deck (Figures 5, 6, and 7). The steam generators, RCPs, and gratings were made of steel and the other structures were constructed of reinforced concrete. All of the structures were painted with an epoxy-base paint. Figure 8 gives the top view of the Surtsey vessel, showing the orientation and location of the instrument penetrations through the vessel ports at six different levels.

The steam accumulator tank was pressurized to  $\approx 6.3$  MPa with superheated steam. After the pressurization sequence, the iron oxide/aluminum/chromium thermite mixture was ignited remotely with a braided wire fuse placed on top of the compacted thermite. After the thermite was ignited, the pressure in the crucible rapidly increased. This pressure increase verified that the thermite reaction had started, and signaled the operator to fail the burst diaphragm separating the steam accumulator tank and the molten thermite in the melt generator. This brought superheated steam into contact with the molten thermite. Upon contacting and failing a fusible brass plug at the bottom of the crucible, the molten thermite in the crucible was expelled by high-pressure steam into the cavity.

Zero time for HPME was set by the data acquisition system as the time at which the melt failed the brass plug and entered the cavity. This event was signaled by a photodiode located at the melt plug exit. When the hot melt burst through the brass plug, the intense light emitted from the melt caused the photodiode to emit a signal that was used to mark the initiation of the HPME.

## **2.1 Initial Conditions**

The IET-4 test was conducted with the following initial conditions: (1) the melt simulant was 43 kg of iron oxide/aluminum/chromium powder; (2) the driving gas was  $\approx 583$  g-moles of superheated steam ( $\approx 555$  K) at an initial absolute pressure of 6.7 MPa; (3) the initial absolute pressure in the Surtsey vessel was  $\approx 0.2$  MPa of air diluted with nitrogen (9.59 mol.% O<sub>2</sub>); (4) the cavity was filled with 3.48 kg of water (335 K) that was 0.9 cm deep; and (5) the containment basement floor inside the crane wall (floor area = 4.6 m<sup>2</sup>) was filled with  $\approx 71$  kg of water (286 K) that was 1.5 cm deep. Table 2 lists the initial conditions of the IET-4 experiment, along with IET-1 and IET-3 initial conditions for comparison.

## **2.2 Measurements and Instrumentation**

The most significant variables to measure in the Integral Effects Tests (IETs) are: (1) the increase in pressure and temperature in the Surtsey vessel, (2) the cavity pressure, (3) the number of moles of hydrogen generated by the reaction of metallic debris with steam driving gas, and with water in the cavity and on the containment basement floor, (4) the debris temperature as it exited the instrument tunnel, (5) the debris temperature as it struck the concrete structure, (6) the debris interaction times, (7) the debris particle size, (8) and the mass of debris recovered from specific locations in the Surtsey vessel. The instrumentation and techniques used to make these measurements are described in the sections below.

### **2.2.1 Pressure Measurements**

Six pressure transducers with a range of 0-0.69 MPa, two at each level 1, 3, and 5 (Channels 21 through 26 in Figures 1 and 8), were used to measure the pressure in the upper dome of the Surtsey vessel in the IET-4 experiment. These transducers were mounted in tapped holes in instrument penetration ports in the sides of the Surtsey vessel and had their sensing ends protected with steel turnings. Pressure transducers with a range of 0-6.9 MPa were used to measure the gas pressure in the accumulator tank (Channel 32 in Figure 4), in the crucible above the thermite (Channels 34 and 35 in Figures 2, 3, and 4), and in the scaled reactor cavity (Channel 36 in Figures 3 and 4). Pressure transducers with a range of 0-0.69 MPa were used to measure the gas pressure in the subcompartment structures and in the seal table room (Channels 39 and 40 in Figures 5, 6, and 7). These transducers were metal diaphragm strain gauge-type pressure transducers (Model 141-1, Precise Sensor, Inc., Monrovia, CA). In addition, two pressure transducers were embedded in the concrete walls of the round section of the cavity under the melt generator (labeled P1 and P2 in Figures 3 and 4), and were piezoelectric-type gauges with a range of 0-6.9 MPa. The specified accuracy from the manufacturer for the pressure transducers is less than  $\pm 0.50$  percent at full-scale output. These instruments are routinely recalibrated at SNL against the National Bureau of Standards, and accuracies are always within manufacturer's specifications. The frequency response is 22 kHz (16  $\mu$ s rise time) for the 0-0.69 MPa range pressure transducers, and is 36 kHz (10  $\mu$ s rise time) for the 0-6.9 MPa range pressure transducers. The data acquisition system recorded data from the pressure transducers at a rate of 1400 data points per second from thermite ignition to about 60 seconds following the HPME transient.

## 2.2.2 Temperature Measurements

Following the HPME transient, the gas temperatures in the Surtsey vessel were measured with five aspirated thermocouple assemblies. An aspirated thermocouple assembly consisted of three bare, type-K thermocouples (0.127 mm wire) mounted in an anodized aluminum tube. Each tube was opened with a solenoid-operated valve that was actuated remotely by a signal from the photodiode under the melt plug immediately after the HPME transient. One of these assemblies was installed through instrumentation ports at each level 1, 3, and 5 (Channels 41 through 49 in Figures 1 and 8). A thermocouple assembly was also installed through the refueling canal wall just above the radial concrete beam on the same side as the instrument tunnel exit. This thermocouple assembly was used to measure gas temperature inside the subcompartment structures (Channels 51, 52, and 53 shown in Figures 5, 6, and 7). Another thermocouple assembly was installed through the crane wall into the seal table room (Channels 54, 55, and 56 in Figures 5, 6, and 7). Calculations by SNL have shown that the worst-case temperature underprediction by the thermocouple assemblies would be 13 percent at the beginning of the HPME event (when the gas temperatures are low) to 6 percent at equilibrium (when the gas temperatures have peaked).<sup>3</sup>

Two type-K thermocouple arrays (Channels 68 through 77 in Figures 6, 7, and 9) were installed in the Surtsey vessel to measure bulk gas temperature above the operating deck. Each array consisted of five approximately equally spaced thermocouples suspended near the northeast vent (above the 1C RCP) and above the west end of the refueling canal. Note that the vessel wall near the chute exit has been referenced as the north wall. Figure 9 gives the spacing and relative position of the thermocouple arrays. All type-K thermocouples are made of 0.254 mm wire with a 1.5875 mm sheath. The temperature range is 273-1523 K. The maximum limit of error using the manufacturer's calibration is  $\pm 9.4$  K at 1523 K, with a 0.3 s time constant. The thermocouples had the sheath removed at the tip, exposing the junction to ensure a fast time response. The thermocouples were located  $\approx 71$  cm from the Surtsey vessel wall.

Two type-K thermocouples (Channels 66 and 67 in Figures 6 and 7) were installed inside the triangular vent space above the 1A and 1D RCPs. These thermocouples measured the temperature of the gas as it exited the subcompartment structures.

The temperature of the driving gas in the steam accumulator tank was measured using two type-K thermocouples (Channels 91 and 92 in Figure 4) that extended through the accumulator shell and were secured in place using pressure-tight fittings. Measurements from these thermocouples were important because the measured temperature and pressure in the accumulator tank were used to calculate the number of moles of steam driving gas.

Two pyrometers (Channels 37 and 38 in Figures 5, 6, and 7) were used to measure the temperature of the debris as it exited from the instrument tunnel exit. An optical pyrometer (type 11x20, Ircon Inc., Niles, IL) was located inside the biological shield wall and was focused just above the instrument tunnel exit through a fused silica window sealed in the

---

<sup>3</sup> Thomas Blanchat, May 1992, "Aspirated Thermocouple Calculations," Letter Report to the U.S. Nuclear Regulatory Commission, Sandia National Laboratories, Albuquerque, NM.

biological shield wall. Another optical pyrometer (type 11x30, Ircon Inc., Niles, IL) was located outside the crane wall and was focused just above the instrument tunnel exit through a fused silica window sealed in the crane wall. A debris emissivity of 0.9 was assumed when converting the results (in mV) from the optical pyrometers to temperature (in K). A debris emissivity near the blackbody value was assumed because the debris appeared black when inspected posttest. The calculated debris temperature is not very sensitive to the assumed debris emissivity. For example, at approximately 2000 K a 13 percent change in the assumed emissivity resulted in only a 1.9 percent change in the calculated debris temperature.

The optical pyrometers had a response time of 1.5 ms to 95 percent of their full range. A new, low-range, controller was installed on both pyrometers for the IET-4 test. This controller was capable of measuring temperatures between 1323 K and 1773 K with a specified accuracy of 1 percent of the full-scale temperature. In a transient event such as a HPME experiment, the accuracy of the pyrometer measurements was expected to be no better than  $\pm 25$  K. The pyrometers were factory calibrated and the type 11x30 pyrometer is routinely recalibrated by the Sandia Radiant Heat Facility. (Note that since the type 11x20 optical pyrometer is sealed inside the biological shield wall, it cannot be recalibrated.)

A thin-foil graphite calorimeter (Channel 1 in Figures 5 and 6) was embedded in the crane wall directly in the flight path of the debris to measure the debris contact temperature as it impacted the structure. Another thin-foil graphite calorimeter (Channel 4 in figures 5 and 6) was embedded in the seal table room floor, facing the chute exit. Two other thin-foil graphite calorimeters (Channels 2 and 3 in Figures 5 and 6) were embedded in the containment basement floor between the chute exit and the biological shield wall. Each graphite calorimeter consisted of a 1-mm thick graphite disk with a diameter of 25.4 mm. Each graphite disk had a type-S thermocouple attached to the backside of the disk and was set in a ceramic holder that was embedded in the concrete structure. The response time of these graphite calorimeters was on the order of 10 ms.

Data points from the thermocouples and the pyrometers were recorded by the data acquisition system at a rate of 10 per second prior to thermite ignition. Then, just prior to thermite ignition, the data acquisition system was switched to the fast data acquisition mode, in which data points were recorded at a rate of 1400 per second.

### 2.2.3 Gas Composition

Twelve pre-evacuated 500-cm<sup>3</sup> gas grab sample bottles were used to collect samples from the vessel (Labeled L2, L4, L6, and B in Figures 1, 5, 6, 7 and 8) at the following locations and times: three background samples at levels 2, 4, and 6 were obtained by opening solenoid valves remotely for 10 s just prior to ignition of the thermite; three gas grab sample bottles located at levels 2, 4, and 6 were opened remotely for 10 seconds at 2 minutes after the HPME; three gas grab sample bottles at levels 2, 4, and 6 were opened manually for 10 seconds at  $\approx 30$  minutes after the HPME; two gas grab sample bottles inside the subcompartment structures were opened 2 s after the HPME and remained open for 5 s; and one gas grab sample bottle that had its inlet inside the subcompartment structure was opened 2 minutes after the HPME for 10 s. In addition, two gas grab samples were taken from the cavity following the HPME; one was opened as the HPME was initiated and remained open

for 2 s, and the other was opened at 0.5 s following the HPME and remained open for 2 s (Labeled C in Figure 3). The gas samples were analyzed using gas mass spectroscopy by Battelle Pacific Northwest Laboratories in Richland, WA.

Tests were performed to measure the fill times of the 500-cm<sup>3</sup> gas grab sample bottles at three different initial pressures (atmospheric, 0.26 MPa, and 0.43 MPa). An evacuated bottle was separated from a pressure source by a remotely operated solenoid valve. A pressure transducer was installed downstream of the valve and pressure source, and the fill time was recorded by the data acquisition system. Figure 10 shows the results of these tests. The data indicate that all bottles were filled in less than 2 s, regardless of the upstream pressure.

#### **2.2.4 Posttest Debris Recovery**

The total debris mass dispersed into the Surtsey vessel and the debris mass in specific locations were determined by a very careful posttest debris recovery procedure. The following measurements were made: (1) mass of the molten debris in the cavity and inclined portion of the instrument tunnel; (2) mass on the horizontal surfaces outside the subcompartment structures; (3) mass on the vertical surfaces outside the subcompartment structures; (4) mass recovered from the floor inside the structures; (5) mass recovered from the horizontal surfaces other than the floor inside the structures; (6) mass recovered from the vertical surfaces inside the structures; (7) mass recovered from the doorways inside the structures; (8) mass recovered from the seal table room; (9) mass recovered from the rooms adjacent to the seal table room; and (10) mass recovered from the melt generator/crucible.

#### **2.2.5 Debris Velocity**

Breakwires were placed across the opening from the containment basement to the seal table room and at the seal table room exit plug (Channels 16 and 17 in Figures 5 and 6). When the debris front severed the breakwire, a timing signal was recorded by the data acquisition system. The breakwire was intended to give timing information on entry of debris into and out of the seal table room.

### **3.0 EXPERIMENTAL RESULTS**

The experimental results of the IET-4 test are described in this section. The crane wall suffered significant damage in IET-4 that had not occurred in previous experiments [Allen et al. 1992c,d]. A ≈40x80 cm hole was blown out of the crane wall near the top of the seal table room. The area of the crane wall that formed the outside wall of the seal table room was 63 cm<sup>2</sup> and the hole was 21 cm<sup>2</sup>; thus, ≈33% of the outside wall of the seal table room was blown out. The crane wall was also cracked near the walls of the seal table room about 30 cm from the top of the operating deck. It is believed that repeated, direct hits of molten debris from previous experiments may have dehydrated and weakened the concrete in this region. The ramification of this anomaly and the effects on the experimental results are still being studied.

### **3.1 Blowdown History**

Figure 11 shows the blowdown pressure history of the IET-4 experiment. In the experiment, the free volume in the crucible and in the 10-cm diameter pipe above the crucible was purged with nitrogen. The accumulator tank (volume = 0.29 m<sup>3</sup>) was pressurized with superheated steam to ≈6.3 MPa. After the thermite was ignited, the burst diaphragm separating the steam accumulator tank and the molten thermite was failed remotely by the operator; this brought steam into contact with the molten thermite at an experiment time of about -2 s. The steam driving gas pressure for the IET-4 test was determined from the blowdown pressures shown in Figure 11. The horizontal dotted line across Figure 11 shows that the steam driving gas pressure at the initiation of the HPME was 6.7 MPa.

The number of moles of steam driving gas can be calculated using accumulator steam pressure, temperature and volume. In IET-4, the number of moles of steam driving gas was calculated at two times: before burst diaphragm failure (t = -5 s) and at HPME initiation (t = 0 s). At t = -5 s, the steam pressure was 6.35 MPa, the steam temperature was 580 K, and the volume of the accumulator tank was 0.29 m<sup>3</sup>. The steam driving gas was calculated to be 489 g-moles. At t = 0, the steam pressure was 6.7 MPa, the steam temperature was 555 K, and the volume of the accumulator tank plus the piping and void in the crucible was 0.308 m<sup>3</sup>. The steam driving gas was calculated to be 582 g-moles. A small amount of water inside the piping or burst diaphragms must have been introduced at burst diaphragm failure, which vaporized upon contact with the molten thermite. This resulted in a small pressure increase in the accumulator/crucible, shown in Figure 11 at t = -1.5 s.

Figure 11 shows that steam blowdown from the accumulator tank was complete at ≈4 s. The IET-3 experiment had a similar steam blowdown curve. Figure 12 gives the steam temperature history in the accumulator during the blowdown.

In the IET tests, it is more difficult to distinguish single-phase thermite ejection and steam blowthrough from the changes in shape and inflection points in the blowdown curve (Figure 11) than in earlier experiments [Allen et al. 1991, 1992a, 1992b]. The IET tests used a melt generator that was a 1:10 linear scale model of the hemispherical bottom head of a RPV. This geometry produced a more rounded shape in the early portion of the steam blowdown curve compared to the previous tests, which used a relatively long, narrow cylinder as the melt generator. Steam blowthrough occurred earlier in the IET experiments than in previous tests due to the new melt generator design.

### **3.2 Pressure Measurements**

Pressure transducers were used to measure the pressure increase due to the HPME transient in the Surtsey vessel, in the cavity, in the seal table room, and in the subcompartment structures. The following sections describe the results of the pressure measurements.

### 3.2.1 Surtsey Vessel Pressure

Figures 13, 14, and 15 show the absolute pressure in the Surtsey vessel versus time measured at levels 1, 3, and 5, respectively. These figures have a horizontal dotted line across the graph at the initial pressure in Surtsey prior to the HPME transient. The initial absolute pressure was  $\approx 0.20$  MPa as listed in the table of initial conditions (Table 2). These figures also have a horizontal dotted line across the graph at the peak pressure caused by the HPME. These figures show that the pressures measured at levels 1, 3, and 5 in the Surtsey vessel with three different pressure transducers were virtually identical. The pressure increase in the IET-4 experiment was 0.262 MPa, and the peak pressure was reached at  $\approx 2.5$  s after the beginning of the HPME transient.

Figure 16 compares the Surtsey vessel pressure measured in IET-4 to the pressure measured in IET-1 and IET-3 from 0 to 60 s. The peak pressure increase was 0.098 MPa in IET-1, 0.246 MPa in IET-3, and 0.262 MPa in IET-4; and the general shape of the pressurization curves were similar. The peak pressure was reached at  $\approx 2.5$  s in all tests, but the pressure decreased more rapidly after 2.5 s in IET-3 and IET-4. This may be due to the fact that the hydrogen burn was complete after a few seconds. Figure 16 dramatically shows the effect of the hydrogen burn on the vessel pressure in IET-3 and IET-4.

### 3.2.2 Cavity Pressure

The timing of debris ejection from the cavity into the subcompartment structures is important when analyzing a HPME/DCH event. The timing of debris ejection is best understood by comparing the cavity pressure to the Surtsey vessel pressure. Figure 17 shows the cavity pressure and Surtsey vessel pressure versus time for the IET-4 experiment. This figure shows a relatively small peak in the cavity pressure just after the HPME began. This peak was due to gas expansion caused by hot thermite entering the cavity. The large second peak, which started at  $\approx 0.05$  s and had an absolute pressure of  $\approx 0.95$  MPa, had a shock wave associated with it. This was a small steam explosion, as was observed in IET-1 [Allen et al. 1992d]. There is previous evidence [Allen et al. 1992a] that small steam explosions in the reactor cavity have little effect on the HPME/DCH event. The third broad peak, which occurred between  $\approx 0.4$  and  $\approx 0.8$  s, was due to thermite entrainment from the cavity caused by the steam blowdown; thus the debris entrainment interval lasted  $\approx 0.4$  s.

In previous Surtsey experiments with a 3.5 cm exit hole (LFP-1A, LFP-2A, LFP-8A, [Allen et al. 1991] and WC-1 [Allen et al. 1992a]), the debris entrainment interval was  $\approx 1$  s. In IET-1, IET-3 and IET-4 the debris entrainment interval was  $\approx 0.45$  s. Differences in the debris entrainment interval observed in the IET experiments compared to earlier Surtsey tests are probably due to the new melt generator/crucible design. The present design used a 1:10 linear scaled hemispherical bottom head, whereas the melt generator used in previous experiments had a relatively long, narrow cylindrical shape, and the molten thermite was pushed out with a piston-like motion.

Figure 18 is a plot comparing the cavity pressures measured in the IET-1, IET-3, and the IET-4 experiments. In all experiments, a small initial pressure spike was caused by gas expansion due to hot thermite entering the cavity. The second peak in the IET-1 and the

IET-4 curves were clearly due to steam explosions. The second peak in the IET-3 curve was due to rapid vaporization of water, and lagged the IET-1 peak because the vaporization process was slower than a steam explosion. The third peak in all tests was the result of debris entrainment by the steam blowdown.

High speed photography (16 mm color camera at 1000 frames per second) was employed in the IET-4 test. Plexiglas ports (Figure 8) were installed in the top head of the vessel and at level 3 (looking from south to north above the seal table room ceiling plug). The side view camera at Surtsey mid-level provided the best qualitative view of the HPME event. At  $\approx 1$  s, a bright orange plume of fire could be seen rising up and filling the vessel centerline, indicative of a hydrogen burn. This was quickly followed by molten debris particles. Debris velocity was calculated to be  $\approx 14$  m/s at level 3, similar to the 16 m/s calculated from the breakwire array data obtained in the LFP-8A experiment [Allen et al. 1991].

### 3.2.3 Pressure Measured Inside the Seal Table Room

Figure 19 shows the absolute pressure measured inside the seal table room and the pressure measured in Surtsey plotted against time. The seal table room pressure was negative with respect to the Surtsey vessel pressure between  $\approx 0.2$  s and  $>5$  s. This was confirmed by a negative seal table room differential pressure, also shown in Figure 19. This was different than the seal table room pressure behavior measured in IET-3 [Allen et al. 1992c], where the seal table room pressure was equal to the vessel pressure except during the debris entrainment interval from  $\approx 0.4$  to 0.7 s. The large amount of steam produced when the hot thermite hit the water on the containment basement floor effectively cooled the gas within the subcompartment structures. Apparently, hydrogen burned in the upper dome of Surtsey while steaming of water cooled the subcompartment atmosphere, resulting in a negative pressure with respect to the pressure in the Surtsey upper dome.

Figure 20 shows the absolute pressure in the seal table room and Surtsey vessel plotted against an experiment time between 0 and 0.45 s. The first peak in the seal table room pressure was caused by hot thermite entering the cavity. The second larger pressure peak was probably caused by a small steam explosion. The vertical dotted lines in Figure 20 mark the resonance in the Surtsey vessel caused by the steam explosion. The frequency of the resonance was 20 Hz. This phenomenon was also observed in IET-1 [Allen et al. 1992d].

A breakwire was placed across the opening in the seal table room floor to measure the timing of debris ejection into the seal table room. Another breakwire was placed across the operating deck at the opening in the seal table room ceiling. Figure 21 shows the breakwire signals plotted on the same curve with the cavity pressure. Apparently, a steam explosion created a shock wave that caused the breakwires to fail in succession, so no timing information on debris ejection was obtained from these breakwires. The time between failure of the breakwires was  $\approx 0.003$  s, giving a calculated velocity for the shock wave on the order of 300 m/s.

### 3.2.4 Pressure Measured Inside the Subcompartment Structures

Figure 22 shows the absolute pressure measured in the subcompartment structures and in the Surtsey vessel plotted for an experiment time of 0 to 1 s. This figure also shows the differential pressure between the subcompartment structures and the Surtsey vessel upper dome. Figure 22 shows the same phenomenon as in Figure 19, i.e, negative pressure inside the subcompartment structures compared to the vessel pressure. Note that in IET-3 [Allen et al. 1992c], there was never a negative differential pressure between the inside of the subcompartment structures and the upper dome of the Surtsey vessel during the HPME transient.

### 3.3 Gas Temperature Measurements

Figure 23 compares the temperature measurements from the type-K thermocouples installed on the cavity floor, at the chute exit, and at the seal table room floor opening. At 0.1 s, the melt was on the cavity floor. At 0.2 s, the debris was being ejected through the chute exit. This is verified by the increase in temperature at the seal table room at 0.2 s. Note that all three type-K thermocouples were over-ranged at 1530 K.

Figure 24 shows the gas temperatures measured at the Surtsey vessel walls with aspirated thermocouples at levels 1, 3, and 5 during the IET-4 experiment. The gas temperatures measured at level 3 in the Surtsey vessel were substantially higher than the temperatures measured at levels 1 and 5. The higher temperature at level 3 was caused by hydrogen burning as it exited the vent spaces above the RCPs. The peak temperature at level 3 in IET-4 was 1100 K, comparable to 1050 K temperature in IET-3 [Allen et al. 1992c], and both were noticeably higher (and shorter in duration) than the 635 K temperature measured at level 3 during the IET-1 [Allen et al. 1992d] test. A noticeable difference between IET-3 and IET-4 is that temperature at level 1 did not rise. This may be attributed to the steam produced in the subcompartment structures cooling the lower level areas in the vessel, or due to a different flow path for debris/gas due to the crane wall damage.

Since no hydrogen was burned in IET-1 [Allen et al. 1992d], hydrogen combustion clearly caused the greater magnitude and different shape of the IET-3 and IET-4 temperature peak at level 3. The gas temperature at level 5, which is relatively high in the vessel, was barely above the ambient temperature. This is an indication that not much debris was dispersed into the upper dome of the vessel, and that no hydrogen burns occurred at this level. High-speed films of the IET-3 and IET-4 experiments support this explanation.

Figure 25 shows the gas temperature in IET-1, IET-3, and IET-4 experiments measured inside the subcompartment structures with an aspirated thermocouple. This thermocouple was located through the refueling canal wall just above the radial beam at the RCP deck level, and was on the same side of the refueling canal as the instrument tunnel opening into Surtsey (Channels 51, 52, and 53 in figures 5, 6, and 7). All three of the type-K thermocouples in the aspirated thermocouple assembly that sampled gas from inside the subcompartment structures showed identical temperature-versus-time curves. The large, broad peak in Figure 25 corresponds to debris entrainment from the cavity. The gas temperature reached a peak of  $\approx 1120$  K at  $\approx 0.9$  s in IET-4. Although no hydrogen combustion occurred in IET-1, the peak

gas temperatures in the subcompartment structures in IET-1, IET-3, and IET-4 were almost identical. This indicates that the primary mechanism for heating the subcompartment atmosphere may be debris/gas heat transfer, not hydrogen combustion.

Figure 26 compares IET-3 and IET-4 temperature-versus-time curves for the aspirated thermocouple assembly in the seal table room; the aspirated thermocouple at the same location in IET-1 was destroyed and no data were obtained. Figure 26 shows a peak temperature of  $\approx 1200$  K at  $\approx 0.7$  s in IET-4, which corresponds to the end of the debris entrainment interval, at which point the thermocouple was destroyed. The peak temperature probably coincides with the time at which the maximum amount of debris was suspended in the seal table room atmosphere.

Figure 27 shows the measured temperatures in the triangular vent spaces above the 1A and 1D RCPs plotted against time for the IET-3 and IET-4 tests. The 1A RCP vent space was diagonally across the operating deck from the 1D vent space (Channels 66 and 67 in Figure 7). The peak temperature in the 1A vent space was 925 K at  $\approx 1$  s in IET-4, compared to a peak temperature 1370 K at  $\approx 1$  s in IET-3. The temperature in the 1D vent space reached a peak of 780 K at  $\approx 1.1$  s in IET-4, compared to a peak temperature 870 K at  $\approx 1$  s in IET-3. The higher temperatures measured in IET-3 and IET-4 compared to those measured in IET-1 [Allen et al. 1992d] indicate that hydrogen burned as it was pushed out of the vent spaces above the RCPs. The difference in peak temperatures in the 1D vent space for IET-3 and IET-4 can probably be attributed to the steam production in the subcompartment structures and/or the new flow path for hot gas through the hole in the crane wall.

Bulk gas temperatures from the east and west thermocouple arrays used in IET-4 are shown in Figures 28 and 29. These thermocouples measured temperature from about level 3 to halfway between level 5 and level 6. Typically, the bottom thermocouple measured a higher temperature than the top thermocouple. An average bulk temperature is also plotted on Figure 28 and Figure 29. Since it appears that thermocouples 2 and 3 on the west array were destroyed, they were removed from the average at 2.0 s and 4.74 s, respectively.

Figure 30 plots the relative magnitude at the east and west average bulk gas temperature increase against the relative magnitude increase in vessel pressure in IET-4. As expected (assuming an ideal gas), the relative magnitude increase ( $\approx 2.3$ ) in both pressure and temperature are similar.

### **3.4 Debris Temperature Measurements**

Two optical pyrometers were used in IET-4 to measure the temperature of the debris as it exited the instrument tunnel chute. Figures 31 and 32 give the raw pyrometer voltage signals for the type 11x20 and the type 11x30 pyrometers. Note that voltage signals less than 2 mv are below the temperature calibration range; however, these signals are valuable because they give important information about the timing of debris ejection into the scaled containment basement. Figure 31 indicates that luminous debris passed through the focal point of the type 11x20 optical pyrometer between  $\approx 0.2$  and  $\approx 0.9$  seconds. The data from the type 11x30 pyrometer (Figure 32) indicates that luminous debris entered the containment basement between  $\approx 0.4$  and  $\approx 0.9$  seconds.

Figures 33 and 34 give the converted temperature measurements for the pyrometers. Figure 33 shows a peak debris temperature of 1640 K occurring at  $\approx 0.75$  s for the type 11x20 pyrometer. Figure 34 shows a peak debris temperature of 1560 K occurring at  $\approx 0.70$  s for the type 11x30 pyrometer. Note that these temperatures were below peak temperatures of 2000-2300 K determined during the LFP and WC tests [Allen et al. 1991; Allen et al. 1992a,b]. It is suspected that the lower temperatures determined by the optical pyrometers may be caused by the trapping of aerosols in the subcompartment structures, partially obscuring the optical path between the sensing head and the focal point above the chute exit. The flow area for aerosols out of the subcompartment is 15 percent of the flow area around the structure used in the LFP tests, and the flow path is much more tortuous.

The Surtsey vessel pressure started to increase at  $\approx 0.2$  seconds, as soon as the pyrometers indicated that molten debris entered the subcompartment structures. Thus, some molten debris must have entered the subcompartment structures at  $\approx 0.2$  seconds. From the pyrometer data, debris ejection may have ended at 0.9 seconds, or the pyrometer output may have been completely obscured by a dense aerosol cloud rebounding off the cold concrete structures in the containment basement. Note that the cavity pressure curve in Figure 17 indicates that debris ejection ended at  $\approx 0.8$  seconds.

Figure 35 shows the debris contact temperatures for IET-4 at the surface of the concrete structure measured with four thin-foil graphite calorimeters: one embedded in the crane wall just under the seal table room directly in the path of the debris, one in the ceiling directly over the chute exit, and two in the containment basement floor between the instrument tunnel opening and the biological shield wall. Figure 35 shows that the calorimeter in the crane wall measured a peak debris contact temperature of  $\approx 1100$  K at 1.0 s. The calorimeter embedded in the containment basement floor near the instrument tunnel exit reached a peak temperature of 400 K in  $\approx 4$  seconds, as did the calorimeter in the containment basement floor near the biological shield wall. Note that these calorimeters are under a hot (possibly boiling) layer of water. A 0.4 MPa saturation temperature reference line is also shown in Figure 35.

### **3.5 Gas Composition Measurements**

Fourteen gas grab samples were taken from the Surtsey vessel in the IET-4 experiment. The gas concentrations ( $N_2$ ,  $O_2$ ,  $H_2$ ,  $CO$ , and  $CO_2$ ) measured in the gas grab samples are listed in Table 3. A 10 s background sample of the vessel was obtained just prior to ignition. The measured background oxygen concentration was 9.59 mol.%. The results of the six gas samples taken from levels 2, 4, and 6 in the Surtsey vessel at 2 and 30 minutes after the HPME transient are in excellent agreement. The mean oxygen and hydrogen concentrations  $\pm$  standard deviations for these two samples were 7.975 mol.%  $O_2 \pm 0.043$ , and 0.827 mol.%  $H_2 \pm 0.036$ . The total amount of hydrogen generated was  $\approx 297$  g-moles in IET-4. The amount of hydrogen generated was determined from the difference between the posttest hydrogen gas grab sample value and the summation of the pre-existing hydrogen gas grab sample value plus the amount of hydrogen burned. Oxygen depletion calculations indicate that 236 g-moles of hydrogen burned and 61 g-moles of hydrogen remained unreacted.

Two gas grab samples were taken from inside the subcompartment structures. These bottles were opened at 2 s after the initiation of the HPME and were closed 5 s later. These samples

showed hydrogen concentrations of 3.88 and 3.85 mol.% H<sub>2</sub>. This indicates that there were high H<sub>2</sub> concentrations inside the subcompartment structures soon after the HPME. These samples also indicated oxygen concentrations of 7.90 and 8.00 mol.% O<sub>2</sub>. Thus, there was some oxygen depletion inside the subcompartment structures shortly after the beginning of the HPME, either from displacement or hydrogen combustion. The above background concentration of CO and CO<sub>2</sub> was due to the ablation of concrete, the graphite limiter plate, and the burning of paint on structures.

Two gas grab samples were taken from the cavity in the IET-4 experiment. The results of these samples indicate that there were high hydrogen concentrations in the cavity during the HPME transient (23.8 and 35.4 mol.%). The result indicates that the entraining gas in the cavity was a mixture of steam and hydrogen, and is important because many analytical entrainment models require the composition of the entraining gas.

### 3.6 Debris Recovery Summary

The posttest water on the containment basement floor was 1.27 cm deep, compared to an initial depth of 1.52 cm. Evaporation of the water was complete in a few days. Debris in the Surtsey vessel was recovered from four basic locations: (1) from inside the subcompartment structures, (2) from the Surtsey vessel outside the structures, (3) from the cavity and instrument tunnel chute, and (4) from the crucible. Table 4 gives the debris recovery summary of the IET-4 experiment, and compares it to the IET-1 [Allen et al. 1992d] and IET-3 experiments [Allen et al. 1992c]. The total molten mass available for dispersal into the vessel is usually about 20 percent greater than the initial thermite charge due to the melting of the inner wall of the crucible, vaporization of the fusible brass plug, ablation of concrete in the cavity and structures, and oxidation of metallic debris. Table 4 indicates that ≈81 percent of the molten debris that was ejected into the cavity was dispersed into the vessel in IET-4, ≈67 percent in IET-3, and ≈86 percent in IET-1. Total debris dispersed into Surtsey in IET-4 was 40.7 kg, compared to 34.3 kg in IET-3, and 43.0 kg in IET-1. The reason for the difference in debris dispersal may be due to the stochastic nature of debris entrainment from the cavity.

Table 4 also shows the mass balance based on transport fractions. The entries for the transport fractions indicate how they are computed from the mass balance. The transport fractions depend on the mass recovered from the locations specified in Table 4. For example, the mass transported to the upper dome is computed from

$$M_{d,dome} = f_{eject} f_{disp} f_{dome} M_d^0 \quad (1)$$

This method predicts that 5.30 kg of thermite were transported to the upper dome, which is less than the 8.04 kg of material that were actually recovered in the upper dome. The difference represents contaminants and oxygen uptake. The transport fractions are computed based on the assumption that the bulk of contaminants and oxygen uptake occurred in the cavity. This introduces an element of subjectivity into the definition of transport fractions; however, the adopted procedure is recommended because it more closely represents the fraction of thermite dispersed to each location.

The debris plume apparently impacted the crane wall and the concrete ceiling near the seal table. Some of the debris was deflected to the containment basement floor, and some of the debris entered the seal table room. Debris impacting the crane wall inside the seal table room apparently caused it to fail. Some debris was ejected through the hole in the crane wall. Of the 32.6 kg recovered from within the subcompartment structures, 8.0 kg was in the seal table room. The concrete plug in the ceiling of the seal table room (i.e., in the operating deck) was intentionally left out, as it had been in IET-3.

A video taken from a port in the upper head of the Surtsey vessel shows a violent hydrogen burn above the operating deck in the sealed structures. Early in the HPME transient, the video shows a horizontal, bright orange flame jetting violently out of the seal table room door. The video taken from the upper port shows orange flames leaping out of the vent spaces above the reactor coolant pumps and then filling the entire vessel and propagating toward the upper head, but only reaching about the midpoint of Surtsey. Individual, luminous debris particles are evident in IET-4.

Figure 36 shows particle size analysis from debris recovered from the Surtsey vessel outside the subcompartment structures. The particle size analysis discounted all debris with size >9.4 mm. The particle size distribution is not lognormal, and was similar to the results of the IET-3 experiment. The sieve mass median diameter of debris recovered outside the subcompartment structures was 0.52 mm.

### 3.7 Energy Balance

A single-cell equilibrium model was used to perform an energy balance on the IET experiments [Allen et al. 1992c,d], neglecting the presence of water in the cavity. Simple calculations based on the actual IET initial conditions were performed to determine the amount of energy that might be added to the Surtsey vessel atmosphere by the steam blowdown, exothermic steam/metal chemical reactions, debris/gas heat transfer, and hydrogen combustion. The total amount of energy was used to calculate an upper limit to the possible pressure increase in the Surtsey vessel,  $\Delta P_{\text{equilibrium}}$ . The result could then be compared to the measured peak pressure increase,  $\Delta P_{\text{measured}}$ , to determine the total DCH efficiency,  $\eta = \Delta P_{\text{measured}} / \Delta P_{\text{equilibrium}}$ , in the IET experiments [Allen et al. 1992c,d].

The presence of water in the cavity during the IET experiments provided a potential heat sink in the system, since some portion of the thermal and chemical energy in the debris would be used to vaporize the water. In the WC-2 experiment [Allen et al. 1991a], the results indicated that less than 15 percent of the water initially present in the cavity was vaporized, despite the fact that the thermite in that experiment contained approximately five times the amount of energy necessary to vaporize all of the water that was present. This result suggests that water was ineffective as a heat sink. Furthermore, the HIPS tests with water in the cavity [Tarbell et al. 1991] suggest that the bulk of the water was ejected prior to debris dispersal. In the IET experiments [Allen et al. 1992c,d], the thermite contained approximately 17 times the amount of energy necessary to vaporize all of the water that was present in the cavity. The actual amount of water that was vaporized in the IET experiments cannot be determined from the experimental results, but there was probably very little water vaporized in the cavity.

Derivation of the single-cell model has been documented by Pilch [1991]. The resulting model is given here. Thermal equilibrium between airborne debris and the containment atmosphere yields a simple, bounding expression for the DCH load,

$$\frac{\Delta U}{U^o} = \frac{\Delta P}{P^o} = \frac{\sum_i \Delta E_i}{U^o(1 + \psi)} \quad (2)$$

where

- $\Delta U$  = total internal energy gained by the containment atmosphere,
- $U^o$  = initial internal energy of the entire containment atmosphere,
- $\Delta P$  = pressure rise in the containment resulting from the DCH event,
- $P^o$  = initial containment pressure,
- $\Delta E_i$  = maximum energy that could be added to the containment atmosphere by the  $i^{\text{th}}$  process, where the  $i$  processes are steam blowdown, debris/gas heat transfer, debris oxidation by steam in an otherwise inert atmosphere, and hydrogen combustion, and
- $\psi$  = heat capacity ratio.

The heat capacity ratio appears because the debris still carries sensible heat that is not available for containment pressurization at thermal equilibrium between airborne debris and the atmosphere. The heat capacity ratio is defined by

$$\psi = \frac{N_d C_d}{(N^o + N_b) C_v} \quad (3)$$

where

- $N_d$  = number of g-moles of debris participating in DCH,
- $C_d$  = molar heat capacity of debris,
- $N^o$  = number of gas g-moles initially in the containment,
- $N_b$  = number of gas g-moles added to the containment by RCS blowdown, and
- $C_v$  = molar heat capacity of the containment atmosphere.

The g-moles of debris participating in DCH can be expressed in terms of the initial charge of thermite by

$$N_d = f_{eject} f_{disp} \frac{M_d^o}{MW_d} \quad (4)$$

where

- $f_{\text{eject}}$  = fraction of the initial charge that is ejected from the melt generator to the cavity,
- $f_{\text{disp}}$  = fraction of the melt ejected into the cavity that is subsequently dispersed into the containment,
- $M_d^{\circ}$  = initial (mass) charge of thermite, and
- $MW_d$  = the effective molecular weight of thermite, 0.0631 kg/g-mole.

Table 4 lists all the information necessary to complete this calculation.

Blowdown of the steam accumulator adds both mass and energy to the containment atmosphere. The maximum amount of energy that the accumulator can contribute to Surtsey pressurization is given by

$$\Delta E_b = \frac{P_{acc}^{\circ} V_{acc}}{\gamma - 1} \left( 1 - \frac{P^{\circ}}{P_{acc}^{\circ}} \right) , \quad (5)$$

where

- $P_{acc}^{\circ}$  = equilibrium pressure of the accumulator/melt generator system just prior to plug failure,
- $V_{acc}$  = total free volume of the accumulator and melt generator, and
- $\gamma$  = ratio of specific heats.

The term preceding the brackets represents the total internal energy of the accumulator, while the bracketed term represents the fraction of this total that is convected into the containment.

Molten debris dispersed from the reactor cavity carries both latent and sensible heat that can be transferred to the atmosphere. The maximum energy source associated with debris thermal energy,

$$\Delta E_t = N_d \Delta e_t , \quad (6)$$

is equal to the amount of dispersed debris,  $N_d$ , times the specific molar internal energy of the debris,  $\Delta e_t$ , which has a value of 0.147 MJ/g-mole for thermite.

The energy source due to debris oxidation,

$$\Delta E_r = N_d \Delta e_r , \quad (7)$$

is equal to the amount of debris participating in DCH times the specific molar oxidation energy of the debris. Assuming all the metals react with steam, the specific molar oxidation energy,  $\Delta e_r$ , has a value of 0.054 MJ/g-mole for thermite.

The energy source due to hydrogen combustion is

$$\Delta E_{H_2} = N_{H_2, tot} \Delta e_{H_2} = (N_{H_2, pre} + U_{H_2} N_d) \Delta e_{H_2} \quad (8)$$

where

$N_{H_2, pre}$	=	g·moles of pre-existing hydrogen in the containment atmosphere prior to the DCH event,
$U_{H_2}$	=	the effective stoichiometric coefficient for debris oxidation, 0.892 g·moles- $H_2$ /g·mole-debris, and
$\Delta e_{H_2}$	=	the specific combustion energy for hydrogen, 0.242 MJ/g·mole- $H_2$ .

The second term in the brackets,  $U_{H_2} N_d$ , represents the totals of g·moles of hydrogen that can be produced from complete oxidation of the metallic constituents of the dispersed debris. There is sufficient steam in the accumulator and water in the cavity or on the basement floor to achieve complete oxidation of debris.

The initial internal energy of the atmosphere is computed from

$$U^o = N^o C_v T^o \quad (9)$$

where

$T^o$  = initial temperature of the Surtsey atmosphere.

Table 5 summarizes the energy balance for IET-1, IET-3, and IET-4. The thermal (latent and sensible heats) and chemical energy (debris oxidation) are computed for the dispersed thermite mass only. For IET-1, the calculated pressure rise at equilibrium is 0.384 MPa compared to a measured pressure of 0.098 MPa; thus the DCH efficiency for IET-1 is 26 percent. For IET-3, the calculated pressure rise at equilibrium is 0.608 MPa compared to a measured pressure of 0.246 MPa. The DCH efficiency for IET-3 is 40 percent. The calculated pressure rise at equilibrium for IET-4 is 0.704 MPa compared to a measured pressure rise of 0.262 MPa. The DCH efficiency for IET-4 was 37.2 percent. The efficient combustion for hydrogen ( $\approx 80$  percent) produced during the DCH event in IET-3 and IET-4 resulted in a pressure rise that more than doubled the pressure rise observed in IET-1. This large contribution due to efficient hydrogen combustion is reflected in the substantially larger overall efficiencies reported for IET-3 and IET-4.

#### 4.0 SUMMARY

A comparison of the IET-1, IET-3, and IET-4 experiments gave a quantitative measurement of the incremental increase in peak pressure in the Surtsey vessel due to combustion of hydrogen produced by the steam-driven HPME. Pressure and temperature measurements showed that a vigorous hydrogen burn occurred as gas was pushed out of the subcompartment structures. IET-3 gave the first experimental evidence that DCH conditions can result in almost complete combustion of hydrogen. IET-4 confirmed this evidence.

An unusual phenomenon was seen in IET-4. This was the negative pressures (relative to vessel pressure) measured in the subcompartment structures, and also in the seal table room. This effect may be attributed to the water on the basement floor inside the crane wall. Overall, water on the basement floor inside the crane wall appeared to have little effect on the Surtsey vessel peak pressure. The additional hydrogen burned in IET-4 (236 g-moles) compared to IET-3 ( $\approx 186$  g-moles) and the additional debris dispersed outside the subcompartment structures in IET-4 (8 kg) compared to IET-3 (3 kg) were apparently at least partially compensated for by quenching of debris by water on the containment basement floor.

Table 6 summarizes the comparative results of the IET-1, IET-3, and IET-4 experiments.

Table 1

**IET-4 Instrumentation Location and Purpose**

<b>Channel Number</b>	<b>Instrument</b>	<b>Location</b>	<b>Purpose</b>
1	Disk Calorimeter*	In Crane Wall	Measure Debris Contact Temperature
2	Disk Calorimeter*	On Vessel Floor Next to Chute	Measure Debris Contact Temperature
3	Disk Calorimeter*	On Vessel Floor Next to Shield	Measure Debris Contact Temperature
4	Disk Calorimeter*	In Ceiling over Chute	Measure Debris Contact Temperature
7	Thermocouple	Chute Exit	Measure Temperature Inside Subcompartment Structures
8	Thermocouple	Seal Table Room Floor	Measure Temperature Inside Subcompartment Structures
16	Breakwire	Seal Table Room Plug	Measure Debris Velocity
17	Breakwire	On Seal Table Room Floor	Measure Debris Velocity
18	Photodiode	Photodiode	Signal Initiation of HPME
19	Pressure Transducer	Refueling Canal Wall	Measure Gas Pressure Inside Subcompartment Structures
20	Pressure Transducer	Seal Table Room	Measure Gas Pressure Inside Seal Table Room
21	Pressure Transducer	Level 1	Measure Gas Pressure in Surtsey Vessel
22	Pressure Transducer	Level 1	Measure Gas Pressure in Surtsey Vessel
23	Pressure Transducer	Level 3	Measure Gas Pressure in Surtsey Vessel

<b>Channel Number</b>	<b>Instrument</b>	<b>Location</b>	<b>Purpose</b>
24	Pressure Transducer	Level 3	Measure Gas Pressure in Surtsey Vessel
25	Pressure Transducer	Level 5	Measure Gas Pressure in Surtsey Vessel
26	Pressure Transducer	Level 5	Measure Gas Pressure in Surtsey Vessel
32	Pressure Transducer	Accumulator	Measure Gas Pressure in Accumulator Tank
33	Pressure Transducer	Burst Diaphragm	Measure Gas Pressure
34	Pressure Transducer	Crucible	Measure Gas Pressure
35	Pressure Transducer	Crucible	Measure Gas Pressure
36	Pressure Transducer	Cavity	Measure Gas Pressure in the Cavity
37	Optical Pyrometer Type 11x20	Inside Biological Shield Wall - Focused Above Instrument Tunnel Exit	Measure Debris Temperature as it Entered Subcompartment Structures
38	Optical Pyrometer Type 11x30	Outside Crane Wall - Focused Above Instrument Tunnel Exit	Measure Debris Temperature as it Entered Subcompartment Structures
39	Pressure Transducer	Refueling Canal	Measure Gas Pressure Inside Subcompartment Structures
40	Pressure Transducer	Seal Table Room	Measure Gas Pressure Inside Seal Table Room
41	Aspirated Thermocouple	Level 3	Measure Gas Temperature at Surtsey Vessel Walls
42	Aspirated Thermocouple	Level 3	Measure Gas Temperature at Surtsey Vessel Walls

<b>Channel Number</b>	<b>Instrument</b>	<b>Location</b>	<b>Purpose</b>
43	Aspirated Thermocouple	Level 1	Measure Gas Temperature at Surtsey Vessel Walls
44	Aspirated Thermocouple	Level 1	Measure Gas Temperature at Surtsey Vessel Walls
45	Aspirated Thermocouple	Level 1	Measure Gas Temperature at Surtsey Vessel Walls
46	Aspirated Thermocouple	Level 5	Measure Gas Temperature at Surtsey Vessel Walls
47	Aspirated Thermocouple	Level 5	Measure Gas Temperature at Surtsey Vessel Walls
48	Aspirated Thermocouple	Level 5	Measure Gas Temperature at Surtsey Vessel Walls
49	Aspirated Thermocouple	Level 3	Measure Gas Temperature at Surtsey Vessel Walls
50	Ignitor	Crucible	Timing Signal for Thermite Ignition
51	Aspirated Thermocouple	Refueling Canal Wall	Measure Gas Temperature Inside Subcompartment Structures
52	Aspirated Thermocouple	Refueling Canal Wall	Measure Gas Temperature Inside Subcompartment Structures
53	Aspirated Thermocouple	Refueling Canal Wall	Measure Gas Temperature Inside Subcompartment Structures
54	Aspirated Thermocouple	Seal Table Room	Measure Gas Temperature Inside Seal Table Room

<b>Channel Number</b>	<b>Instrument</b>	<b>Location</b>	<b>Purpose</b>
55	Aspirated Thermocouple	Seal Table Room	Measure Gas Temperature Inside Seal Table Room
56	Aspirated Thermocouple	Seal Table Room	Measure Gas Temperature Inside Seal Table Room
57	Thermocouple	Cavity Floor	Measure Gas Temperature Inside Cavity
58	Thermocouple	Crucible	Measure Gas Temperature Inside Crucible
59	Pressure Transducer	Coolant Pump 1A	Measure Pressure Caused by Heating RCP 1A
62	Pressure Transducer	Coolant Pump 1B	Measure Pressure Caused by Heating RCP 1B
63	Pressure Transducer	Coolant Pump 1C	Measure Pressure Caused by Heating RCP 1C
64	Pressure Transducer	Coolant Pump 1D	Measure Pressure Caused by Heating RCP 1D
65	Pressure Transducer	Lower Head	Measure Pressure Under Containment Basement Floor
66	Thermocouple	Vent Space 1A	Measure Gas Temperature Above RCP 1A
67	Thermocouple	Vent Space 1D	Measure Gas Temperature Above RCP 1D
68	East Thermocouple Array	Bottom	Measure Local Gas Temperature
69	East Thermocouple Array	Bottom/Middle	Measure Local Gas Temperature

<b>Channel Number</b>	<b>Instrument</b>	<b>Location</b>	<b>Purpose</b>
70	East Thermocouple Array	Middle	Measure Local Gas Temperature
71	East Thermocouple Array	Middle/Top	Measure Local Gas Temperature
72	East Thermocouple Array	Top	Measure Local Gas Temperature
73	West Thermocouple Array	Bottom	Measure Local Gas Temperature
74	West Thermocouple Array	Bottom/Middle	Measure Local Gas Temperature
75	West Thermocouple Array	Middle	Measure Local Gas Temperature
76	West Thermocouple Array	Middle/Top	Measure Local Gas Temperature
77	West Thermocouple Array	Top	Measure Local Gas Temperature
80	Pressure Transducer	Level 5	Measure Gas Pressure in Surtsey Upper Dome
81	Thermocouple	Accumulator	Measure Gas Temperature 0.32 cm From Inner Wall
82	Thermocouple	Accumulator	Measure Gas Temperature 0.32 cm From Inner Wall
83	Thermocouple	Accumulator	Measure Gas Temperature 0.32 cm From Inner Wall

<b>Channel Number</b>	<b>Instrument</b>	<b>Location</b>	<b>Purpose</b>
84	Thermocouple	Accumulator	Measure Gas Temperature 0.32 cm From Inner Wall
85	Thermocouple	Accumulator	Measure Gas Temperature 0.32 cm From Inner Wall
86	Thermocouple	Accumulator	Measure Gas Temperature 0.32 cm From Inner Wall
87	Thermocouple	Accumulator	Measure Flange Outside Surface Temperature
88	Thermocouple	Accumulator	Measure Accumulator Outside Surface Temperature
90	Thermocouple	Accumulator	Measure Accumulator Outside Surface Temperature
91	Thermocouple	Accumulator	Measure Gas Temperature Inside Accumulator Tank
92	Thermocouple	Accumulator	Measure Gas Temperature Inside Accumulator Tank
93	Thermocouple	10.2-cm Pipe between Accumulator and Melt Generator	Measure Gas Temperature Inside Pipe with Burst Diaphragm
103	Thermocouple	10.2 cm Pipe Elbow Between Melt Generator and Crucible	Measure Skin Temperature
P1	Piezoelectric Pressure Transducer	East Side of Cavity	Measure Pressure in Cavity Wall Under the Melt Generator

<b>Channel Number</b>	<b>Instrument</b>	<b>Location</b>	<b>Purpose</b>
P2	Piezoelectric Pressure Transducer	West Side of Cavity	Measure Pressure in Cavity Wall Under the Melt Generator
P3	Piezoelectric Pressure Transducer	Crane Wall	Measure Gas Pressure Inside Subcompartment Structures
P4	Piezoelectric Pressure Transducer	Refueling Canal	Measure Gas Pressure Inside Subcompartment Structures
L2	Gas Grab Sample	Surtsey Level 2	Measure Gas Composition Prior to and After HPME
L4	Gas Grab Sample	Surtsey Level 4	Measure Gas Composition Prior to and After HPME
L6	Gas Grab Sample	Surtsey Level 6	Measure Gas Composition Prior to and After HPME
C	Gas Grab Sample	Cavity	Measure Gas Composition Prior to and After HPME
B	Gas Grab Sample	Subcompartment Structure	Measure Gas Composition Prior to and After HPME

\* Disk Calorimeters Used Type S Thermocouples  
Other Thermocouples Were Type K

Table 2

## Initial Conditions for the IET-1, IET-3 and IET-4 Experiments

		IET-1	IET-3	IET-4
Thermite composition (kg)				
	iron oxide	29.26	29.26	29.26
	chromium	4.65	4.65	4.65
	aluminum	<u>9.09</u>	<u>9.09</u>	<u>9.09</u>
Mass of the initial thermite charge (kg)		43.00	43.00	43.00
Hole diameter (cm)				
	initial	3.5	3.5	3.5
	final	4.09	4.53	4.22
Steam pressure at plug failure (MPa)		7.1	6.1	6.7
Steam temperature at plug failure (K)		600	585	555
Moles of steam driving gas (g-moles)		440	456	582
Cavity water (kg)		3.48 (0.9 cm deep)	3.48 (0.9 cm deep)	3.48 (0.9 cm deep)
Water on containment basement floor inside crane wall (kg)		0	0	71.1 (1.52 cm deep)
Initial absolute pressure in Surtsey (MPa)		0.20	0.19	0.20
Initial temperature in Surtsey (K)		295	279	286
Initial gas composition in Surtsey (mol.%)	N <sub>2</sub>	99.96	90.6	90.0
	O <sub>2</sub>	0.03	9.0	9.59
	Other	0.01	0.4	0.41
Freeboard volume inside subcompartment structures		4.65 m <sup>3</sup>		
Freeboard volume in Surtsey upper dome		<u>85.15 m<sup>3</sup></u>		
Total freeboard volume inside Surtsey		89.8 m <sup>3</sup>		

Table 3

## Gas Concentrations Measured in the IET-4 Experiment

Location	Start Time → Duration	Species (mol.%)				
		N <sub>2</sub>	O <sub>2</sub>	H <sub>2</sub>	CO	CO <sub>2</sub>
Background	-20 s → 10 s	90.0	9.59	<0.01	<0.1	0.02
Cavity	0.0 s → 2 s	63.4	9.22	28.8	1.80	0.65
Cavity	0.5 s → 2 s	46.9	10.40	35.4	15.30	0.70
Inside Structures	2 s → 5 s	86.0	7.90	3.88	1.40	0.34
	2 s → 5 s	85.4	8.00	3.85	0.90	0.32
	2 min → 10 s	88.9	8.07	1.02	0.31	0.42
Level 2	2 min → 10 s	89.9	7.98	0.82	0.50	0.32
	30 min → 10 s	90.5	7.90	0.86	<0.10	0.32
Level 4	2 min → 10 s	90.4	8.03	0.79	<0.1	0.32
	30 min → 10 s	89.6	7.99	0.85	0.8	0.32
Level 6	2 min → 10 s	90.5	7.96	0.78	<0.1	0.32
	30 min → 10 s	90.4	7.96	0.86	<0.1	0.32
Mean <sup>§</sup>			7.975	0.827		
Standard Deviation <sup>§</sup>			0.043	0.036		

Notes:

§ Mean and standard deviations were computed for the six samples taken after the HPME at levels 2, 4, and 6 in the Surtsey vessel.

Table 4

**Debris Recovery Summary for the IET-1, IET-3 and IET-4 Experiments**

<b>MASS BALANCE (kg)</b>	<b>IET-1</b>	<b>IET-3</b>	<b>IET-4</b>
Initial Thermite Charge, $M_d^0$ (a)	43.0	43.0	43.0
Crucible (b)	4.54	4.50	9.76
Cavity/Chute (c)	7.06	16.80	9.54
Inside Structures (d)	38.03	31.30	32.67
Outside Structures (e)	4.98	3.00	8.04
Total Recovered*	43.01	34.30	40.72
<b>TRANSPORT FRACTIONS</b>			
Ejected into Cavity, $f_{\text{eject}} = 1 - b/a$	0.894	0.895	0.773
Dispersed from Cavity, $f_{\text{disp}} = (d + e)/(c + d + e)$	0.859	0.671	0.810
Transported Outside Subcompartment, $f_{\text{dome}} = e/(d + e)$	0.116	0.087	0.197

Notes: 1. The molten mass available for dispersal into the vessel is usually about 20% greater than the initial iron oxide/aluminum/chromium thermite charge due to melting of the inner wall of the crucible, vaporization of the fusible brass plug, ablation of concrete in the cavity, and oxidation of metallic debris by steam.

Table 5

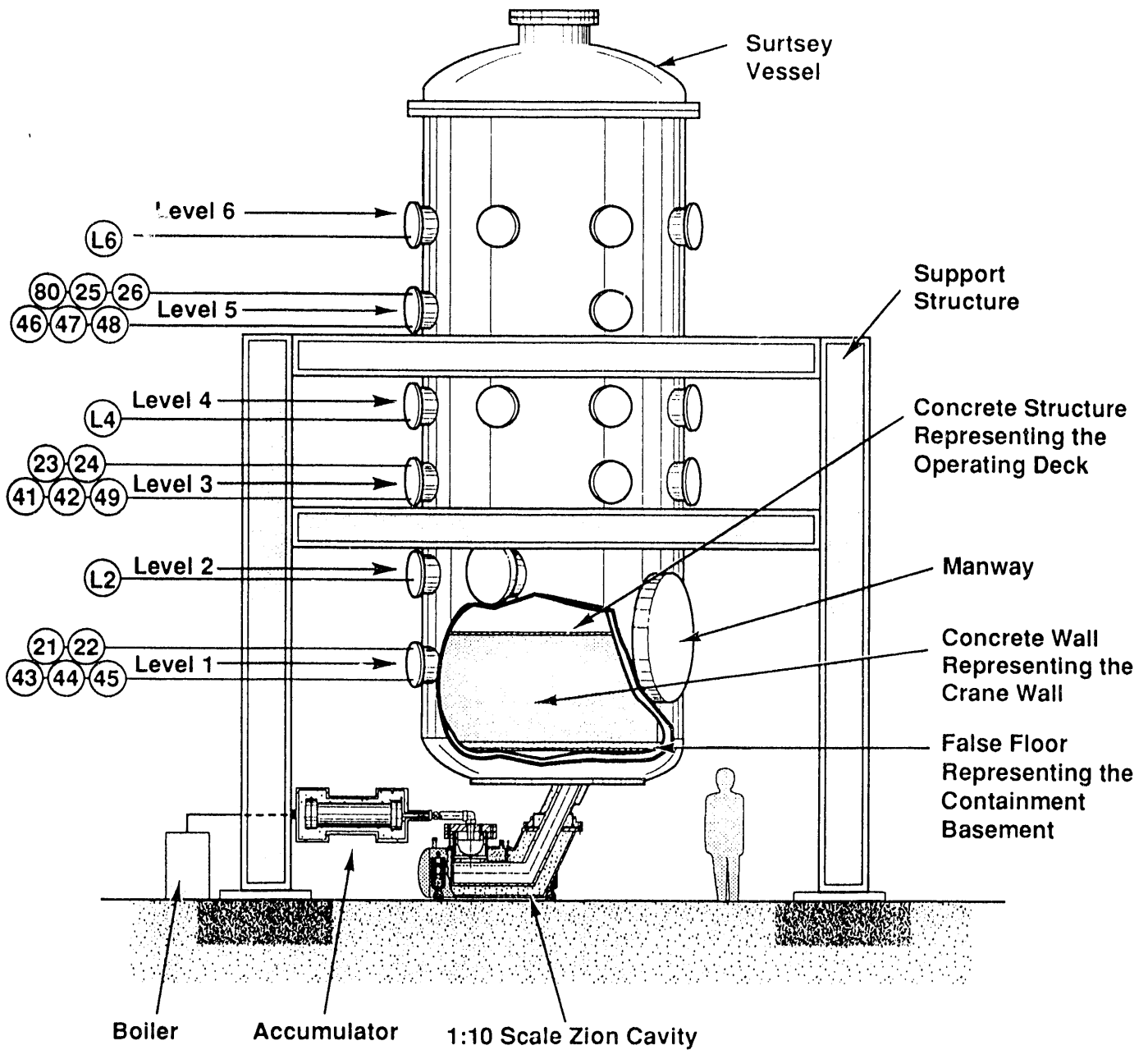
## Energy Balance for the IET-1, IET-3 and IET-4 Experiments

Term	IET-1 Value	IET-3 Value	IET-4 Value	Description
$\Delta E_b$	5.45 MJ	5.29 MJ	5.71 MJ	Blowdown energy
$\Delta E_t$	83.7 MJ	58.2 MJ	60.4 MJ	Latent and sensible heat
$\Delta E_r$	31.9 MJ	23.2 MJ	24.1 MJ	Chemical energy from debris oxidation
$\Delta E_{H_2}$	0.0 MJ	97.7 MJ	122.0 MJ	Hydrogen combustion
$\psi$	0.219	0.156	0.152	Heat capacity ratio
$U^\circ$	51.7 MJ	49.8 MJ	52.4 MJ	Internal energy of atmosphere
$P^\circ$	0.20 MPa	0.19 MPa	0.20 MPa	Initial pressure of atmosphere
$\Delta P$	0.384 MPa	0.608 MPa	0.704 MPa	Calculated pressure rise
$\eta$	26%	40%	37.2%	DCH efficiency

Table 6

## Summary of the Results of the IET-1, IET-3, and IET-4 Experiments

	IET-1	IET-3	IET-4
Driving pressure at plug failure (MPa)	7.1	6.1	6.7
Moles of H <sub>2</sub> O driving gas (g-moles)	440	456	583
Cavity water (g-moles)	193	193	193
Ablated hole diameter (cm)	4.04	4.53	4.22
Total debris dispersed into Surtsey (kg)	43.0	34.3	40.7
$\Delta P$ due to the HPME (MPa)	0.098	0.246	0.262
Moles of H <sub>2</sub> produced (g-moles)	223	223	297
Moles of H <sub>2</sub> burned (g-moles)	≈0	186	236



Note: All pressure transducers have individual penetrations.

Figure 1. Surtsey vessel, high-pressure melt ejection system, and subcompartment structures used in the IET-4 experiment. The figure also shows instrumentation location by channel number.

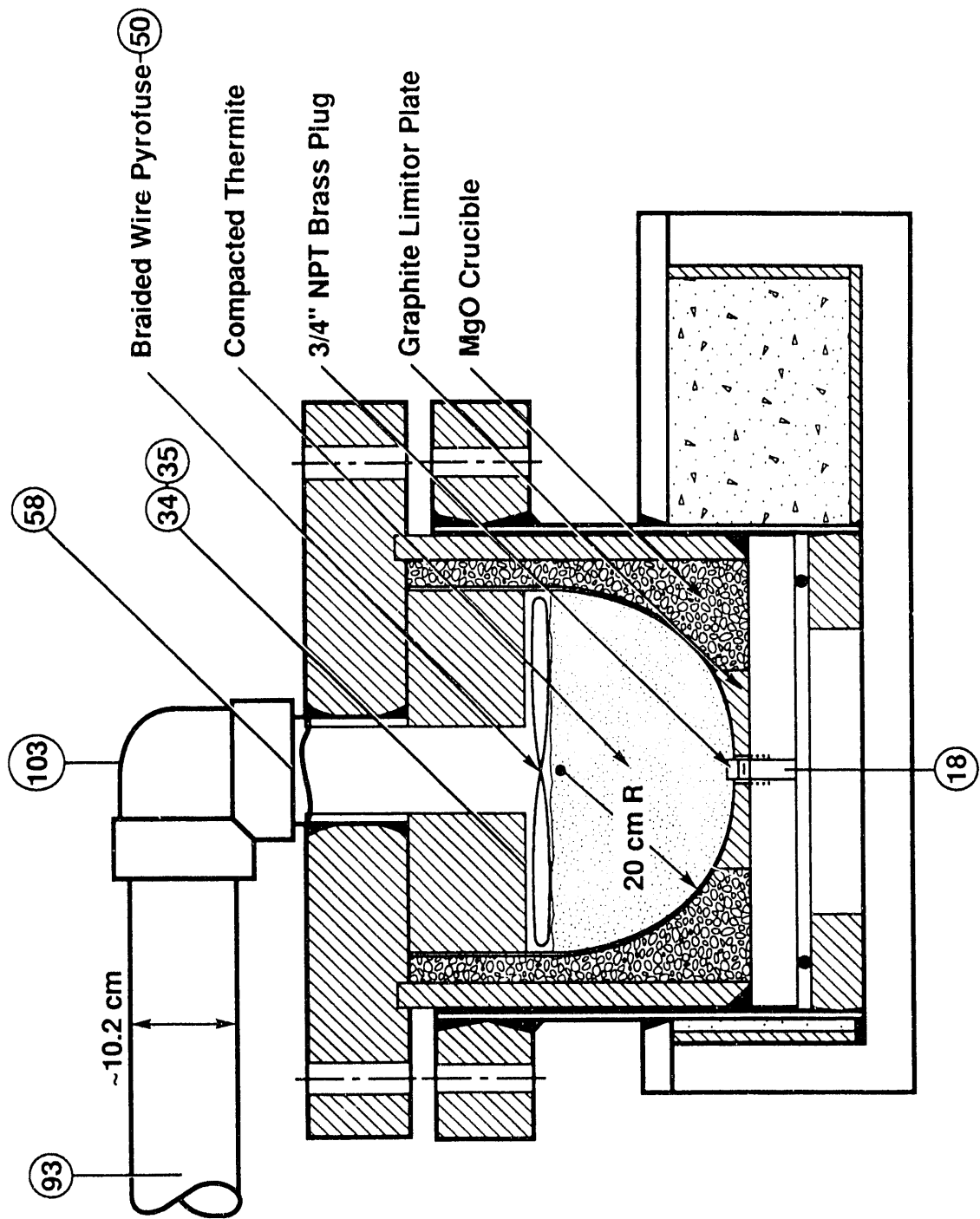


Figure 2. Melt generator and MgO crucible used in the IET-4 experiment. The figure also shows instrumentation location by channel number.

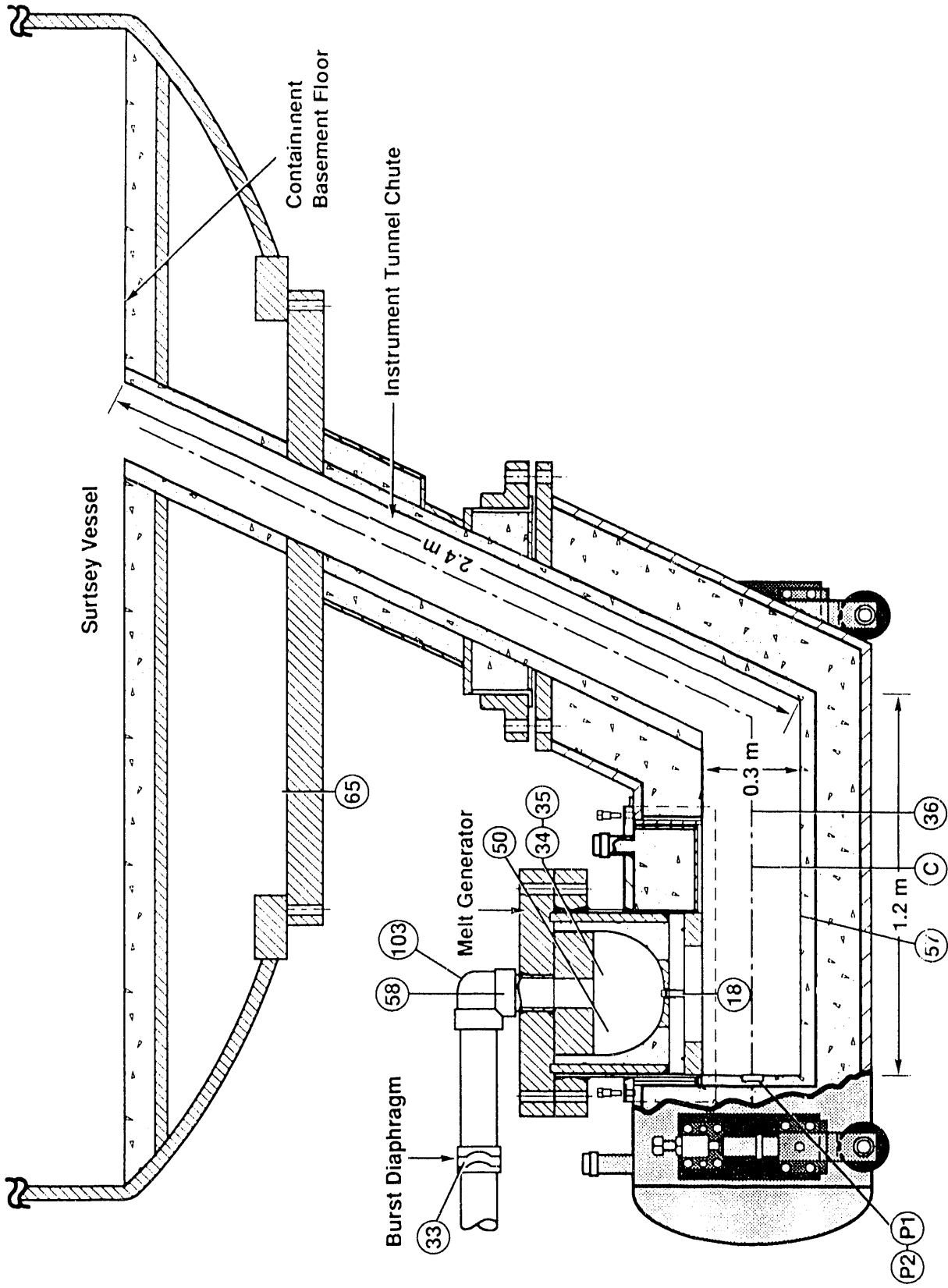


Figure 3. Schematic of 1:10 linear scale model of the Zion reactor cavity. The figure also shows instrumentation location by channel number.

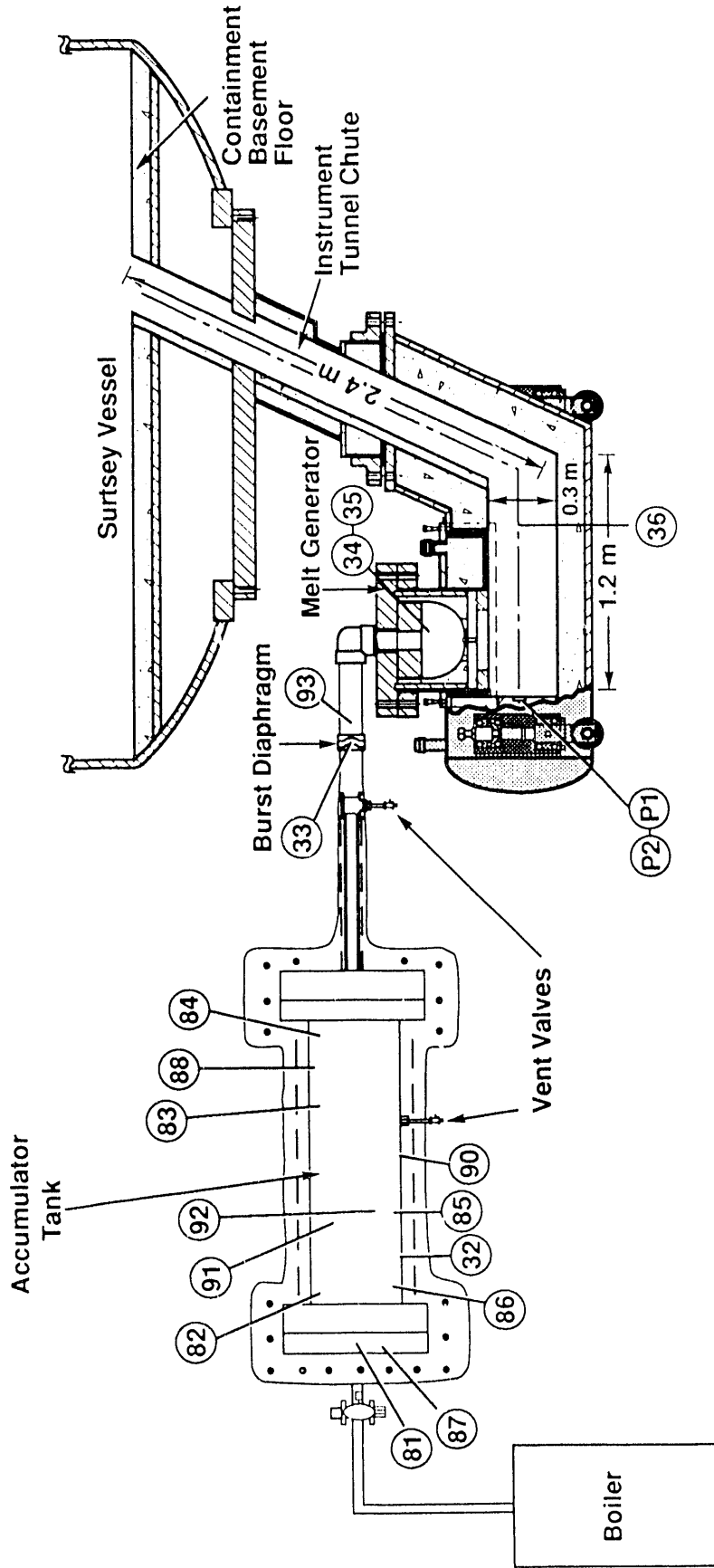


Figure 4. High-pressure steam boiler, steam accumulator, melt generator, cavity, and Surtsey vessel layout. The figure also shows instrumentation location by channel number.

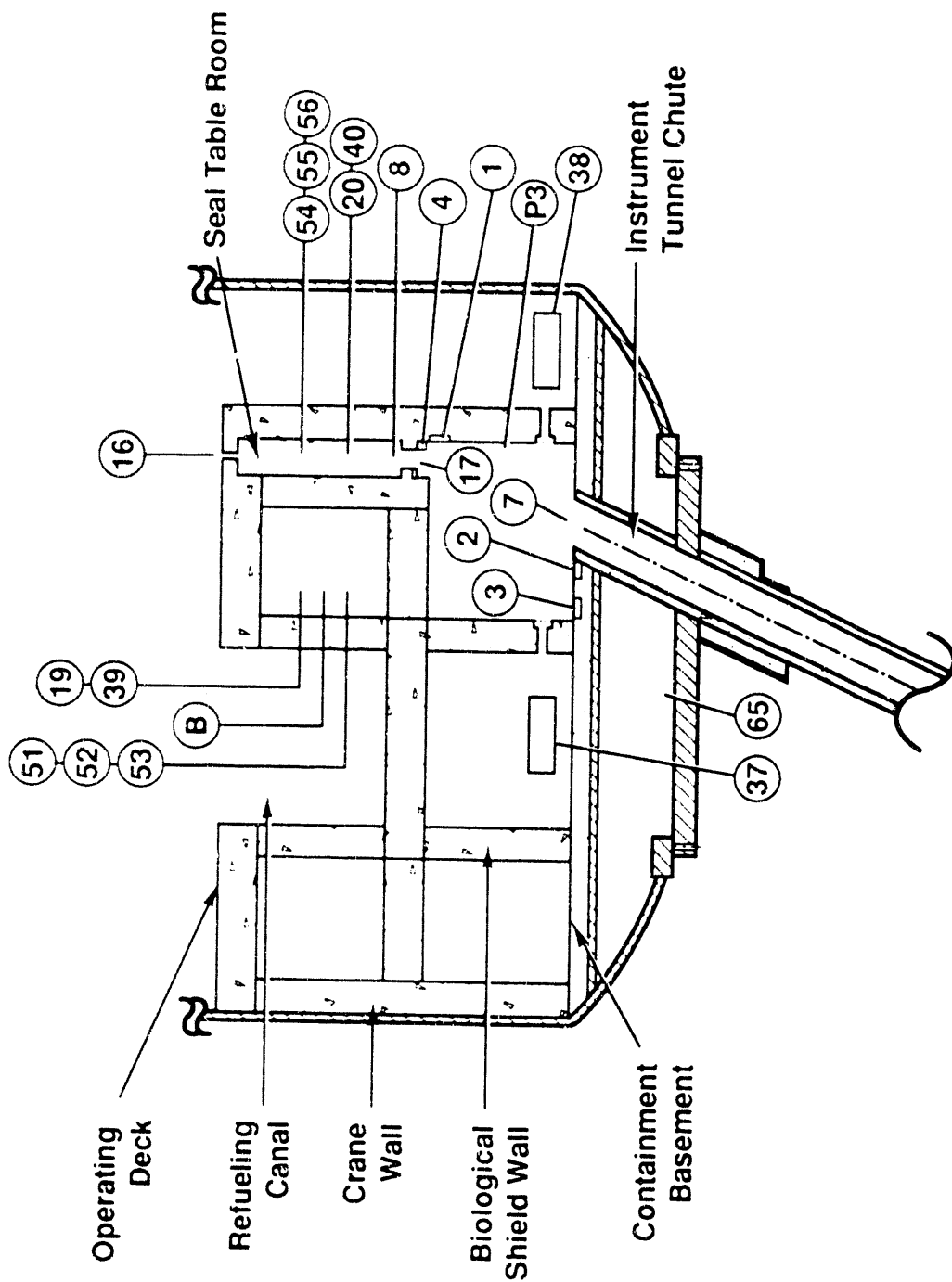


Figure 5. Two-dimensional view of the subcompartment structures inside the Surtsey vessel. The figure also shows instrumentation location by channel number.

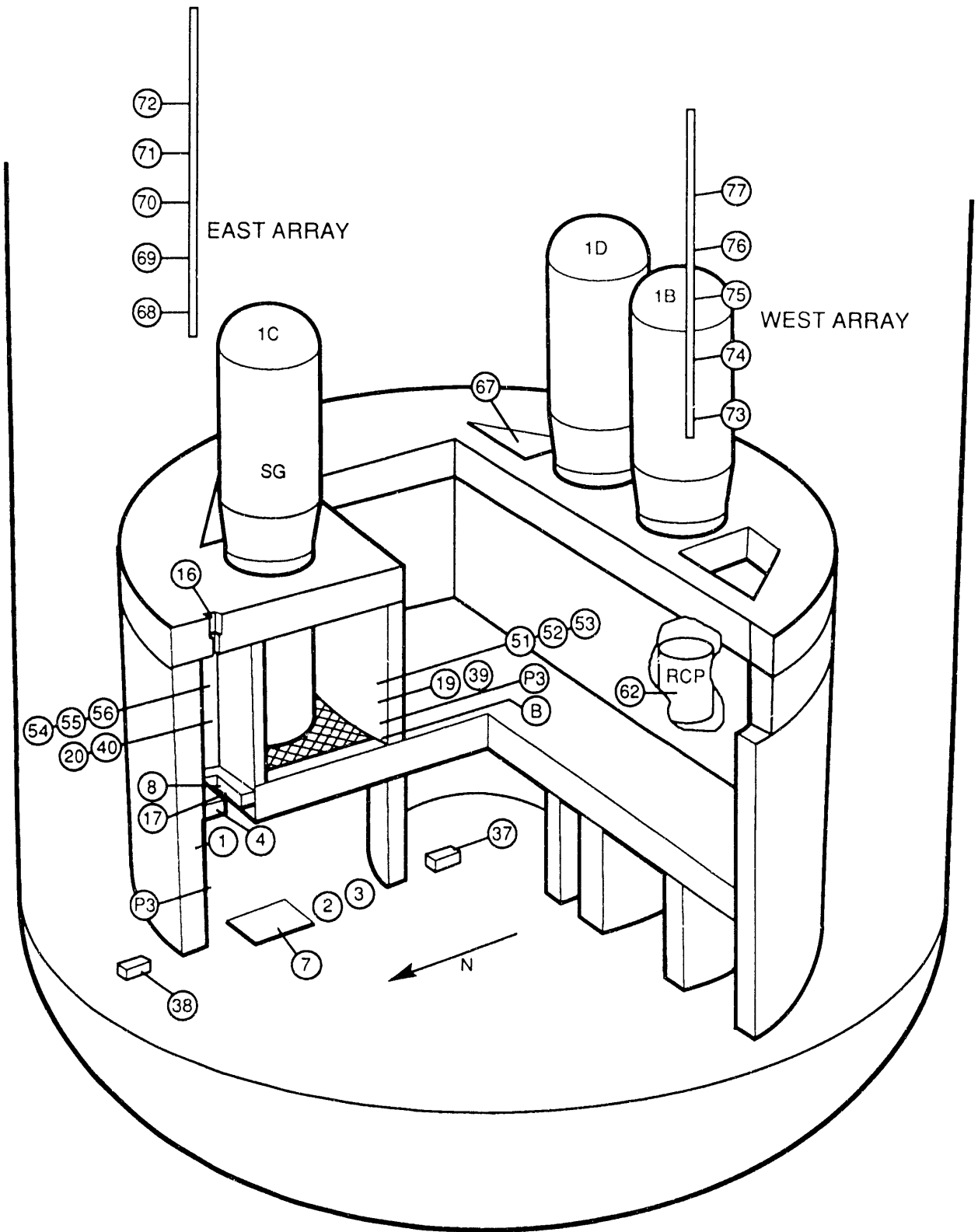


Figure 6. Isometric view of the subcompartment structures inside the Surtsey vessel. The figure also shows instrumentation location by channel number.

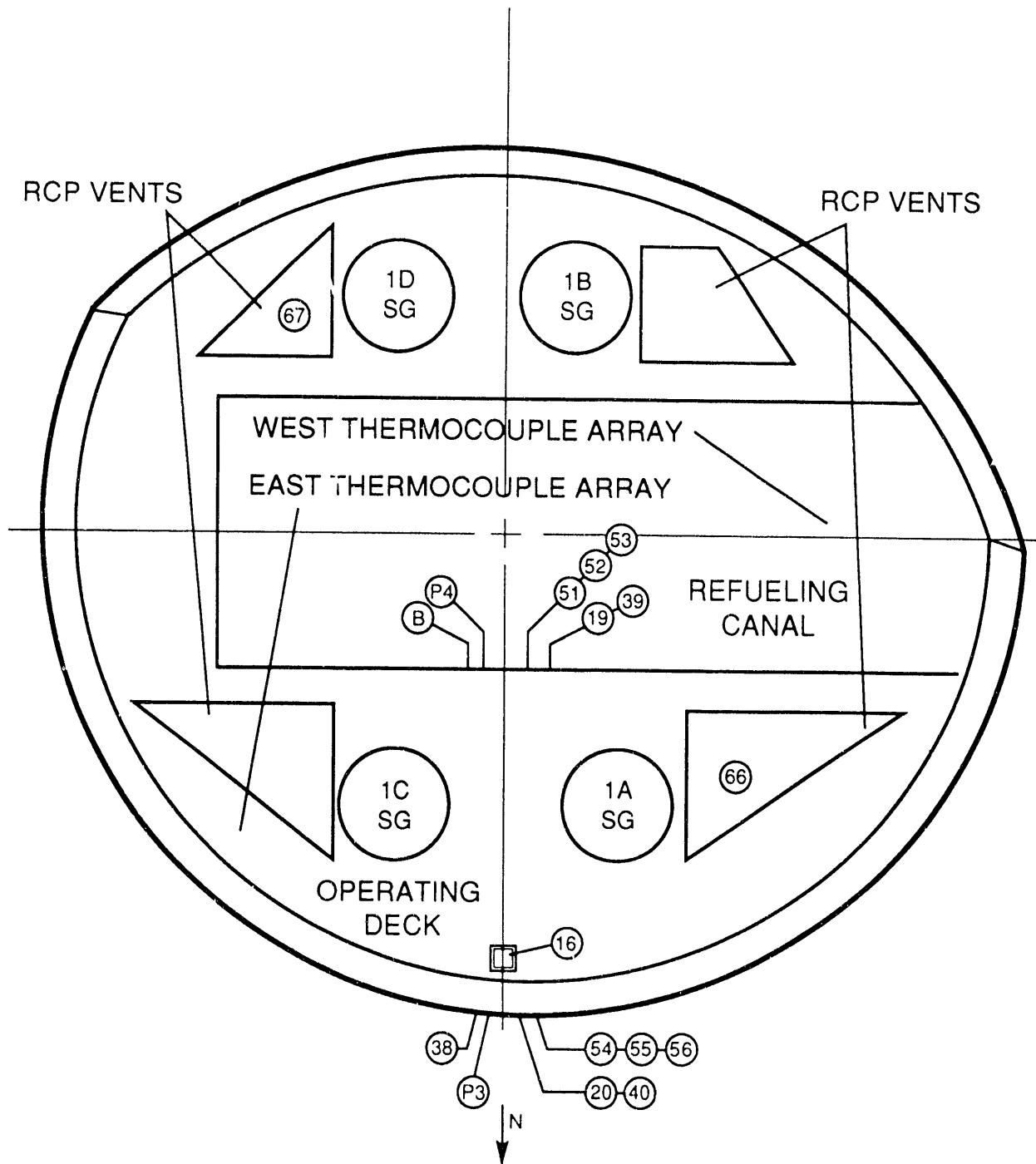


Figure 7. Top view of structures inside the Surtsey vessel. The figure also shows instrumentation location by channel number.

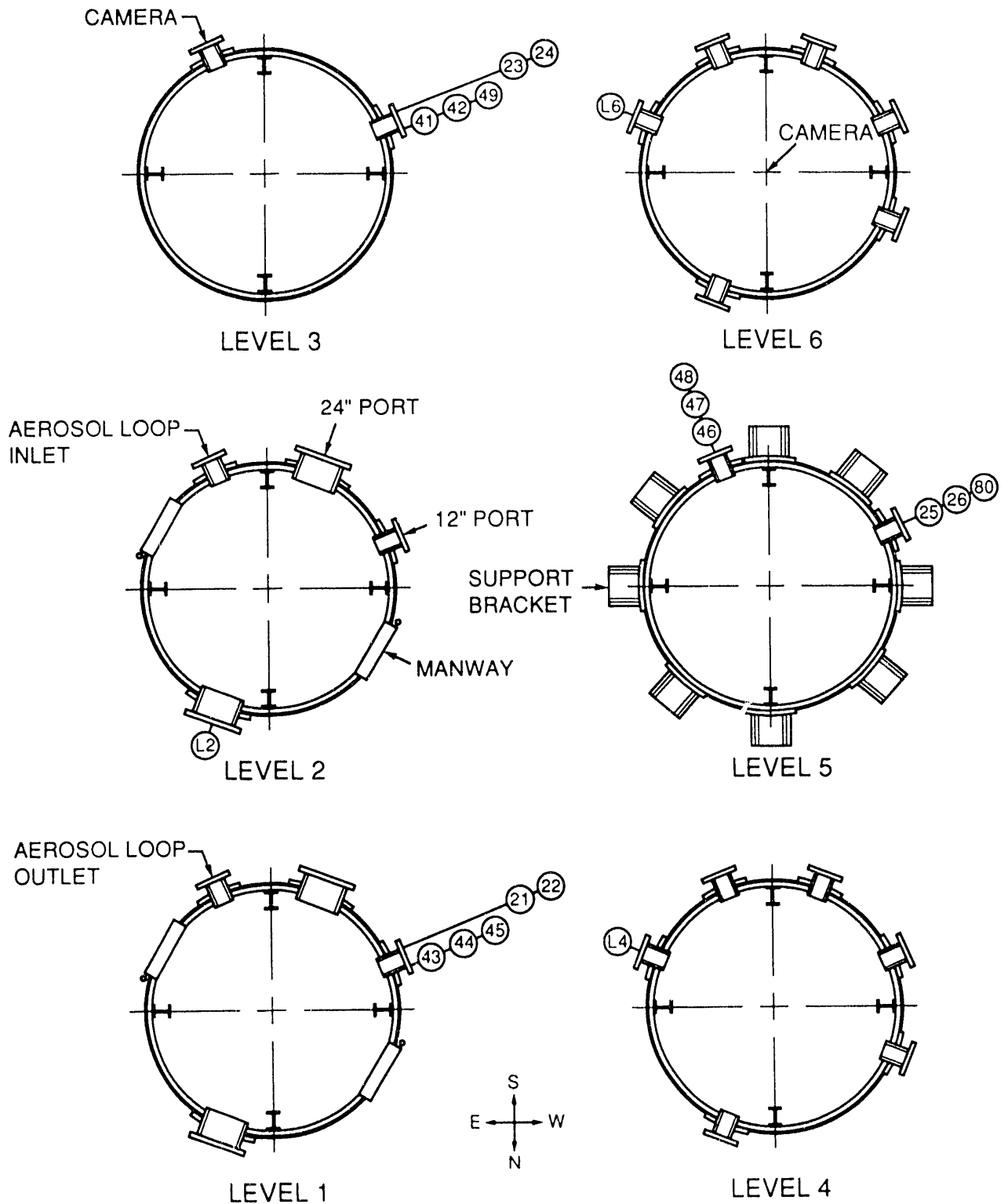


Figure 8. Top view of the Surtsey vessel showing instrumentation ports. The figure also shows instrumentation location by channel number.

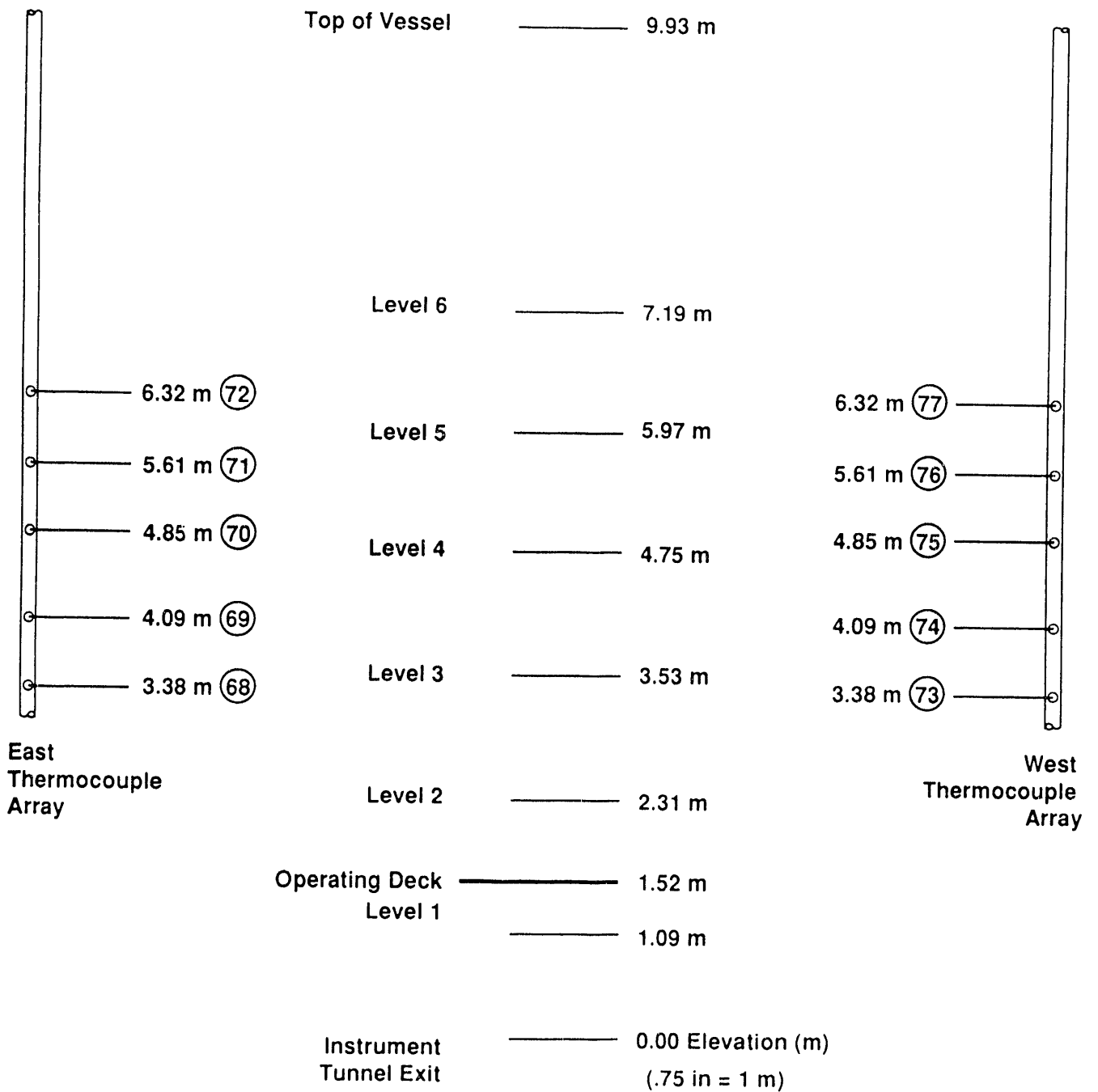


Figure 9. Location of Surtsey vessel bulk gas temperature thermocouple arrays. The figure also shows instrumentation location by channel number.

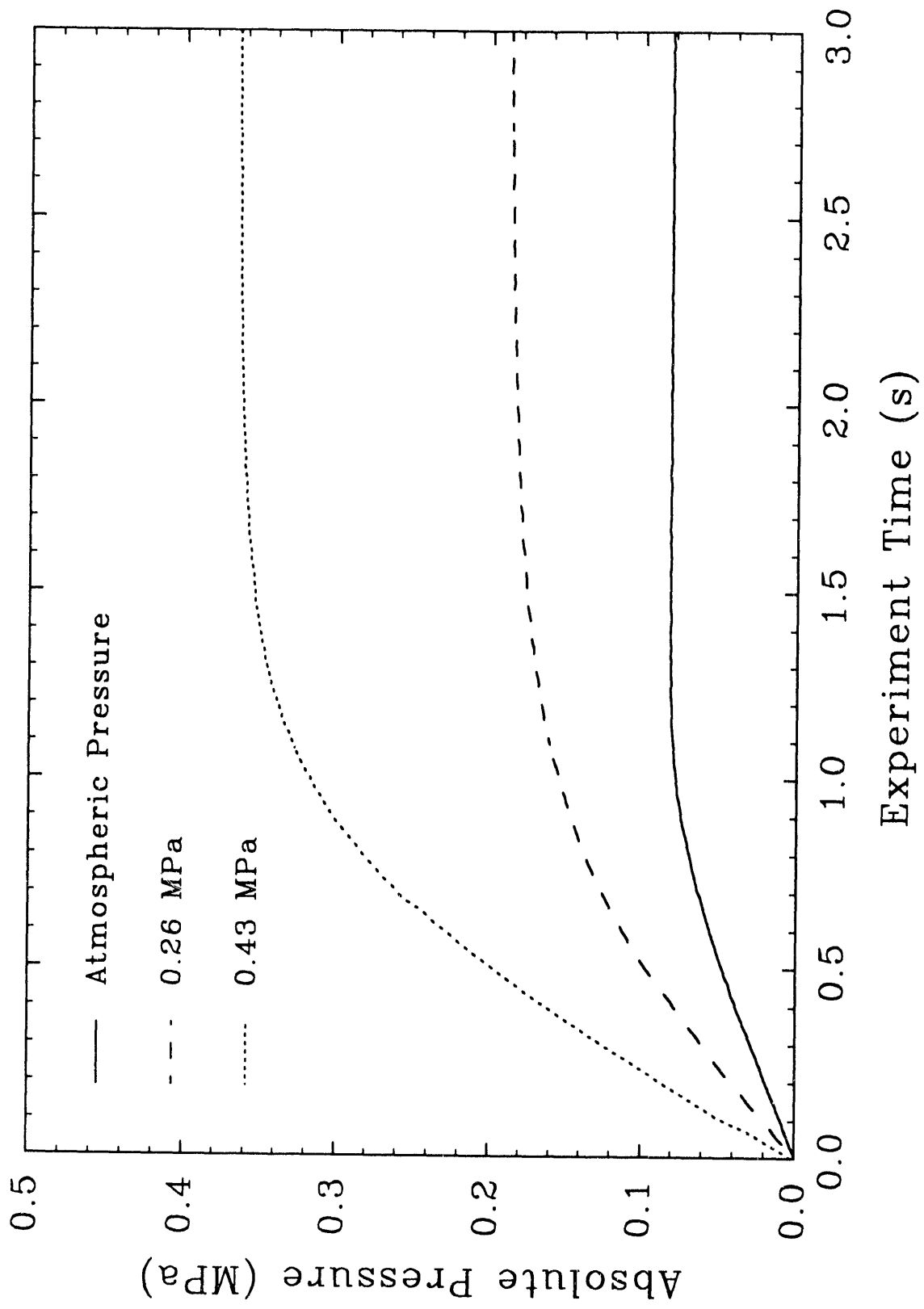


Figure 10. Gas grab sample bottle fill times.

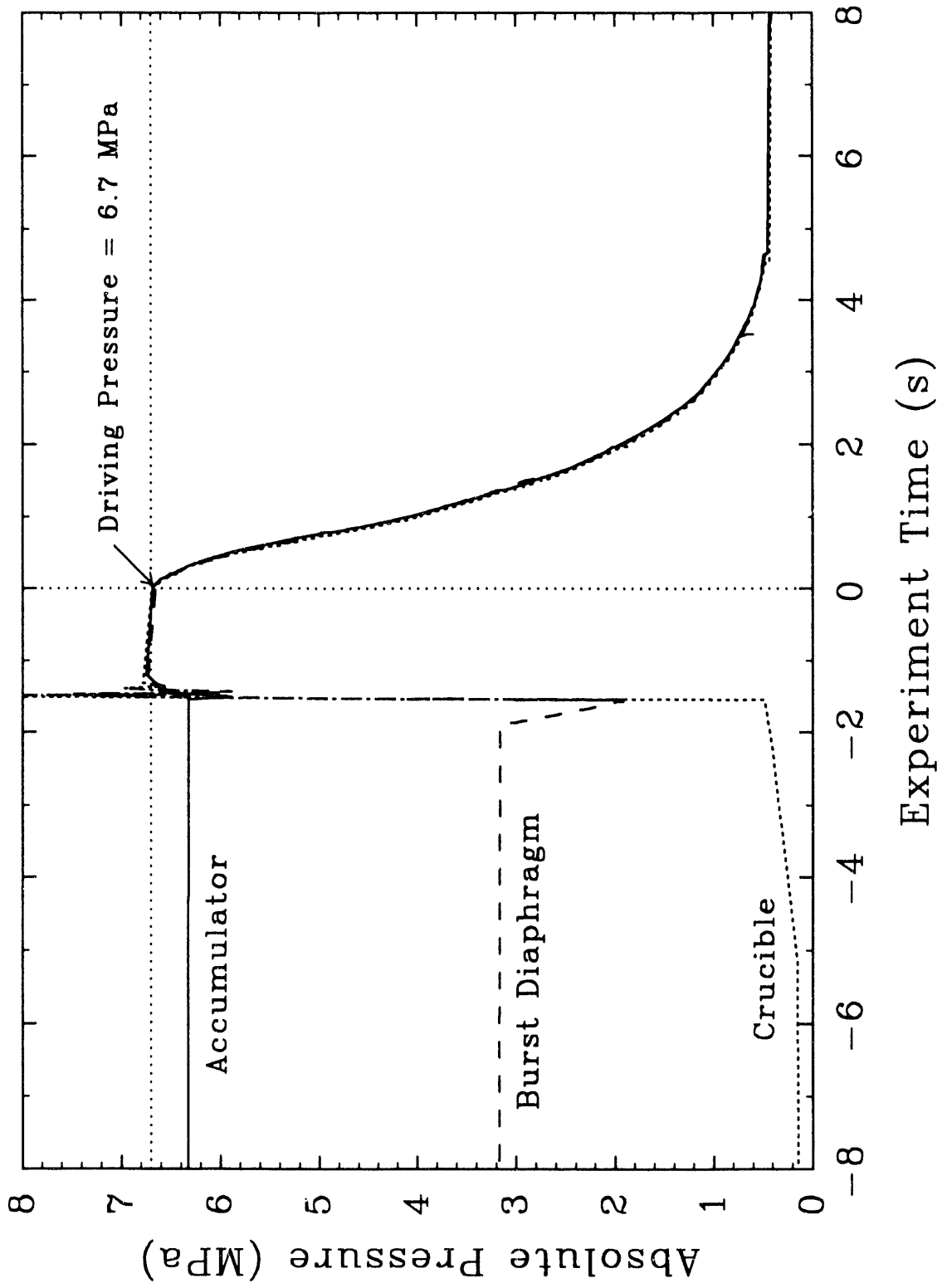


Figure 11. Blowdown pressure history for the IET-4 experiment.

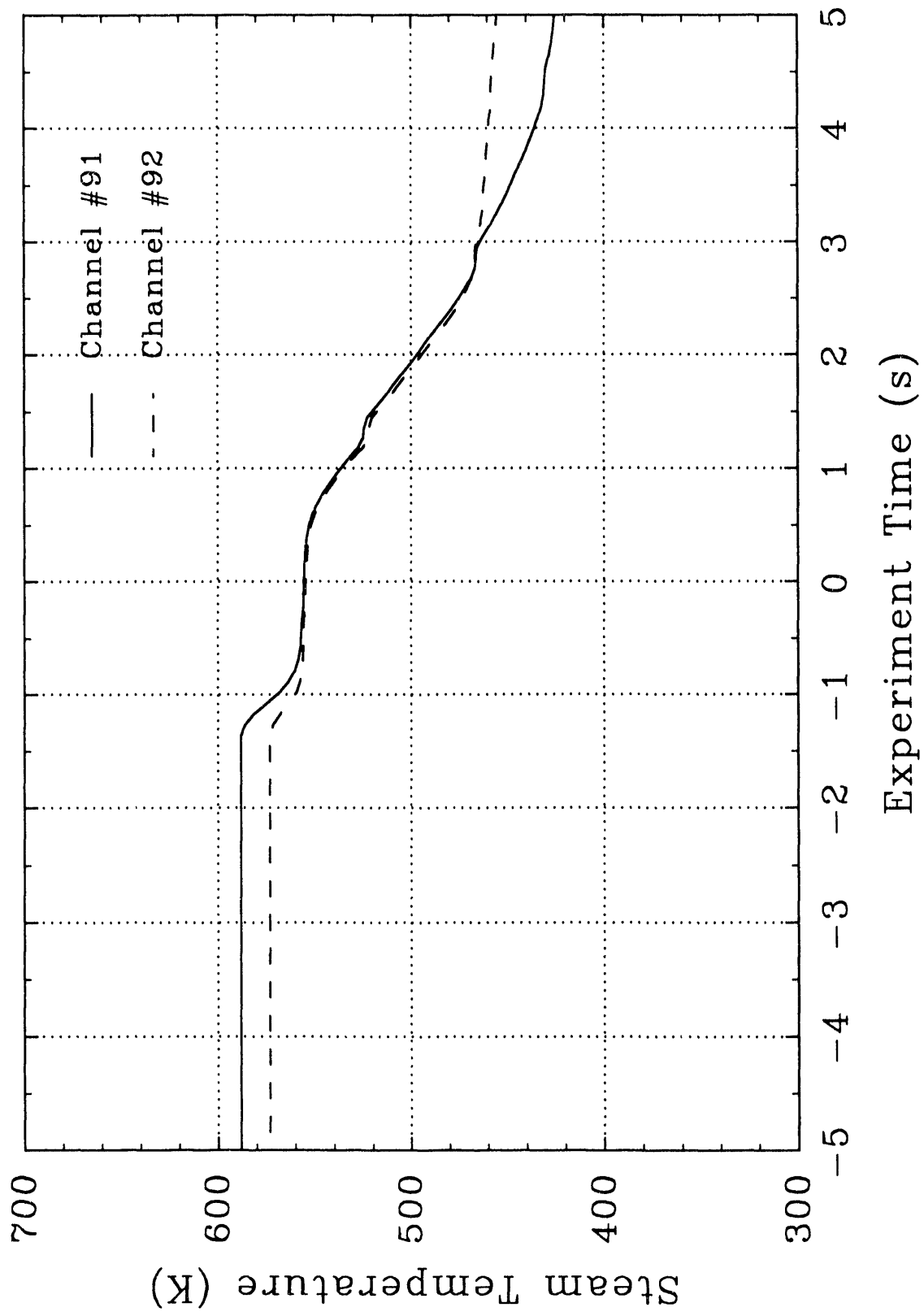


Figure 12. Steam blowdown temperatures measured in the steam accumulator tank with type-K thermocouples in the IET-4 experiment.

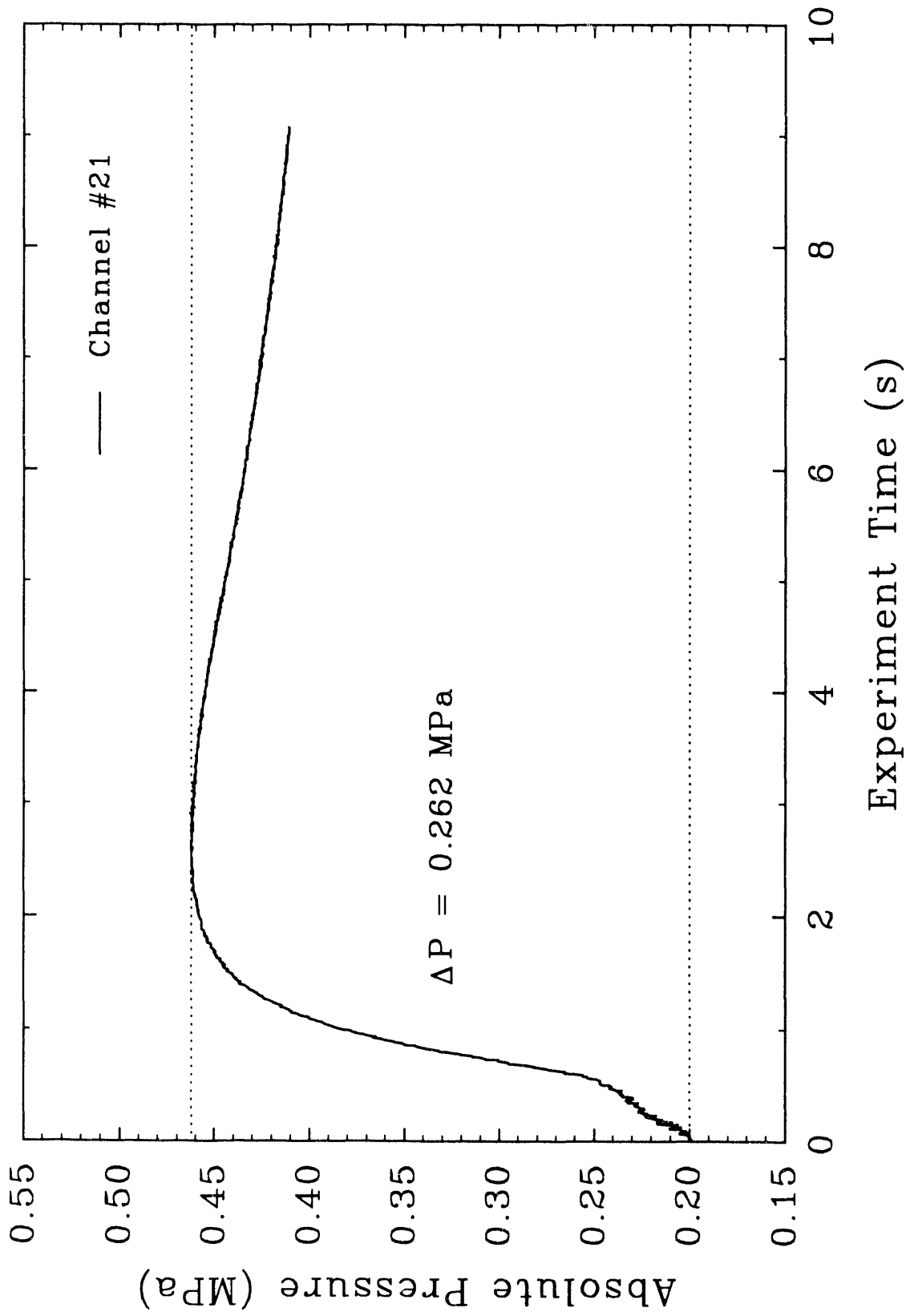


Figure 13. Surtsey vessel pressure versus time measured at level 1 in the IET-4 experiment.

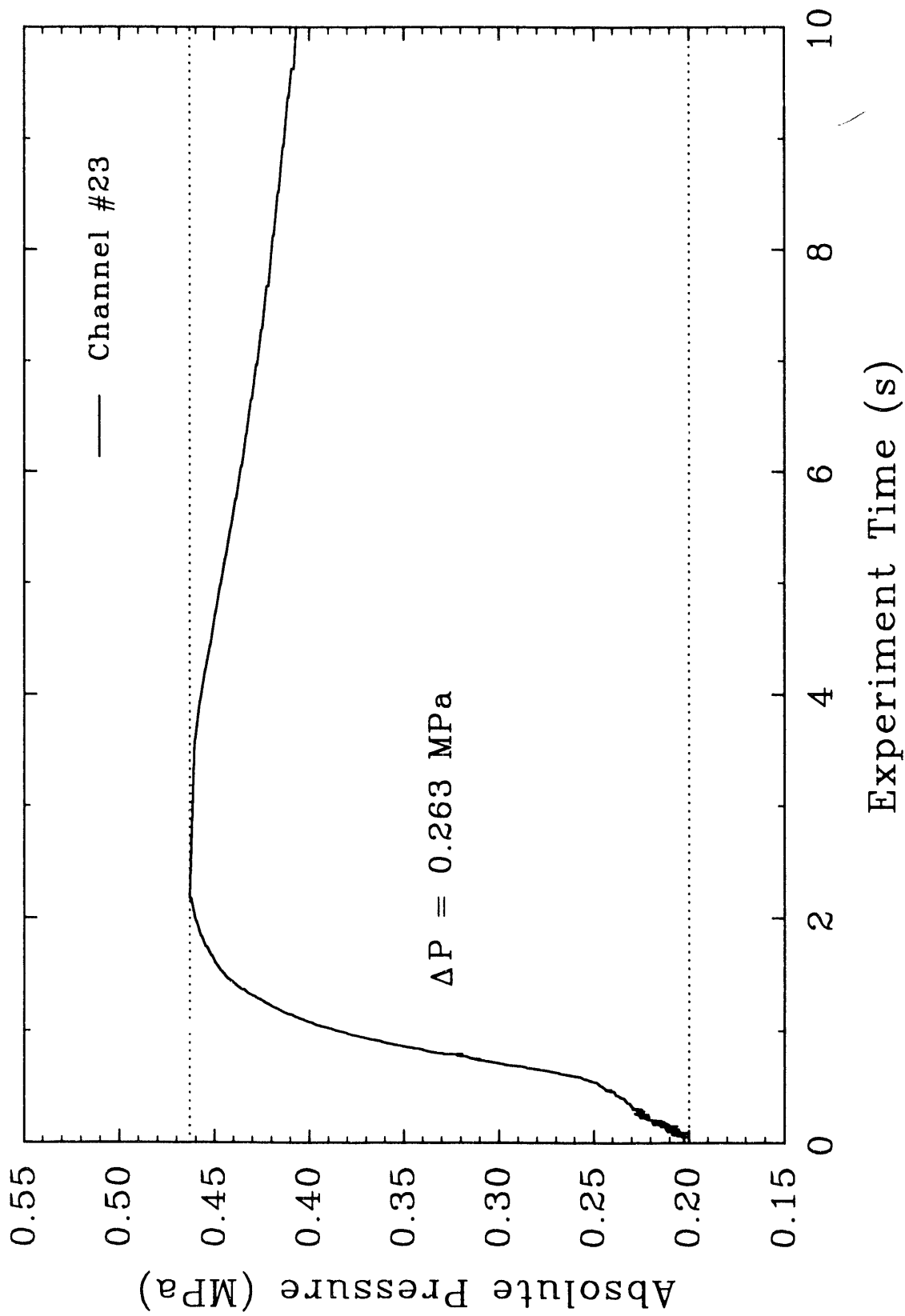


Figure 14. Surtsey vessel pressure versus time measured at level 3 in the IET-4 experiment.

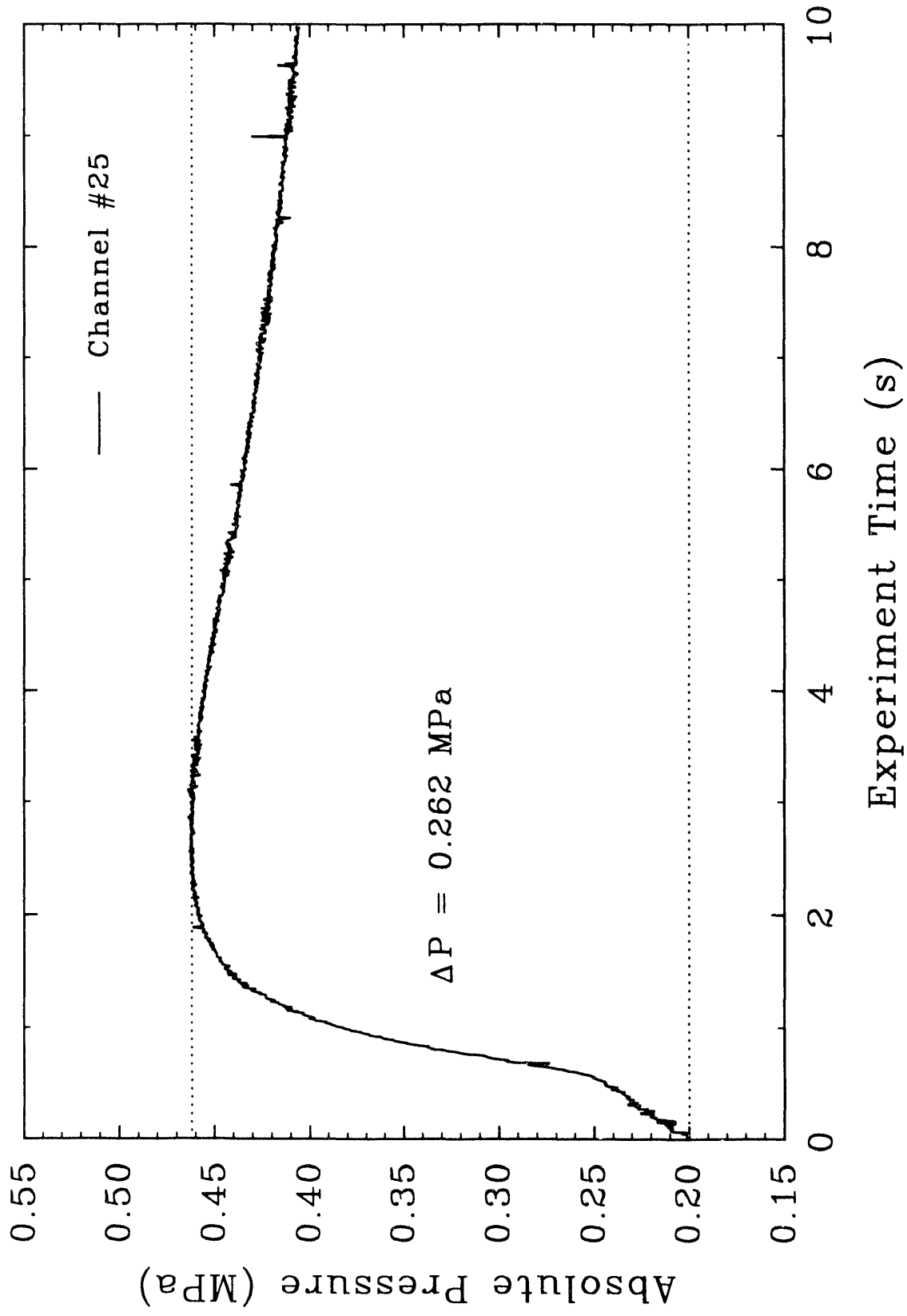


Figure 15. Surtsey vessel pressure versus time measured at level 5 in the IET-4 experiment.

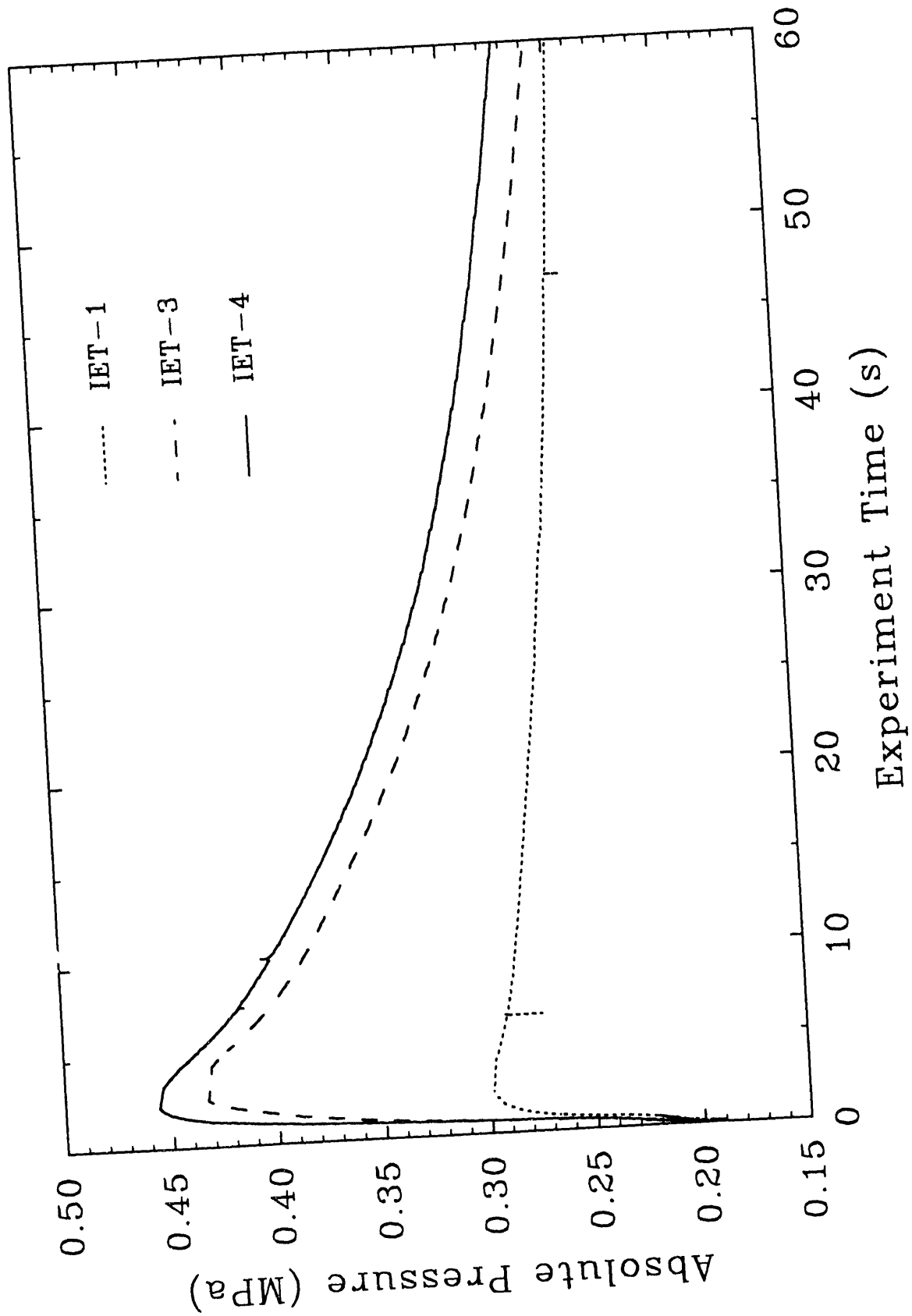


Figure 16. Surtsey vessel pressure comparisons versus time for the IET-1, IET-3, and IET-4 experiments.

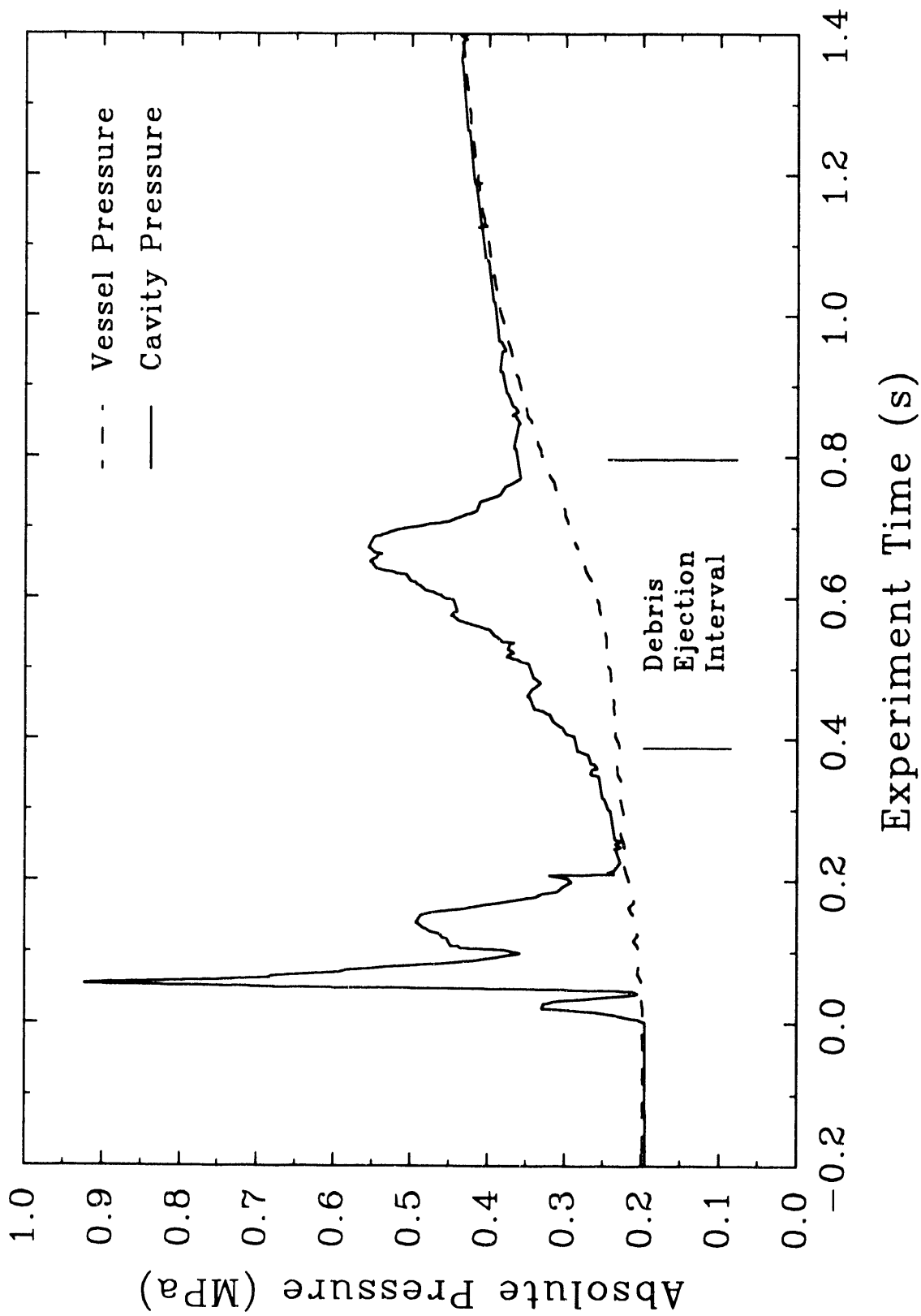


Figure 17. Cavity pressure and Surtsey vessel pressure versus time in the IET-4 experiment.

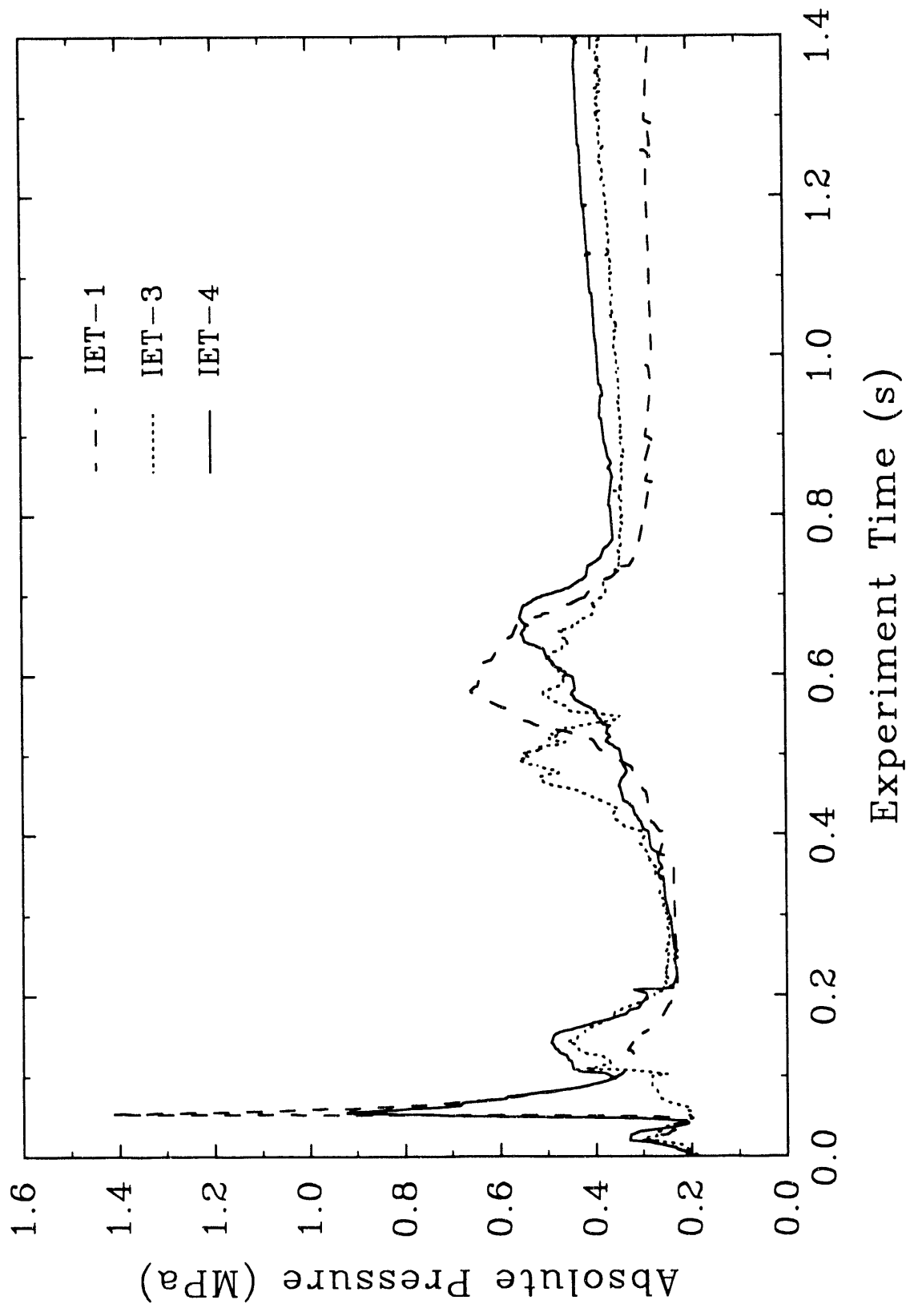


Figure 18. Comparison of the cavity pressures versus time for the IET-1, IET-3, and IET-4 experiments.

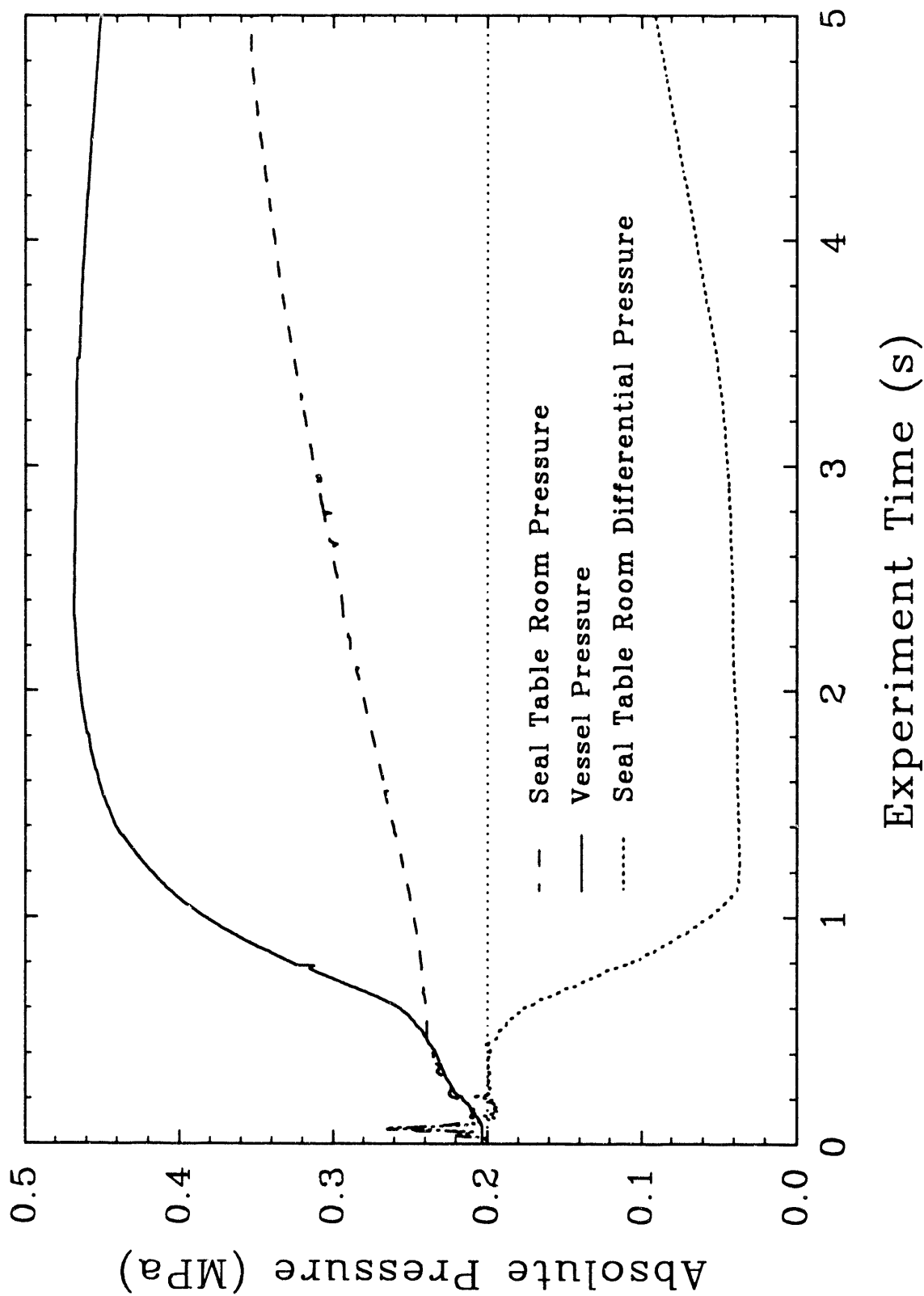


Figure 19. Seal table room absolute pressure and differential pressure compared to Surtsey vessel pressure in the IET-4 experiment.

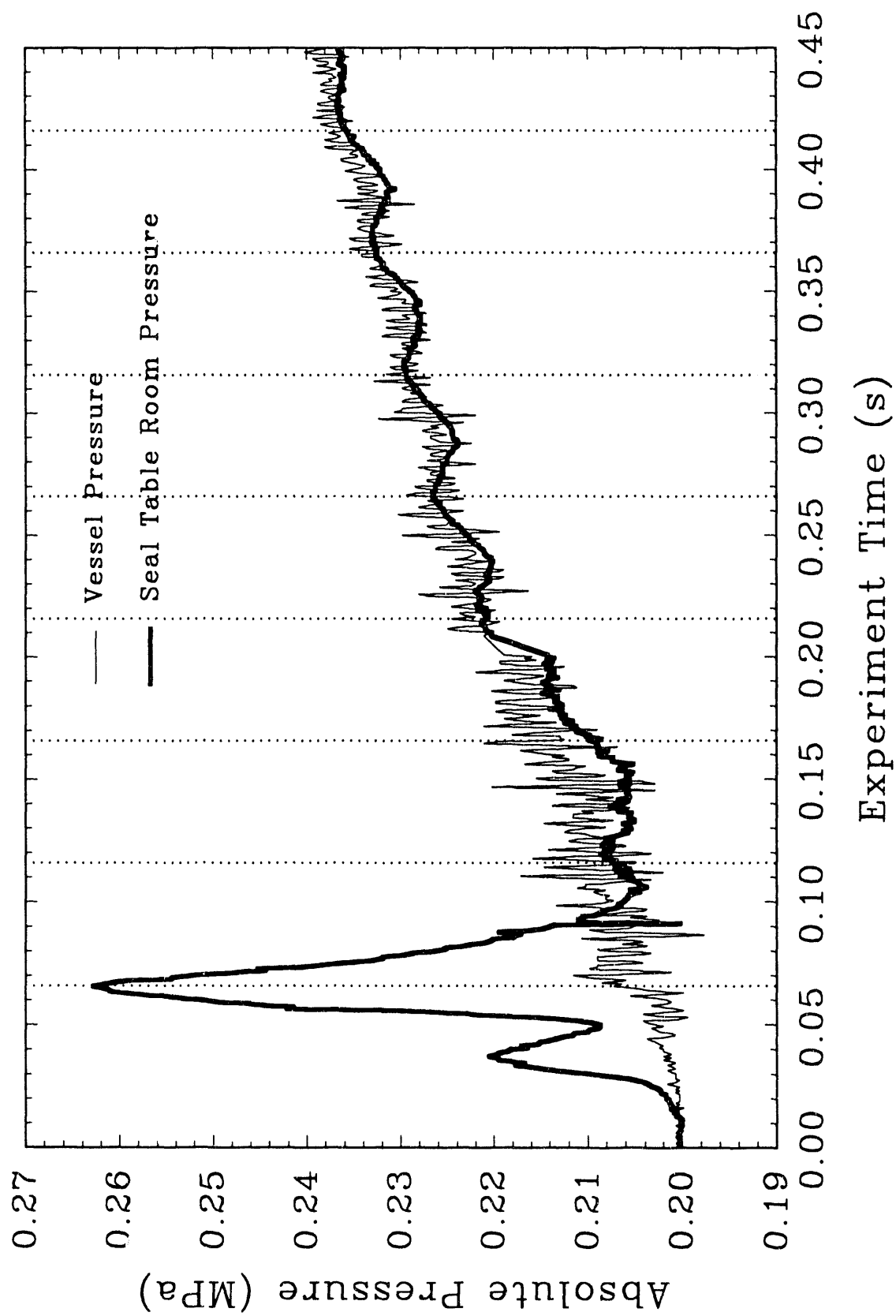


Figure 20. Seal table room and Surtsey vessel pressure versus time in the IET-4 experiment. The vertical dotted lines align with a 20 Hz resonance in the vessel caused by a steam explosion in the cavity.

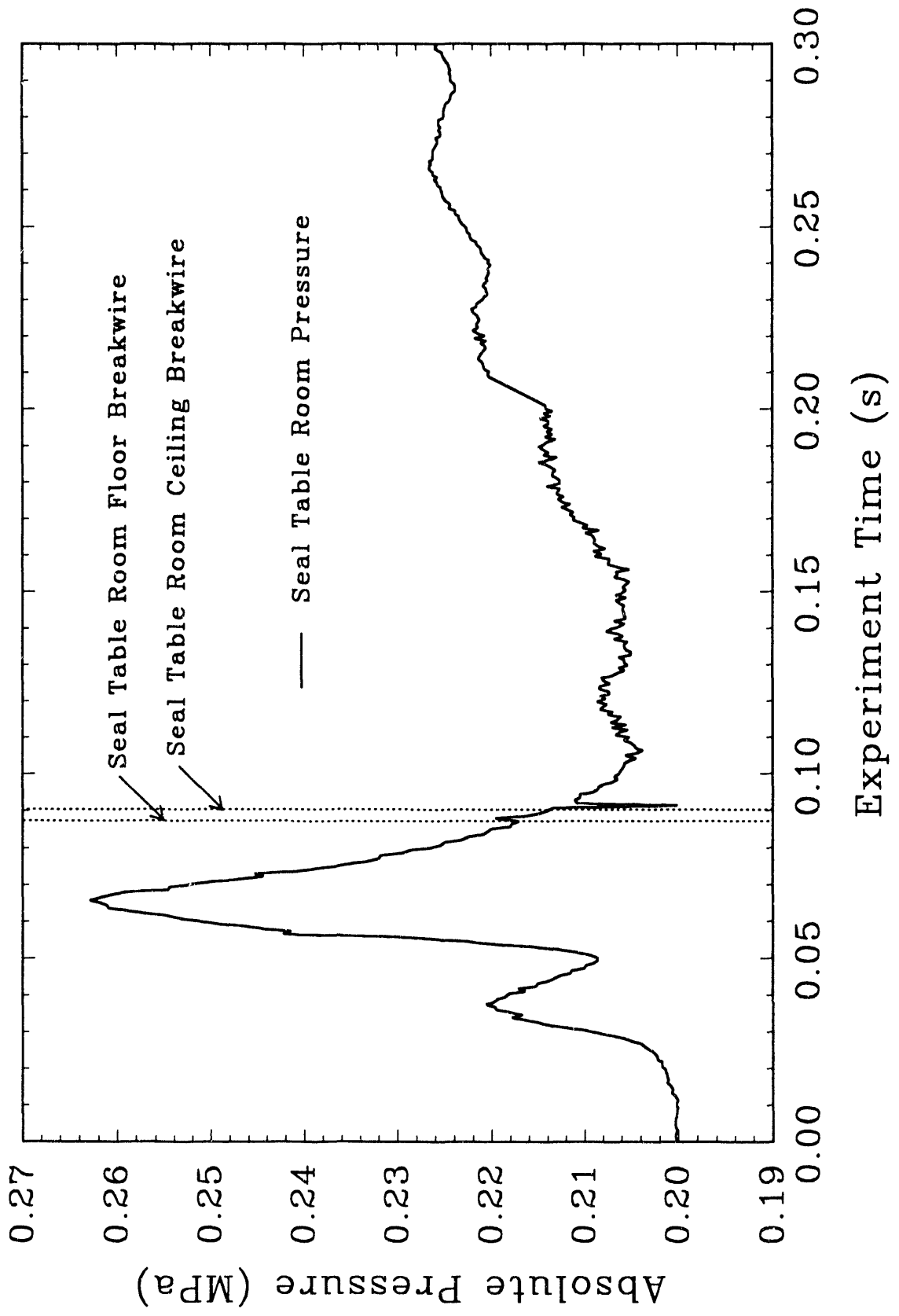


Figure 21. Debris ejection timing into the seal table room in the IET-4 experiment.

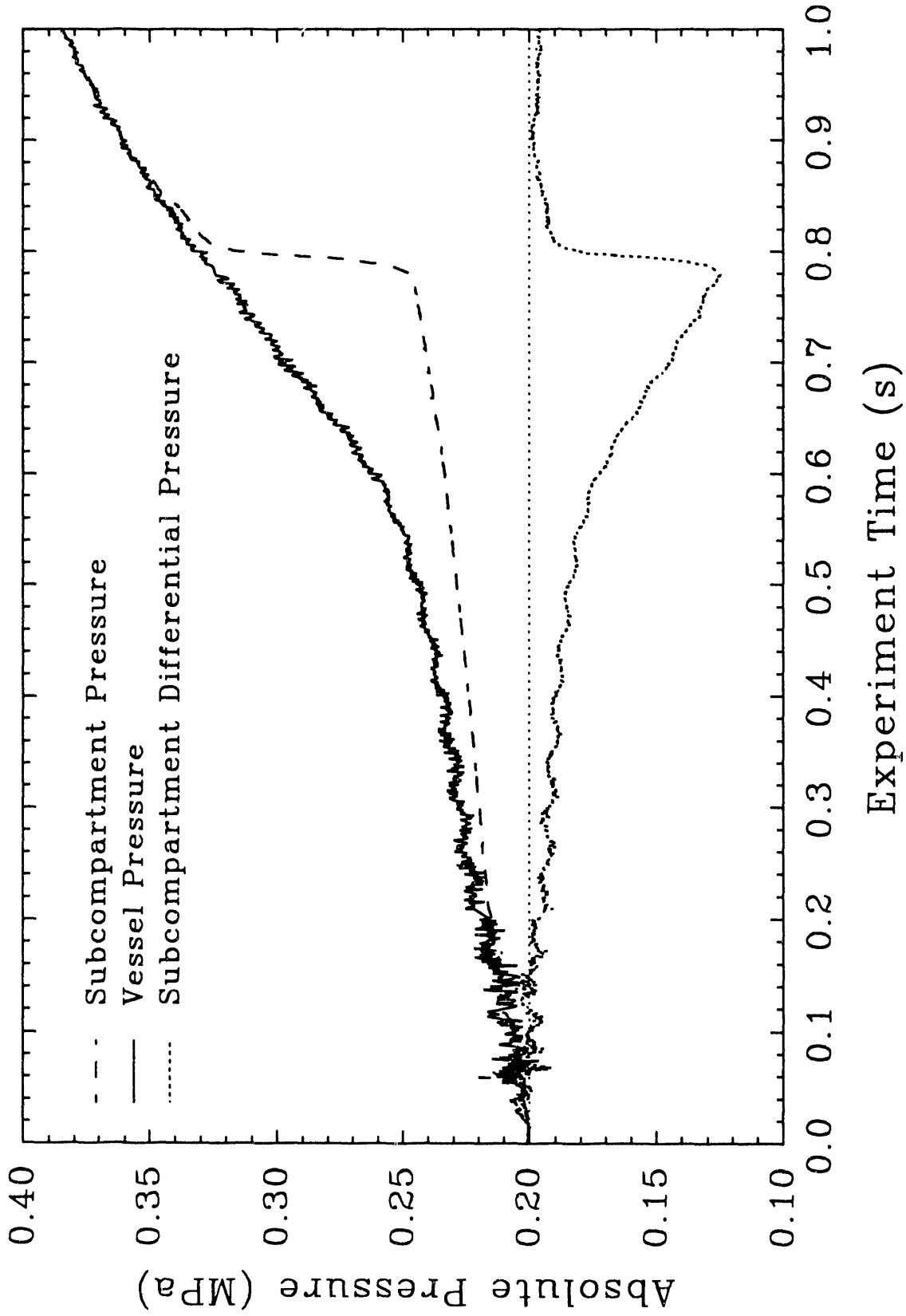


Figure 22. Subcompartment absolute pressure and differential pressure compared to Surtsey vessel pressure in the IET-4 experiment.

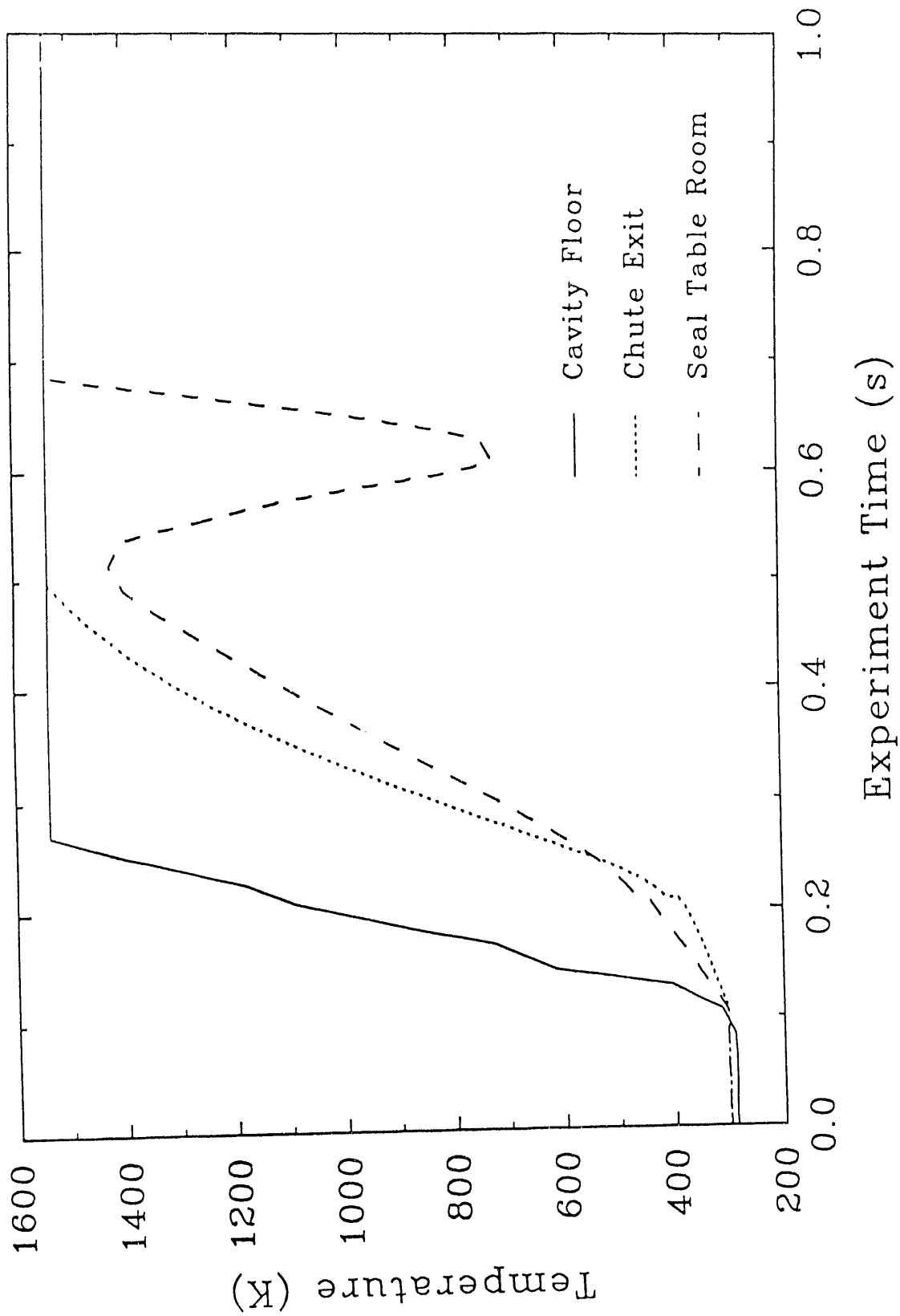


Figure 23. Cavity floor, chute exit, and seal table room temperatures measured with type-K thermocouples in the IET-4 experiment. A type-K thermocouple over-ranges at 1530 K. All three of these thermocouples

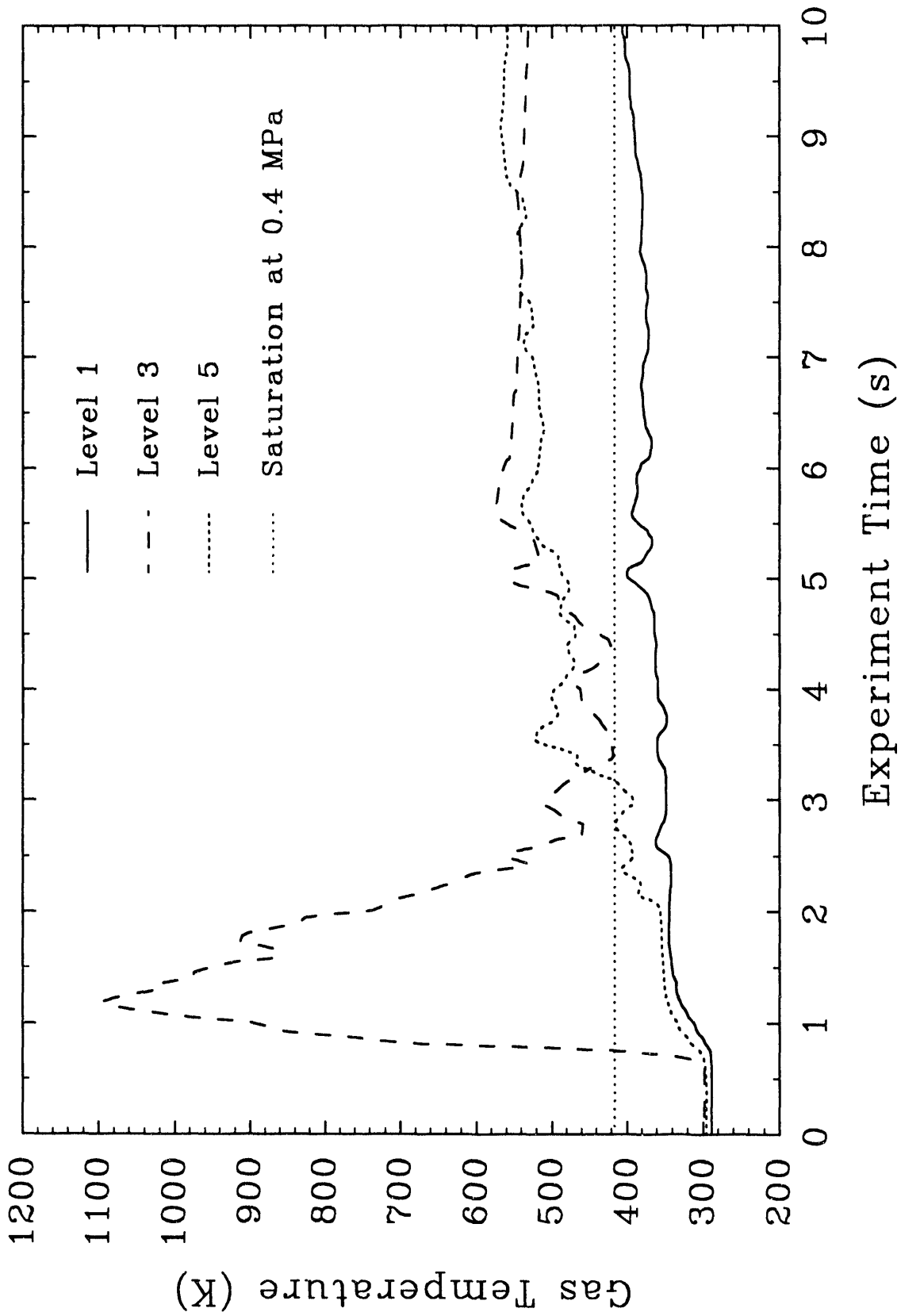


Figure 24. Gas temperatures measured at levels 1, 3, and 5 in the Surtsey vessel with aspirated thermocouples in the IET-4 experiment.

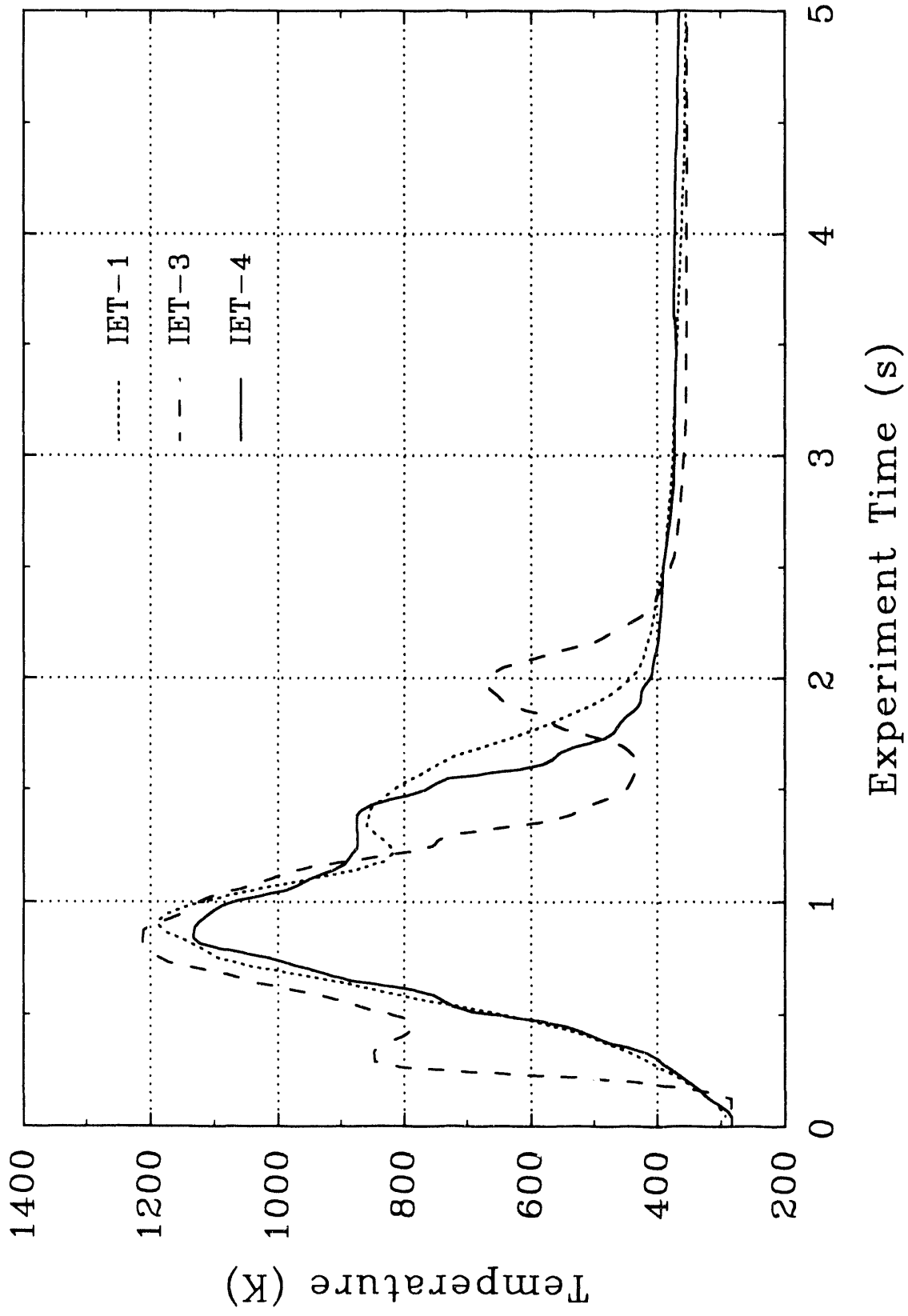


Figure 25. Gas temperatures inside the subcompartment structures measured with aspirated thermocouples in the IET-1, IET-3, and IET-4 experiments.

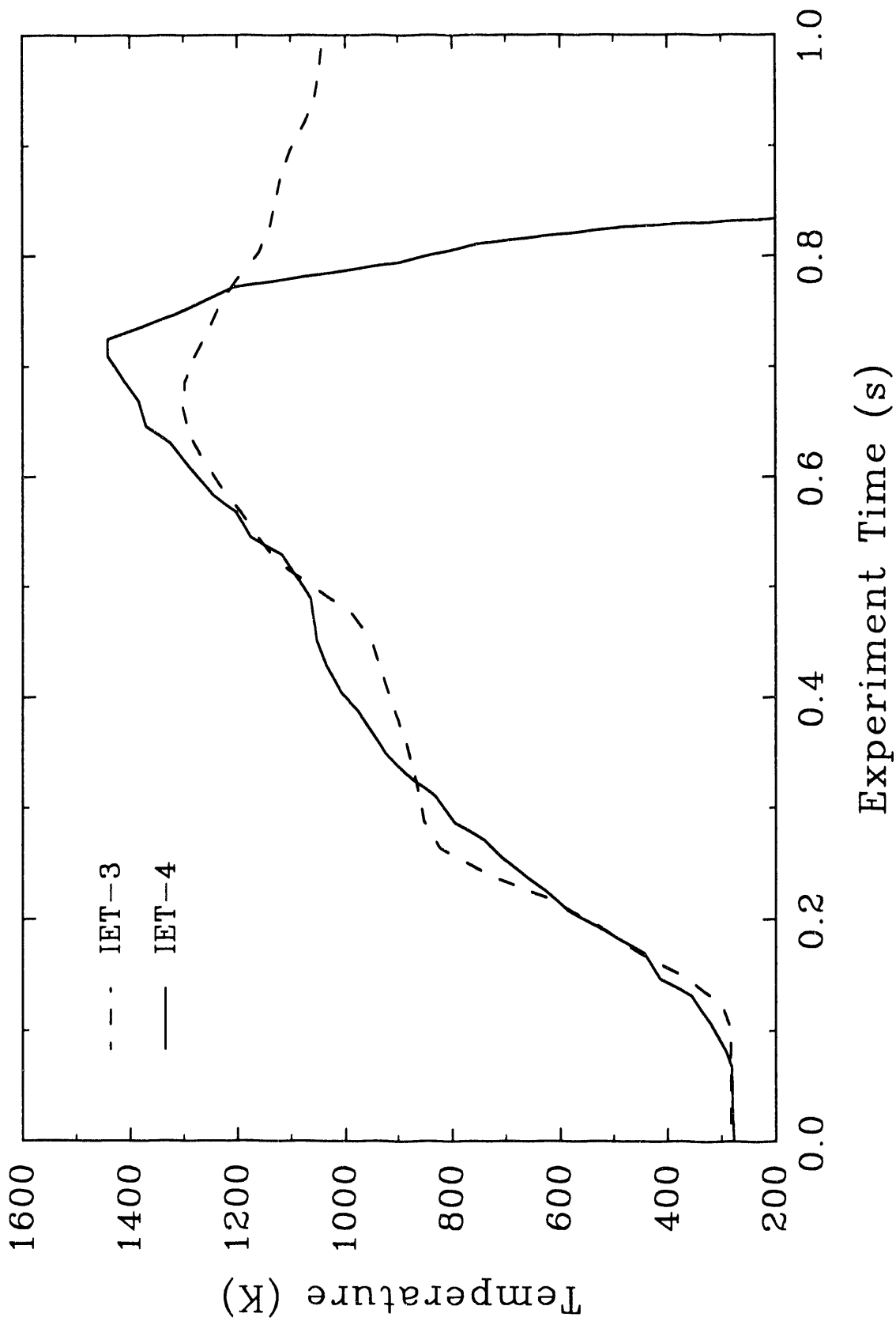


Figure 26. Gas temperatures inside the seal table room measured with type-K aspirated thermocouples in the IET-3 and IET-4 experiments.

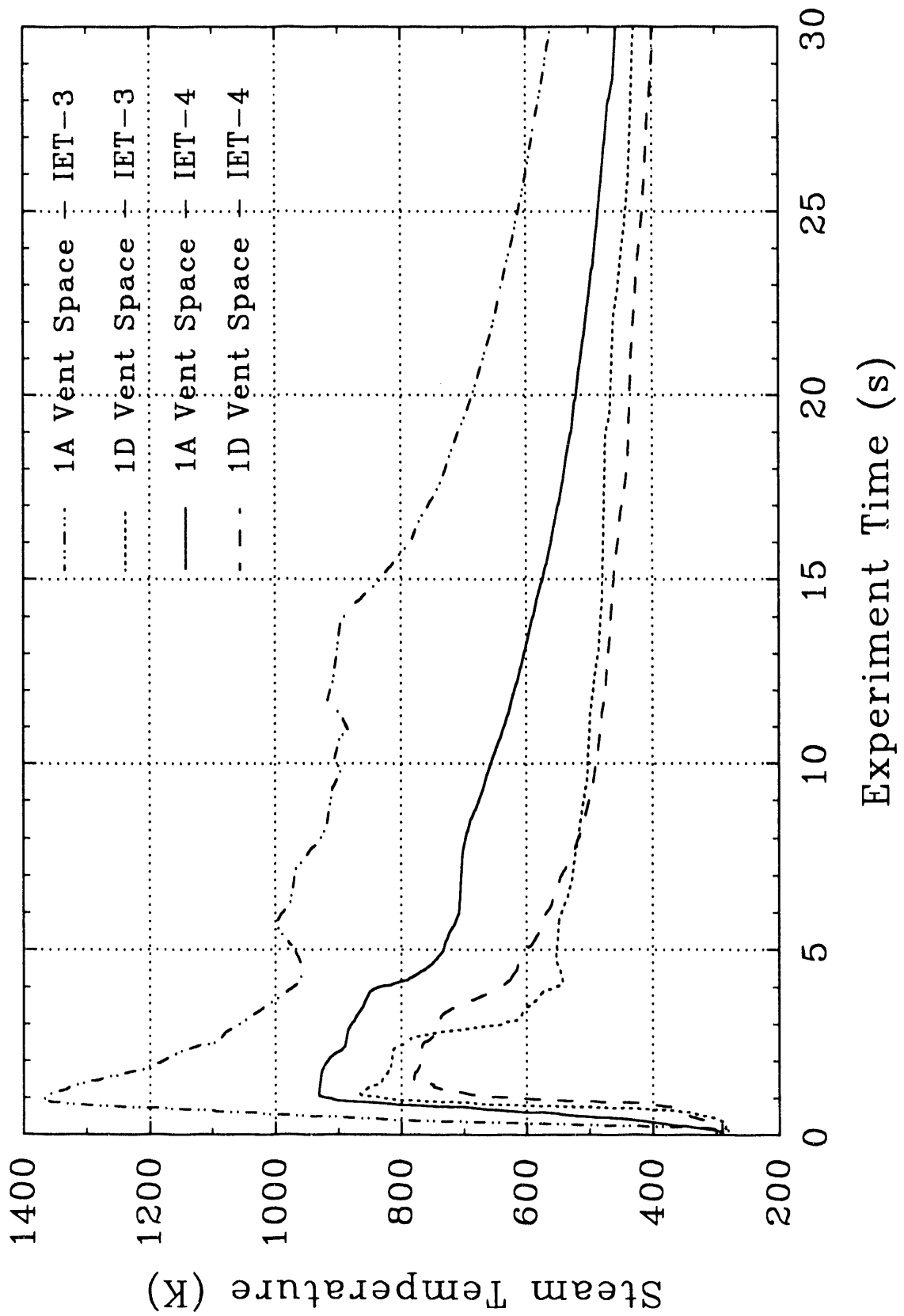


Figure 27. Comparison of the temperatures in the triangular vent spaces above reactor coolant pumps 1A and 1D in the IET-3 and IET-4 experiments.

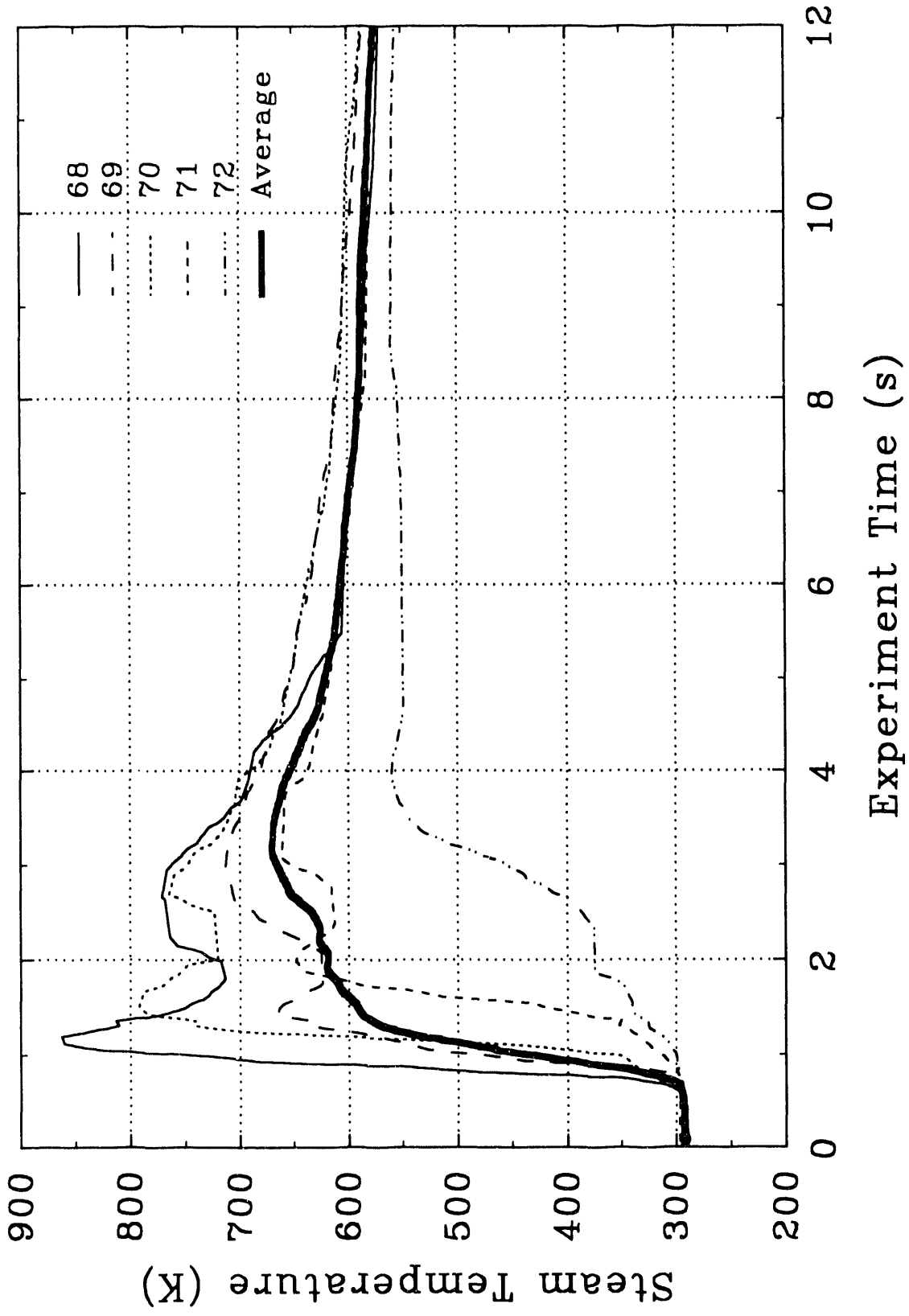


Figure 28. Temperature history of the east thermocouple array in the IET-4 experiment.

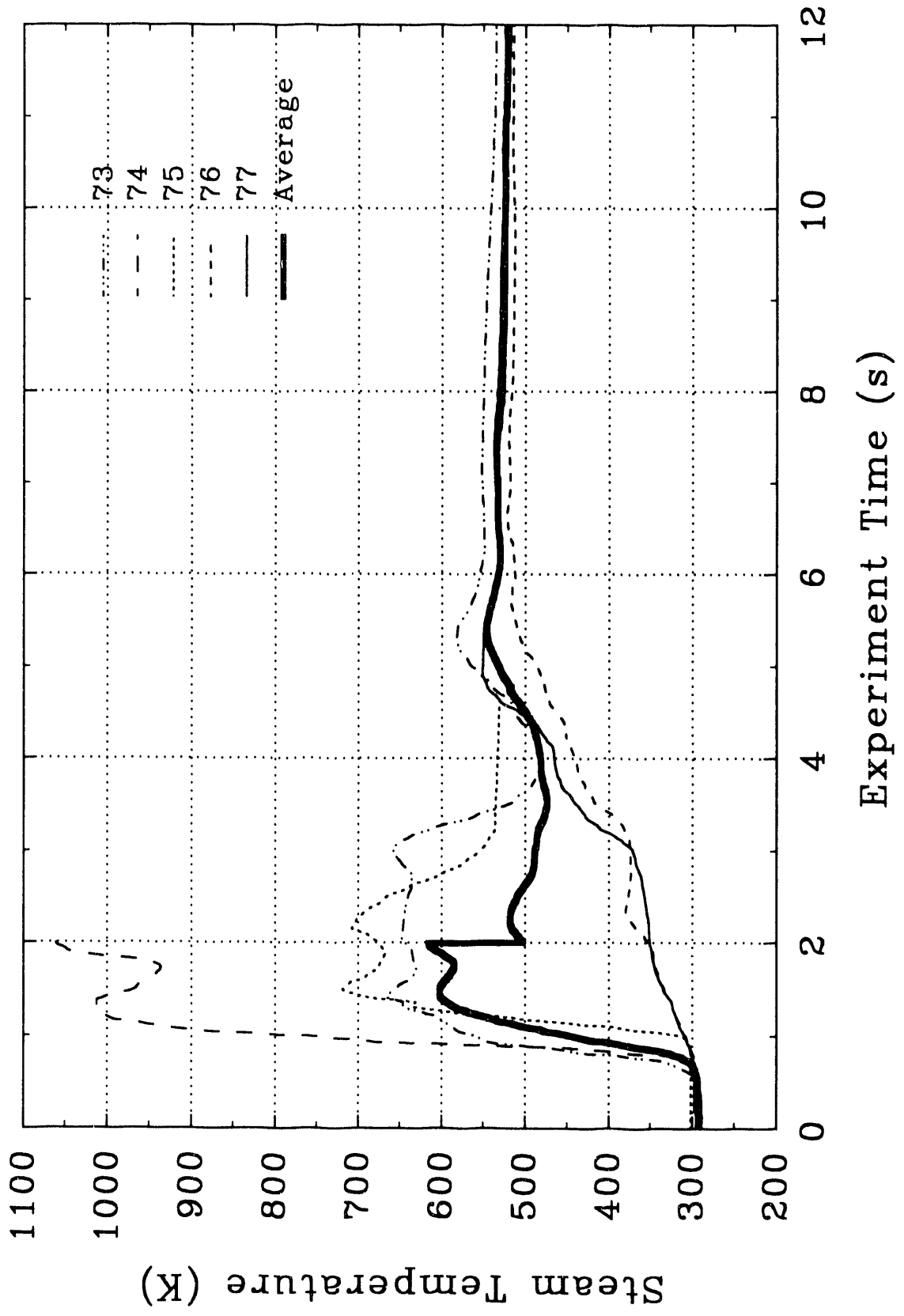


Figure 29. Temperatures history of the west thermocouple array in the IET-4 experiment.

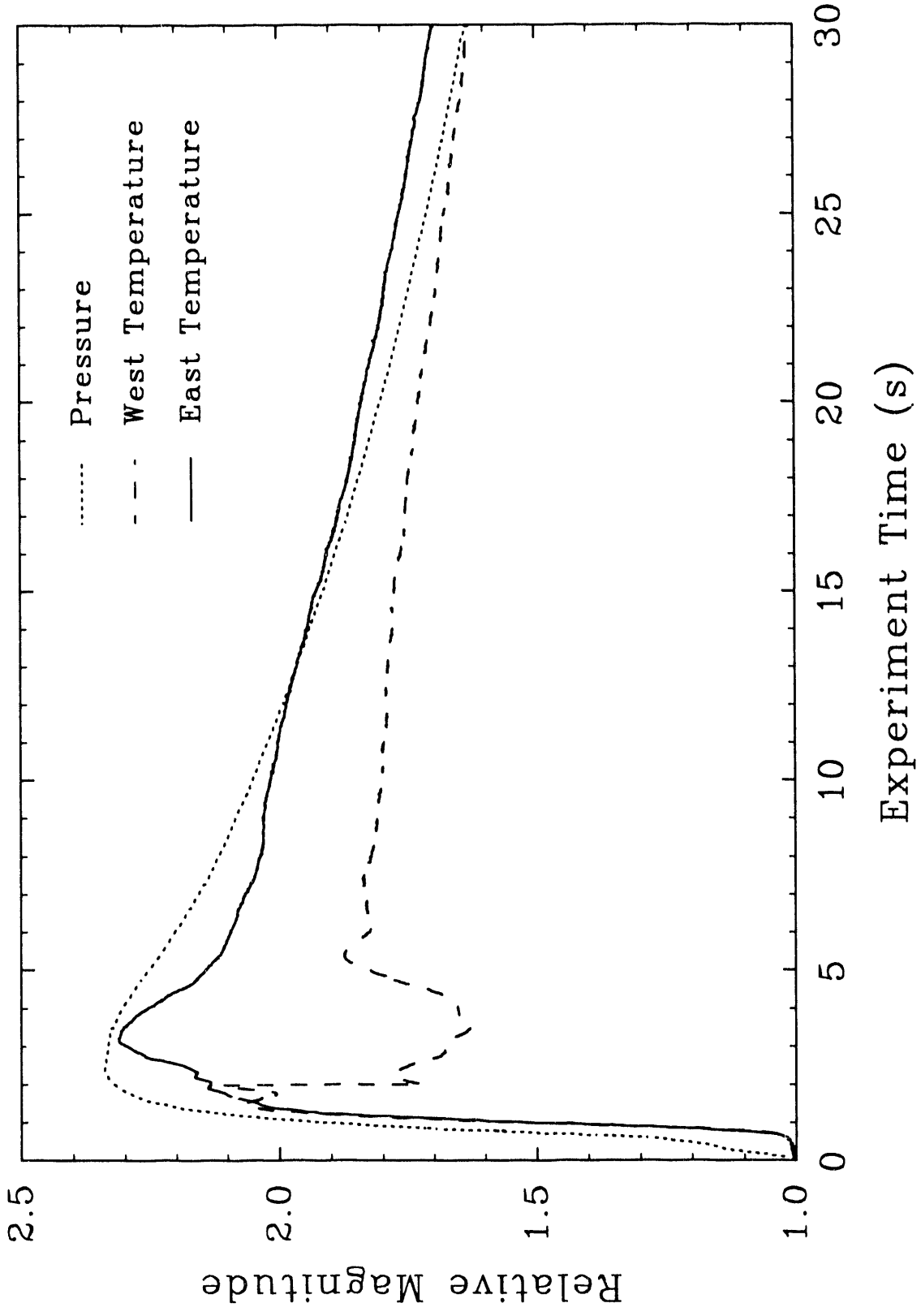


Figure 30. Relative pressure and bulk gas temperature increase in the Surtsey vessel in the IET-4 experiment.

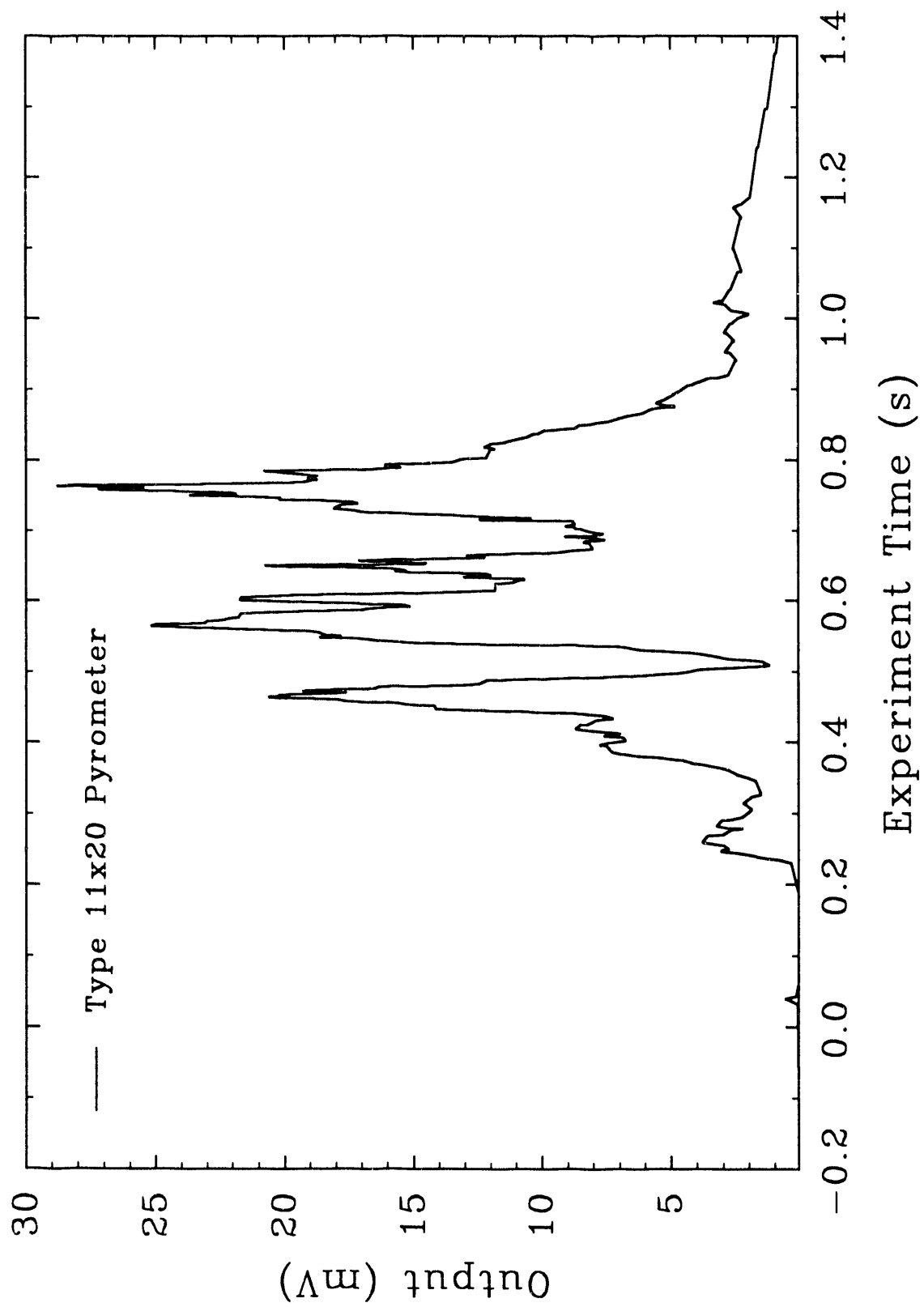


Figure 31. Raw pyrometer output at the chute exit measured with a type 11x20 optical pyrometer in the IET-4 experiment.

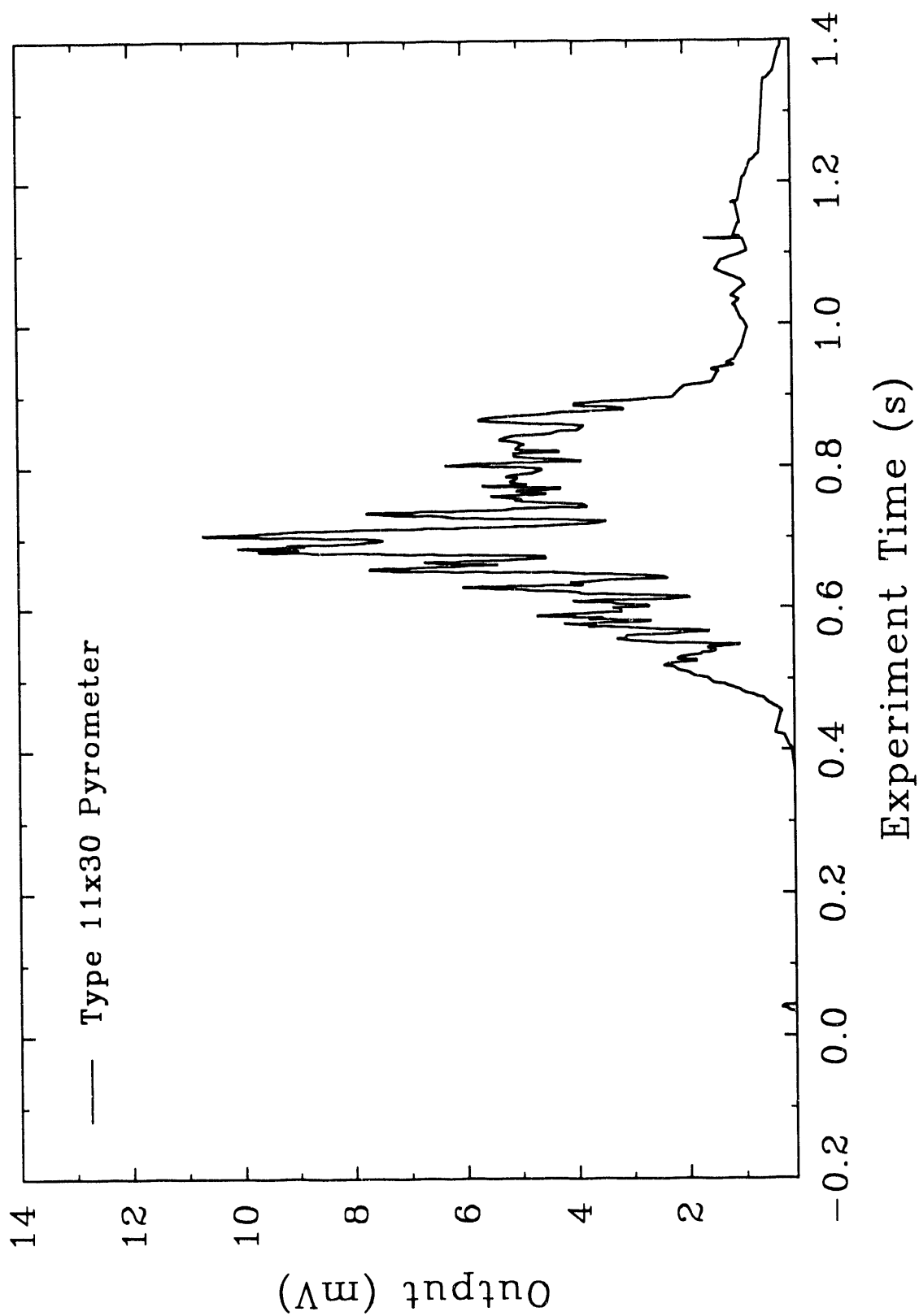


Figure 32. Raw pyrometer output at the chute exit measured with a type 11x30 optical pyrometer in the IET-4 experiment.

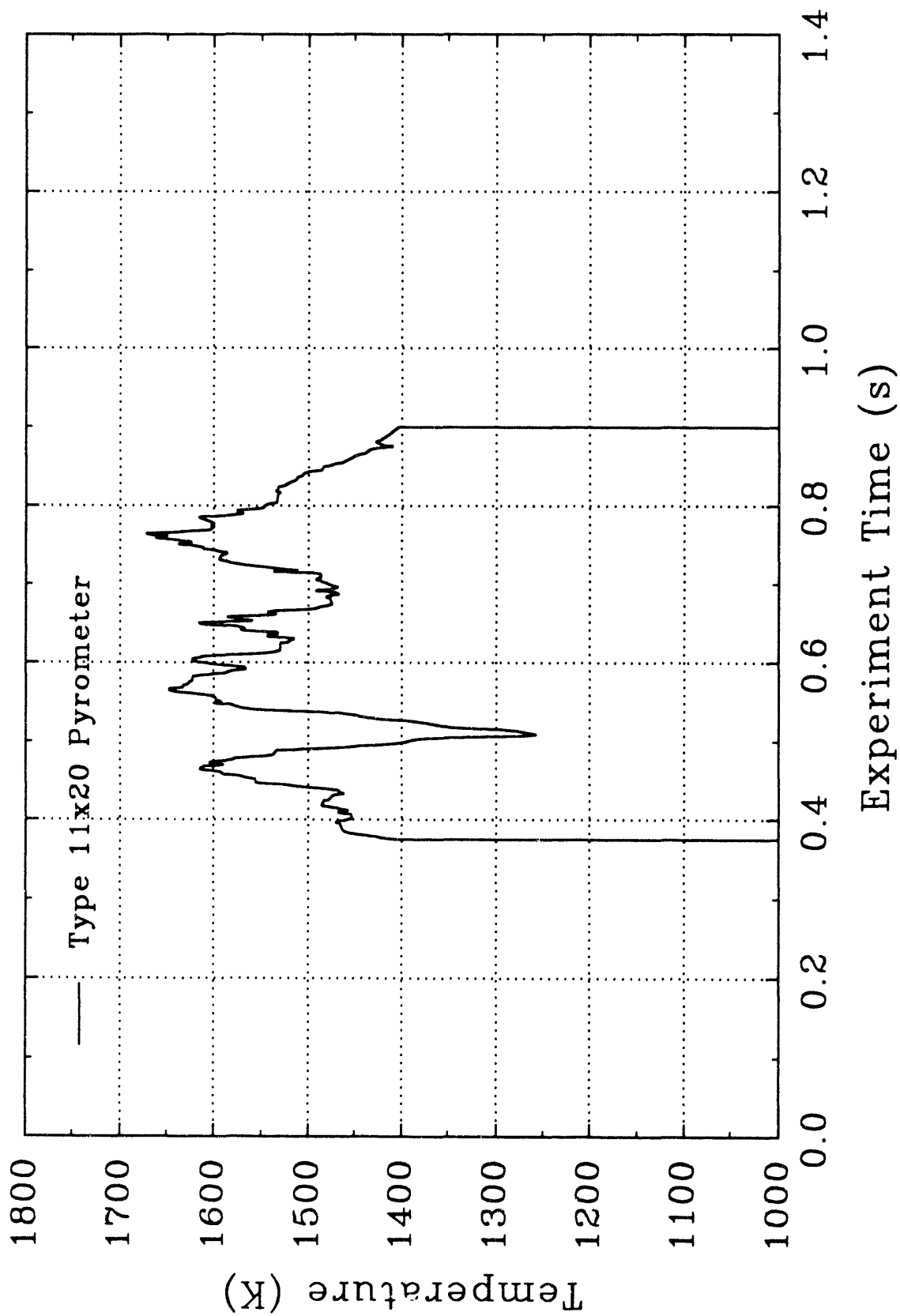


Figure 33. Debris temperature at the chute exit measured with a type 11x20 optical pyrometer in the IET-4 experiment.

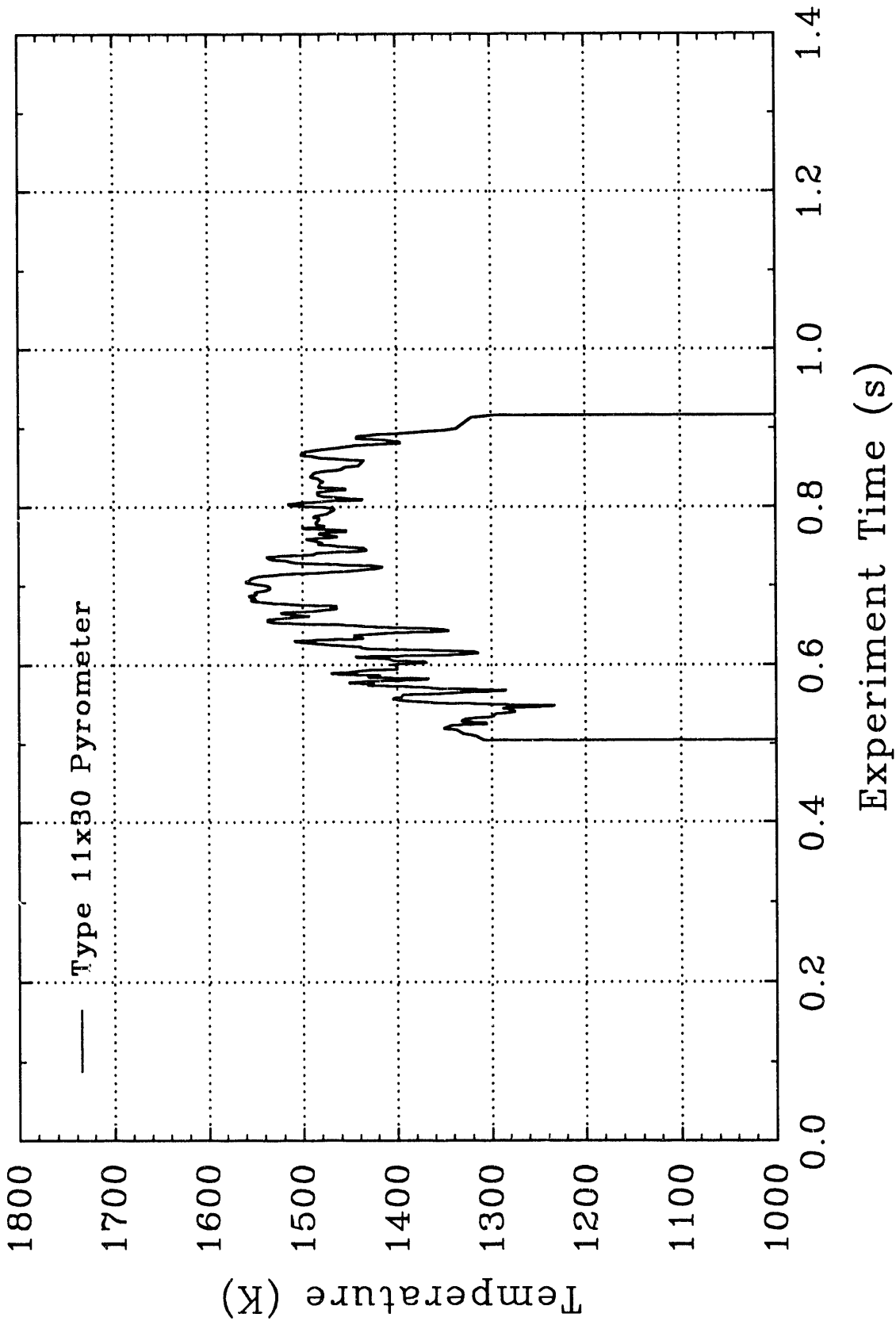


Figure 34. Debris temperature at the chute exit measured with a type 11x30 optical pyrometer in the IET-4 experiment.

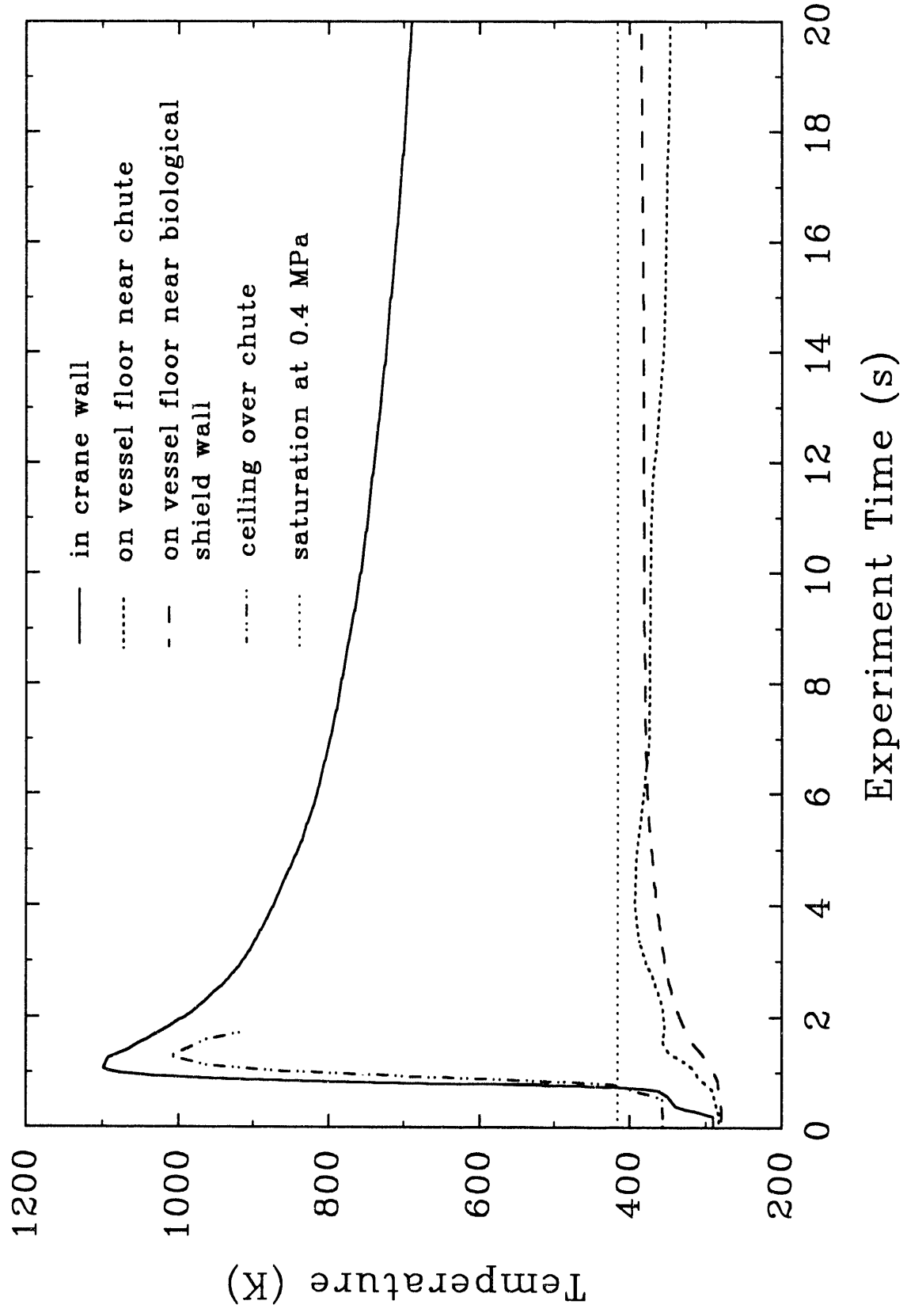


Figure 35. Debris temperature measured with the graphite disk calorimeters in the IET-4 experiment.

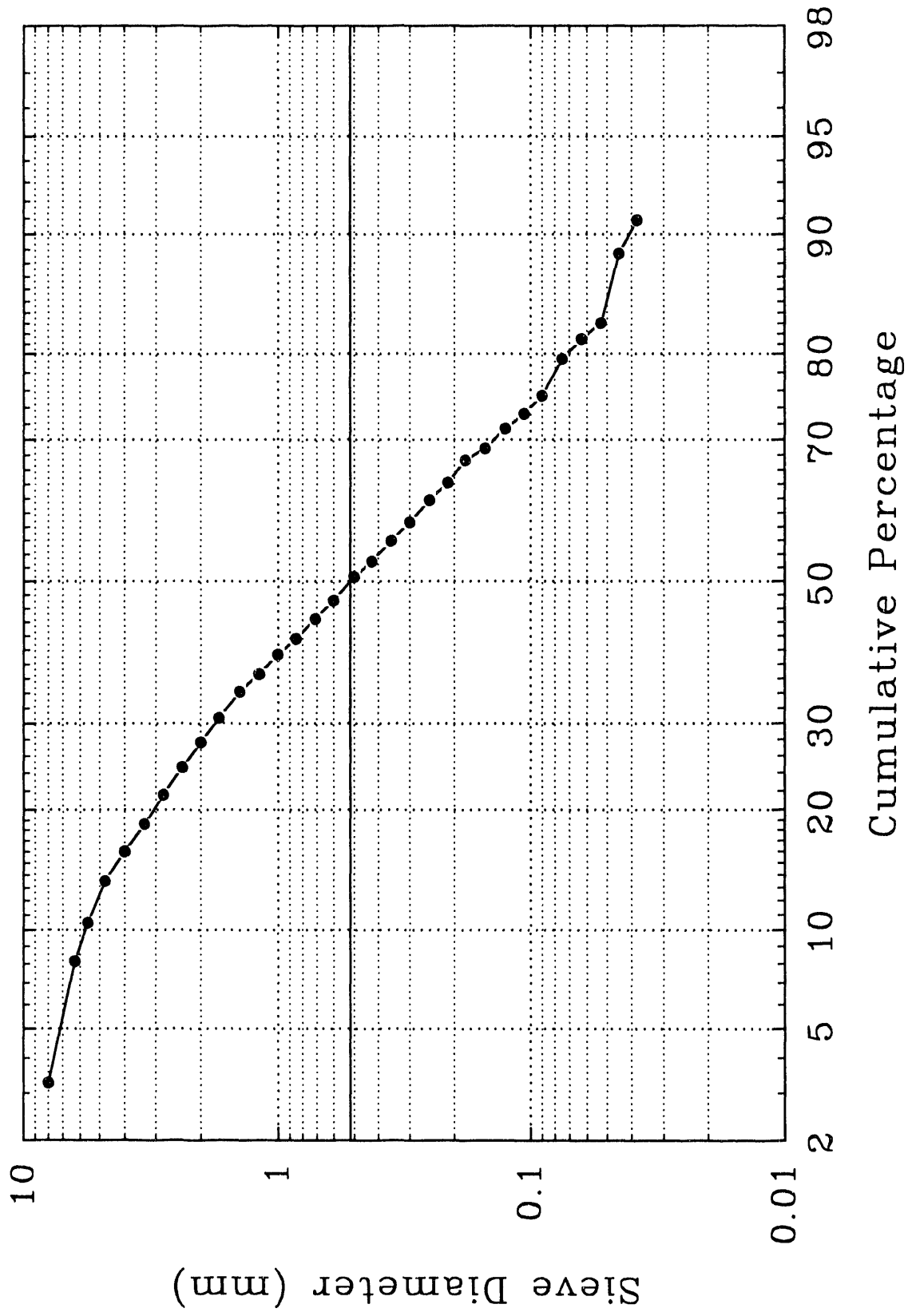


Figure 36. Posttest sieve analysis of debris recovered from outside the subcompartment structures in the Surtsey vessel in the IET-4 experiment.

## 5.0 REFERENCES

- Allen, M. D., M. Pilch, R. T. Nichols and R. O. Griffith, Oct. 1991, Experiments to Investigate the Effect of Flight Path on Direct Containment Heating (DCH) in the Surtsey Test Facility: The Limited Flight Path (LFP) Tests, NUREG/CR-5728, SAND91-1105, Sandia National Laboratories, Albuquerque, NM.
- Allen, M. D., M. Pilch, R. O. Griffith and R. T. Nichols, Mar. 1992a, Experiments to Investigate the Effect of Water in the Cavity on Direct Containment Heating (DCH) in the Surtsey Test Facility - The WC-1 and WC-2 Tests, SAND91-1173, Sandia National Laboratories, Albuquerque, NM.
- Allen, M. D., M. Pilch, R. O. Griffith and R. T. Nichols, Mar. 1992b, Experimental Results of Tests to Investigate the Effects of Hole Diameter Resulting from Bottom Head Failure on Direct Containment Heating (DCH) in the Surtsey Test Facility - The WC-1 and WC-3 Tests, SAND91-2153, Sandia National Laboratories, Albuquerque, NM.
- Allen, M. D., M. Pilch, R. O. Griffith, D. C. Williams and R. T. Nichols, Mar. 1992c, The Third Integral Effects Test (IET-3) in the Surtsey Test Facility, SAND92-0166, Sandia National Laboratories, Albuquerque, NM.
- Allen, M. D., M. Pilch, R. O. Griffith, R. T. Nichols and T. K. Blanchat, June 1992d, Experiments to Investigate the Effects of 1:10 Scale Zion Structures on Direct Containment Heating (DCH) in the Surtsey Test Facility: The IET-1 and IET-1R Tests, SAND92-0255, Sandia National Laboratories, Albuquerque, NM.
- Pilch, M. M., Oct. 1991, "Adiabatic Equilibrium Models for Direct Containment Heating," SAND91-2407C, presented at the 19th Water Reactor Safety Information Meeting, Washington, D.C.
- Tarbell, W. W., M. Pilch, J. W. Ross, M. S. Oliver, D. W. Gilbert and R. T. Nichols, Mar. 1991, Pressurized Melt Ejection Into Water Pools, NUREG/CR-3916, SAND84-1531, Sandia National Laboratories, Albuquerque, NM.

DISTRIBUTION:

U. S. Nuclear Regulatory Commission (7)  
Office of Nuclear Regulatory Research  
Attn: C. Tinkler, NLN-344  
R. Lee, NLN-344  
A. Reuben, NLN-344  
M. Cunningham, NLS-372  
F. Eltawila, NLN-344  
J. Mitchell, NLS-314  
B. Sheron, NLS-007  
Washington, D.C. 20555

U. S. Nuclear Regulatory Commission (3)  
NRC/RES  
Attn: E. Beckjord, NLS-007  
B. Hardin, NLS-169  
T. Speis, NLS-007  
Washington, D.C. 20555

U. S. Department of Energy  
Office of Nuclear Safety Coordination  
Attn: R. W. Barber  
Washington, D.C. 20545

U. S. Department of Energy (2)  
Albuquerque Operations Office  
Attn: C. E. Garcia, Director  
For: C. B. Quinn  
R. L. Holton  
P. O. Box 5400  
Albuquerque, NM 87185

Los Alamos National Laboratories  
Attn: M. Stevenson  
P.O. Box 1663  
Los Alamos, NM 87545

W. Stratton  
2 Acoma Lane  
Los Alamos, NM 87544

Electric Power Research Institute (2)  
Attn: A. Michiels  
R. Sehgal  
3412 Hillview Avenue  
Palo Alto, CA 94303

R. Sherry  
JAYCOR  
P. O. Box 85154  
San Diego, CA 92138

UCLA  
Nuclear Energy Laboratory  
Attn: I. Catton  
405 Hilgaard Avenue  
Los Angeles, CA 90024

Brookhaven National Laboratory (6)  
Attn: R. A. Bari  
T. Pratt  
N. Tutu  
130 BNL  
Upton, NY 11973

Argonne National Laboratory (4)  
Attn: J. Binder  
C. Johnson  
L. Baker, Jr.  
B. Spencer  
9700 S. Cass Avenue  
Argonne, IL 60439

Fauske and Associates, Inc.  
Attn: R. Henry  
16W070 West 83rd Street  
Burr Ridge, IL 60952

Battelle Columbus Laboratory (2)  
Attn: R. Denning  
J. Gieseke  
505 King Avenue  
Columbus, OH 43201

Department of Energy  
Scientific and Tech. Info. Center  
P. O. Box 62  
Oak Ridge, TN 37831

University of Wisconsin  
Nuclear Engineering Department  
Attn: M. L. Corradini  
1500 Johnson Drive  
Madison, WI 53706

EG&G Idaho  
Willow Creek Building, W-3  
Attn: R. Hobbins  
P. O. Box 1625  
Idaho Falls, ID 83415

Battelle Pacific Northwest Laboratory  
Attn: M. Freshley  
P. O. Box 999  
Richland, WA 99352

Professor Agustin Alonso  
E.T.S. Ingenieros Industriales  
Jost Gutierrez Abascal, 2  
28006 Madrid  
SPAIN

Jose Angel Martinez  
Sub. Emplazamientos y Programas Coop.  
CONSEJO DE SEGURIDAD NUCLEAR  
Justo Dorado 11  
28040 MADRID  
SPAIN

Juan Bagues  
Consejo de Seguridad Nuclear  
SOR Angela de la Cruz No 3  
Madrid 28056  
SPAIN

Gesellschaft für Reaktorsicherheit (GRS)  
Postfach 101650  
Glockengrass 2  
5000 Koeln 1  
GERMANY

Technische Universität München  
Attn: Professor H. Karwat  
8046 Garching, Forschungsgelände  
Munich  
GERMANY

Siegfried Hagen  
Kernforschungszentrum Karlsruhe  
P.O. Box 3640  
D-7500 Karlsruhe 1  
GERMANY

Kernforschungszentrum Karlsruhe (2)  
Attn: P. Hofmann  
    B. Kuczera  
Postfach 3640  
75 Karlsruhe  
GERMANY

Klaus Trambauer  
Gesellschaft Fuer Reaktorsicherheit  
Forschungsgelände  
D-8046 Garching  
GERMANY

UKAEA (3)  
Attn: D. Sweet  
    S. Kinnersly 203/A32  
    D. Williams 210/A32  
Winfrith, Dorchester  
Dorset DT2 8DH  
UNITED KINGDOM

UKAEA Culham Laboratory  
Attn: B. D. Turland E5.157  
Abingdon  
Oxfordshire OX14 3DB  
UNITED KINGDOM

UKAEA  
Reactor Development Division  
Attn: T. Butland  
Winfrith, Dorchester  
Dorset DT2 8DH  
UNITED KINGDOM

M. R. Hayns  
AEA Reactor Services  
B329  
Harwell  
Didcot  
Oxfordshire OX11 0RA  
UNITED KINGDOM

Mr. F. Abbey (2)  
AEA Technology  
Safety and Reliability Directorate  
Wigshaw Lane  
Culcheth  
Cheshire WA3 4NE  
UNITED KINGDOM

Simon J. Board  
CEGB National Power  
Barnett Way  
Barnwood, Gloucestershire GL4 7RS  
ENGLAND

Nigel E. Buttery  
Central Elect. Gen. Board, Booths Hall  
Chelford Road, Knutsford  
Cheshire WA16 8QG  
ENGLAND

Nucleare e della Protezione Sanitaria (DISP)  
Attn: Mr. G. Petrangeli  
Ente Nazionle Energie Alternative (ENEA)  
Viale Regina Margherita, 125  
Casella Postale M. 2358  
I-00100 Roma A. D.  
ITALY

G. Caropreso  
Dept. for Environmtl Protection & Health  
ENEA CRE Casaccia  
Via Anguillarese, 301  
00100 Roma Ad.  
ITALY

P. Ficara  
Department for Thermal Reactors  
ENEA CRE Casaccia  
Via Anguillarese, 301  
00100 Roma Ad.  
ITALY

Alan V. Jones  
Thermodynamics & Rad. Physics, TP-650  
CEC Joint Research Center, Ispra  
I-21020 Ispra (Varese)  
ITALY

Dr. K. J. Brinkman  
Reactor Centrum Nederland  
1755 ZG Petten  
THE NETHERLANDS

Mr. H. Bairiot, Chief  
Department LWR Fuel  
Belgonucleaire  
Rue de Champde Mars. 25  
B-1050 Brussels  
BELGIUM

Japan Atomic Energy Research Institute  
Attn: K. Sato  
Fukoku Seimei Bldg.  
2-2-2, Uchisaiwai-cho, Chiyoda-ku, Tokyo  
100  
JAPAN

Japan Atomic Energy Research Institute  
Severe Accident Research Laboratory  
Attn: Dr. K. Soda, Head  
Tokai-mura, Naka-gun, Ibaraki-ken  
319-11  
JAPAN

Japan Atomic Energy Research Institute  
Reactivity Accident Laboratory  
Attn: Toyoshi Fuketa  
Tokai-Mura, Ibaraki-Ken  
319-11  
JAPAN

R. D. MacDonald  
Atomic Energy Canada, Ltd.  
Chalk River, Ontario  
CANADA KOJ IJO

Atomic Energy Canada Ltd.  
Attn: Vijay I. Ngth  
Sheridan Park Res. Comm.  
Mississauga, Ontario  
CANADA L5K 1B2

Oguz Akalin  
Ontario Hydro  
700 University Avenue  
Toronto, Ontario  
CANADA M5G 1X6

K. N. (Kannan) Tennankore  
Safety Research Division  
Whiteshell Nuclear Res. Establishment  
Pinawa, Manitoba  
CANADA ROE 1LO

J. Clive Wood  
Safety Research Division  
Whiteshell Nuclear Res. Establishment  
Pinawa, Manitoba  
CANADA ROE 1LO

M. Jankowski  
IAEA  
Division of Nuclear Reactor Safety  
Wagranesrstrasse 5  
P. O. Box 100  
A/1400 Vienna  
AUSTRIA

Statens Kernkraftinspektion (2)  
Attn: L. Hammer  
W. Frid  
P. O. Box 27106  
S-10252 Stockholm  
SWEDEN

Studvik Energiteknik AB  
Attn: K. Johansson  
S-611 82 Nykoping  
SWEDEN

Korea Adv Energy Research Inst  
Attn: Hee-Dong Kim  
P. O. Box 7  
Daeduk-Danji  
Choong-Nam  
KOREA

Chang K. Park  
Korea Atomic Energy Research Institute  
Korea Advanced Energy Research Institute  
P.O. Box 7, Daeduk Danji  
Taejon 305-353  
KOREA

Jong In Lee  
Severe Accident Assessment Department  
Korea Institute of Nuclear Safety  
P.O. Box 16, Daeduk-Danji  
Daejeon, 305-353  
KOREA

POSTECH  
Department of Mechanical Engineering  
Attn: Moo Hwan Kim  
P. O. Box 125  
Kyungbuk 790-600  
KOREA

Institute of Nuclear Energy Research  
Attn: Yi-Bin Chen  
P. O. Box 3  
Lungtan  
Taiwan 32500  
REPUBLIC OF CHINA

Ms. C. Lecomte  
CEN FAR  
60-68 Av. du G. Leclerc - B.P.6  
92265 Fontenay aux Roses cedex  
FRANCE

Dr. A. Meyer-Heine  
CEN Cadarache  
13108 Saint Paul lez Durance  
FRANCE

Dr. A. Tattegrain  
CEN Cadarache  
13108 Saint Paul lez Durance  
FRANCE

Dr. G. Hache  
CEN Cadarache  
13108 Saint Paul lez Durance  
FRANCE

Jacques Duco  
Centre d'Etudes Nucleaires (IPSN-DAS)  
Commissariat a l'Energie Atomique  
Boite Postale No. 6  
F-92265 Fontenay-aux-Roses Cedex  
FRANCE

Maurice Gomolinski  
Protection and Nuclear Safety Institute  
Commissariat a l'Energie Atomique  
Boite Postale No. 6  
F-92265 Fontenay-aux-Roses Cedex  
FRANCE

Michel Livolant  
Inst. de Protection et de Surete Nucl.  
Commissariat a l'Energie Atomique  
Boite Postale No. 6  
F-92265 Fontenay-aux-Roses Cedex  
FRANCE

Jorma V. Sandberg  
Department of Nuclear Safety  
Finnish Center Radiation & Nucl. Safety  
P.O. Box 268  
SF-00101 Helsinki  
FINLAND

Lasse Mattila  
Nuclear Engineering Laboratory  
Technical Research Center of Finland  
P.O. Box 169  
SF-00181 Helsinki  
FINLAND

S. Chakraborty  
Swiss Federal Nucl. Safety Inspectorate  
CH-5303 Wurenlingen  
SWITZERLAND

J. Peter Hosemann  
Light Water Reactor Safety Program  
Paul Scherrer Institute  
CH-5232 Villigen PSI  
SWITZERLAND

Vladimir Asmolov  
I.V. Kurchatov Institute of Atomic Energy  
Moscow 123182  
Kurchatov Square  
USSR

1810 D. W. Schaeffer  
7141 Technical Library (5)  
7613-2 Document Processing  
for DOE-OSTI (10)  
7151 Technical Publication  
6321 B. D. Zak  
6400 N. R. Ortiz  
6403 W. A. VonRiesemann  
6404 D. A. Powers  
6405 D. A. Dahlgren  
6412 A. L. Camp  
6414 J. E. Kelly  
6415 S. L. Thompson  
6418 R. K. Cole  
6422 M. D. Allen (5)  
6422 T. K. Blanchat (5)  
6422 J. E. Brockmann  
6422 M. Pilch (5)  
6422 R. T. Nichols  
6422 P. Guyer (10)  
6423 K. O. Reil  
6429 K. E. Washington  
6429 R. O. Griffith  
6429 D. C. Williams  
8523-2 Central Technical Files

**END**

**DATE  
FILMED**

**12 / 1 / 92**

